2006

Rock magnetic cyclostratigraphy, orbital forcing, and high-resolution age constraints in an eocene marine flysch, Spanish Pyrenees

Michael L. Newton
Lehigh University

Newton, Michael L.

Rock Magnetic Cyclostratigraphy, Orbital Forcing, and High-Resolution Age Constraints...

May 2006

Rock magnetic cyclostratigraphy, orbital forcing, and high-resolution age constraints in an Eocene marine flysch, Spanish Pyrenees

by

Michael L. Newton

A Thesis
Presented to the Graduate and Research Committee
of Lehigh University
in Candidacy for the Degree of
Master of Science

in
Earth and Environmental Sciences

Lehigh University

April 28, 2006

This thesis is accepted and approved in partial fulfillment of the requirements for the Master of Science

4/28/06
Date

Thesis Advisor: David J. Anastasio

Committee member: Kenneth P. Kodama

Committee member: Josep M. Pares

Chairperson of Department: Peter K. Zeitler

Acknowledgements

Research was supported by collaborative NSF grant EAR-0409077 awarded to DJA & KPK, Lehigh University and JMP, University of Michigan. Advisor Dave Anastasio and committee members Ken Kodama and Josep M. Pares for guidance and support are thanked. Analysis and reviews were assisted by the expertise of Linda Hinnov, John's Hopkins University. Field work was assisted by Christine Regalla, Oscar Royo, and Jim Greenburg.

Table of Contents

Abstract

Determination of high-resolution stratigraphic ages with combined magnetostratigraphic and cyclostratigraphic data minimizes uncertainty related to discontinuous sample spacing, natural variations in sediment accumulation rate, and differential compaction. An 800 m section of the Arguis Formation, a syntectonic Eocene marine flysch deposited within the Jaca Basin in the Spanish Pyrenees, was characterized lithostratigraphically and sampled for magnetostratigraphy, rock magnetic cyclostratigraphy, and magnetic mineralogy analysis. Oriented drill cores were collected strategically to refine a previous magnetostratigraphy. Correlation of the Arguis magnetostratigraphy to the Geomagnetic Polarity Time Scale (GPTS) suggests that the first 600 m of the Arguis formation spans from C18n.1n to C17n.2n. 1220 un-oriented hand samples were collected for rock magnetic cyclostratigraphy (~4 kyr spacing; 0.2-1.5 m). Magnetic mineralogy determined by IRM acquisition modeling, thermal demagnetization of a 3-component IRM, and SIRM/χ ratio analysis consists of magnetite, pyrrhotite, and goethite. Anhysteretic remanent magnetization (ARM) data show hierarchical cyclicity consistent with predicted orbital Milankovitch frequencies. Differential lithologic decompaction was applied using empirical calibration of anisotropy of anhysteretic remanence (AAR) to volume loss from laboratory compaction experiments on comparable lithologies. Spectral analysis of the decompacted ARM data series shows an improvement in orbital power. The ARM depth domain is converted to time by scaling the data to magnetostratigraphy using chron boundary age correlations from three recent

calibrations. The chron boundary ages proposed by Palike et al. (2001) yield the greatest improvement in spectral power at expected Milankovitch frequencies. We refine the magnetostratigraphic time scale by tuning bandpassed ARM data to the precession index according to the new La2004 model. The precessional tuning improves spectral power at all orbital frequencies. Magnetic mineralogy implies a dominant contribution from primary detrital magnetite and a subsidiary contribution from authigenic sulfides to the ARM signal. In addition to the generation of a high-resolution stratigraphic age model, climate encoding mechanisms are suggested to explain the presence of Milankovitch cyclicity in the ARM record. Successful integration of absolute time from magnetostratigraphy with astrochronology allows for high-resolution constraints on sediment accumulation rates in the Arguis section. These bear directly on folding rates in the adjacent Pico del Aguila fold.

1. Introduction

For decades, researchers have observed cyclic patterns in the sedimentary record (Hays et al., 1976). Cyclic patterns exist in carbonates (Fischer, 1991; Preto et al., 2001; Latta et al., 2006), deep-sea sediments (Tiedeman et al., 1994; Shackleton et al., 1999; Palike et al., 2001), lacustrine deposits (Grimm et al., 1993; Rodbell et al., 1999; Curtis et al., 1996; Hodell et al., 2001), and loess (Wu et al., 2005); all of which are formed by a number of different depositional processes and environments. Cyclic changes in the sedimentary record are commonly attributed to climate change, which can occur over a wide array of time scales, from daily changes in solar insolation to million year variations associated with Earth's orbital pattern. In particular, Earth's orbital cycles (Milankovitch rhythms) have been associated with a variety of climate changes responsible for the cyclic deposition of sediments in a number of environments (Hinnov, 2000).

Milankovitch rhythms are composed of three different orbital parameters, precession, obliquity, and eccentricity, which operate at distinct periods and involve particular cycles in Earth's orbit. Precession refers to the wobbling motion of Earth's axis (axial precession) and the rotation of Earth's elliptical shape (precession of the ellipse) and the combined effects lead to two cycles operating at 23 and 19 kyr periods. Obliquity refers to the tilt of Earth's axis from perpendicular to the plane of Earthis orbit. The tilt angle changes through time and a typical period for the tilt cycle is 41 kyr. Eccentricity refers to the ellipticity of Earth's orbit about the sun and has characteristic

cycles with periods of 97 and 127 kyr (short eccentricity) and 404 kyr (long eccentricity). Eccentricity affects the amount of solar radiation on Earth, while precession and obliquity affect the distribution of solar radiation on Earth (Berger et al., 1993). Different climatic processes are associated with each orbital parameter.

A number of climatic indicators have been measured as proxies for climate change in a wide array of environments. Physical properties of sediments such as dust flux (Tiedemann et al., 1994) and carbonate content (Shackleton et al., 1999) were measured to identify orbital climate cycles. Chemical proxies for climate change such as oxygen isotope variations in deep-sea sediments and ice cores (Tiedemann, 1994; Dansgaard et al., 1993) were also used. Recently, rock magnetic parameters have been used as proxies for climate change, including magnetic susceptibility (χ), anhysteretic remanent magnetization (ARM), and saturation isothermal remanent magnetization (sIRM) (Bloemendal et al., 1988; Shackleton et al., 1999; Latta et al., 2006; Mayer and Appel, 1999).

The objective of this study is to provide high-resolution age constraints for a section of syntectonic strata by correlating rock magnetic parameters with expected climate change periodicities (Milankovitch rhythms). In order to understand the mechanism by which climate variations are encoded in rock magnetic parameters, magnetic mineralogy is identified and correlated to plausible climate driven mechanisms that could lead to cyclic variations in rock magnetic parameters. This study also employs a variety of techniques to account for differences in sedimentation rate and lithologic compaction that cause distortion of the climate signal. The syntectonic strata dated by this study were deposited adjacent to a growing anticline, and through the geometric

onlap relationships of the strata to the fold, the high-resolution chronostratigraphy generated by this study allows for direct measurement of the pace of deposition and deformation.

2. Geologic Setting

2.1 Spanish Pyrenees and the Jaca Basin

The Pyrenees are an east-west trending Cretaceous-Tertiary orogen along the border between the Iberian block and the Eurasian Plate (fig. 2.1). The orogen is relatively young, with deformation and synorogenic deposition continuing into the Miocene (~18 Ma) (DePaor and Anastasio, 1988). The orogen is characterized by an axial zone of basement-cored thrusts, with outward-vergent thrust belts to the north and south. The southern Pyrenees consists of the southern thrust sheets, transported syntectonic basins, and the External Sierra, a series of foothills on the southern frontal thrust (Anastasio, 1992). The Jaca Basin is a structurally partitioned piggyback basin located in the southern Pyrenees. Transport of the Jaca basin occurred on a thrust fault in Triasic evaporates associated with the foreland migration of the External Sierra. The Jaca Basin records deposition from middle Eocene through the Miocene (Puigdefabregas, 1975; Hogan and Burbank, 1996). Clastics in the Jaca Basin were deposited from east to west, and represent a marine to continental facies transition, beginning with marine deposition of the Guara Limestone and the Arguis Marls, followed by deltaic deposition

from east to west of the Belsue-Atares Formation, and finally the fluvial deposition of the Campodarbe Group (Millan et al, 1994).

2.2 The Arguis Formation

Significant thickness variations between in the Arguis Formation suggest a syn-folding deposition (fig. 2.1). Thickness differences of the Arguis Formation from anticline to syncline are more drastic at the base of the section than at the top of the section, suggesting a decrease in fold growth up-section (Poblet and Hardy, 1995). The Arguis Formation is composed of alternating beds of marly-siltstones, fine-grained sandstones, medium-grained bioturbated sandstones, coarse-grained sandstones, and interbedded limestones (fig. 2.2). The depositional environment is characterized by a mixed siliciclastic/carbonate setting in which fluvial-, storm-, and tidal-influenced sedimentation dominated (Castelltort et al., 2003), generally trending toward more shallow and coarse facies up-section. The lower boundary of the Arguis Formation is marked by the contact with the marine carbonates of the Guara Formation and the upper boundary by the coarse-grained shallow marine deltaic sandstone of the Belsue-Atares Formation (Puigdefabregas, 1975; Millan et al, 1994).

The age of the Arguis Formation is constrained by detailed biostratigraphy (Canudo, 1990) and magnetostratigraphy (Hogan, 1993; Pueyo et al., 2002; Pares et al., 2006). Canudo et al. (1991) suggests through correlation of calcareous nanoplankton, planktonic foraminifera and nummilite zones that the Arguis Formation formed from earliest Bartonian through early Priabonian. Magnetostratigraphy done by Hogan (1993)

suggests that the Arguis Formation spans in age from C19r into C17n. The magnetochron boundaries for the bottom and top of the Arguis Formation suggested by Hogan (1993) are confirmed by Pueyo et al (2002) and this study.

2.3 Arguis Syncline

The Arguis Formation was divided into three distinct depositional sequences based on sharp lithological and sedimentological facies changes as described in detail by Millan et al. (1994). The first sequence begins at the contact between the Guara Formation and the Arguis Formation and ranges in thickness from 0m at the crest of the Pico del Aguila anticline to ~90 m in the Arguis syncline. This sequence is composed of mainly blue marls and glauconitic sandy marls deposited in a deeper marine environment. Sequence two begins at the top of the last glauconitic and sandy bed found in sequence one. The lower part of this sequence is essentially azoic blue marls while the upper part of the sequence has higher fossil content and decimeter thick interlayers of bioclastic and siliciclastic graded beds. The section is over 400 m thick in the Arguis syncline and about 250 m thick at the crest of the Pico del Aguila anticline. The top of sequence two is marked by a characteristic 'Bryozoan Bed' (Puigdefabregas, 1975), a thick fossiliferous carbonate bed up to 10 m thick in the Arguis syncline. Sequence three begins at the top of the 'Bryozoan Bed'. It is a thick succession of azoic blue marls with coarsening and shallowing upward parasequences in the upper part of the section. The sequence is about 400m thick in the Arguis syncline and only about 100 m thick at the hinge of the Pico del Aguila anticline. Castelltort et al. (2003) also defined a series of

depositional sequences for the Arguis Formation as a progradation/retrogradation cycle of the shoreline related to Pyrenean uplift, sea level change, and sediment supply variations. The sequence stratigraphy of Castelltort et al. (2003) differs from Millan et al. (1994) in that the 'Bryozoan Bed' was assigned its own depositional sequence and the Millan et al. (1994) sequence three was divided into two sequences. The significant thinning and absence of sequences at the crest of the Pico del Aguila fold indicates that sedimentation occurred during fold growth. Structural data correlated with magnetostratigraphic data (Hogan, 1993) was used to develop a structural model for the Pico del Aguila fold (Poblet and Hardy, 1995).

An 800 m stratigraphic section, adjacent to previous transects along the southern margin of the Jaca basin (Puigdefabregas, 1975; Hogan, 1993; Millan et al., 1994; Pueyo, 2001; Castelltort et al., 2003), was measured and described in detail (fig. 2.2). Grain size, bioturbation, fossil composition, and bed thickness were assessed every ~10 cm. The measured section began at the base of the Arguis Formation at the contact with the Guara Limestone. The first 93.2 m of the Arguis Formation corresponds with DS1 of Millan et al. (1994) and the tops of the two glauconite beds of Puigdefabregas (1975) are located at 35.4 m and 93.2 m. Significant glauconite is observed in a number of other beds throughout the lower Arguis Formation and is observed in beds as high as 191.7 m from the base of the Arguis Formation. Grain size in the first 93.2 m ranges from very-fine to fine sand, and the section is very calcareous. Above 93.2 m, grain size decreases to alternating silt and very-fine sand beds that persist until 163.5 m. Alternating beds from very-fine to occasional medium grained sand persist until 355.7 m where grain size increases to alternating beds of fine to medium grained sand and bedding character

becomes more prominent and resistant. Fossil content and bioturbation are high from 355.7 m to 505.6 m. A prominent limestone bed that is traceable throughout the basin is 5.7 m thick, contains abundant fossils including bryozoans, echinoids, and shell fragments, and represents the Bryozoan Bed of Puigdefabregas (1975) and the top of DS2 (Millan et al., 1994). The Bryozoan Bed varies significantly along strike both compositionally and in thickness. The Bryozoan bed can be as thick as 12 m and composed of more sandy horizons with little limestone. Castelltort considers the Bryozoan Bed a separate depositional sequence and representative of a reef facies. Grain size, fossil content, and bioturbation decrease up-section from the Bryozoan Bed to alternating beds of very-fine to fine grained sand. A coarse grained bed with a thickness of 2.5 m and the top of the bed located at 634.7 m represents the Arguis Bed of Poblet and Hardy (1995). Alternating beds of fine to medium grained sand persist above the Arguis Bed and are capped by an easily recognizable fossilifereous bed with bryozoans, shell fragments, and nummilites at 795.4 m where continued sampling was interrupted by steep slopes and extensive cover.

3. Methods

The Arguis Formation was measured, described in detail, and sampled along the Arguis type section adjacent to prior transects by Puigdefabregas (1975), Hogan (1993), Castelltort et al. (2003), and Pueyo et al. (2003). Our section begins at the Arguis-Guara contact (south) and continues until outcrop exposure is lost due to tree cover (north) (fig.

3.1). The section was described using grain size, bed thickness, fossils, bedding, bedform, and other distinguishing characteristics. Grain size was measured in the field using a hand lens comparison to the ϕ grain size scale. The section was measured using a Jacob's staff and Brunton compass. Two suites of samples were collected from the Arguis Formation, one set was collected to analyze rock magnetic cyclostratigraphy and the other set was collected to perform rock magnetic tests on each distinct lithology found throughout the Arguis type section.

3.1 Rock Magnetic Analysis

3.1.1 Sampling

Samples for detailed rock magnetic analysis were collected from six sites representing the six distinct lithologies identified throughout the measured section. The lithologies identified from finest to coarsest are siltstone (<4.0ϕ), very-fine-grained sandstone (4.0-3.5ϕ), fine-grained sanstone (3.5-3.0ϕ), medium-grained bioturbated sandstone (3.0-2.0ϕ), coarse-grained sandstone (2.0-1.5ϕ), and bioclastic limestone. 9-13 oriented cores were collected from each site, generating between 1 and 3 samples per core. Samples were collected using a portable gasoline-powered drill with diamond tipped bit. Samples from each site were used 1) to analyze the effects of volume loss on differential lithologic compaction using anisotropy of anhysteretic remanence (AAR), 2) to identify magnetic mineralogy based on coercivity and Curie temperature from a 3-component thermal demagnetization (Lowrie, 1990), and 3) to separate relative

contributions to remanence from different coercivity phases by measuring and modeling detailed IRM acquisition.

3.1.2 Measurement

ARM for 3 samples from each of 6 sites was applied in a modified Schonstedt GSD-5 AC Geophysical tumbling-specimen demagnetizer in 9 orientations by applying an alternating AC field from 50 mT to 0 mT in the presence of a bias DC field of 0.1 mT with a 90 mT AF demagnetization between each step. ARM was measured in a 2G Enterprises superconducting magnetometer. AAR tensors were determined for each sample based on the ARMs for 9 orientations according to McCabe et al. (1985). To average AAR for each site, individual sample AAR was rotated from core coordinates to stratigraphic coordinates. Once each sample AAR was rotated into the same stratigraphic coordinate system, the six-component tensor was averaged for each site and a site maximum, intermediate, and minimum axis magnitude and orientation was determined.

Isothermal remanent magnetization (IRM) was applied in an ASC Scientific IM-10-30 impulse magnetizer in 3 orthogonal directions to 3 samples from 3 sites representing lithologies found in the Arguis Formation 200-500 m from the base of the section. 1.2 T was applied along the x-axis, 0.6 T was then applied along the y-axis, and finally 0.1 T was applied along the z-axis. Following the application of IRMs, each sample was thermally demagnetized in 50°C steps from 100°C to 600°C. Thermal demagnetization was performed in an ASC Scientific TD-48SC thermal specimen demagnetizer and measured in the magnetometer.

Detailed IRM acquisition experiments were conducted over 27 steps ranging in size from ~17 mT steps to 165 mT to 1 T steps from 3-5 T. Two samples from each of 5 sites (excluding the limestone lithology) were analyzed. Coercivity components were modeled after Kruiver et al. (2001). IRM was applied in an ASC Scientific IM-10-30 impulse magnetizer.

3.1.3 Decompaction

An ARM measured in 9 directions was used to determine the anisotropy ellipsoid tensor for each sample using the AAS program (McCabe et al., 1985). The anisotropy ellipsoid tensor was rotated into stratigraphic coordinates and averaged for each site (lithology). The average anisotropy ellipsoid tensor was converted into eigenvectors using a conversion program developed by Tauxe (1998). A compaction fabric correction was estimated using experimental compaction data from marine sediments (Deamer and Kodama, 1990; Tan and Kodama, 1998). A relationship between $tanI_o/tanI_c$ and volume loss was developed and tied to the Arguis results by their anisotropy (Kodama, written communication) assuming:

$$tanI_o/tanI_c = [K_{max} * (a+2) - 1] / [K_{min} * (a+2) - 1]$$

Where Kmax and Kmin are the maximum and minimum eigenvalues measured by AAR respectively and a is the individual magnetic particle anisotropy. The a value is estimated to be 2 based on a value determinations from fine-grained marine clastics which vary from 1.4-2.25 (Davi and Kodama, 1995; Tan and Kodama, 1998; Vaughn et al., 2005). The value derived for tanIo tanIc was used to estimate volume loss according

to the best-fit curve through experimentally derived empirical compaction data (figure 4.1c).

3.2 Cyclostratigraphy

3.2.1 Sampling

The goal of the sampling strategy for rock magnetic cyclostratigraphy was to obtain a minimum sampling interval to constrain the 20 kyr precession cycle. A minimum of two samples must be measured for every cycle in order to constrain a climate signal (the Nyquist frequency), however, to accurately determine the amplitude of short precession, a sample interval of less than 5 kyr is required. We targeted sampling at a 4 kyr sample interval to ensure enough resolution to observe 20 kyr peaks in spectral analysis. Because sedimentation rates vary significantly from the bottom to the top of the section, and the sedimentation rate estimates were made using data sampled at 20 to 30 meter intervals (Hogan, 1993), significant uncertainty exists in estimating an appropriate sample rate to attain a 4 kyr interval. Estimates based on Hogan's (1993) data were combined with Millan's (1994) depositional sequences (DS) to generate our sampling strategy. DS1 was sampled at a 20 cm interval, DS2 was sampled at a 75 cm interval, and DS3 was sampled at a 1.5 m interval. 1,220 unoriented hand samples were collected in the field.

3.2.2 Measurement

Samples for magnetic cyclostratigraphic analysis were hand crushed and packed into 8cc plastic boxes for rock magnetic analysis. The sample preparation likely integrates approximately 2-3 centuries of time into each box. Mass-normalized MS and ARM were measured for all samples and SIRM was measured for 200 samples from 200-350 m from the base of the Arguis Formation. MS was measured using an Agico KLY-3s Kappabridge. ARM was applied with an alternating magnetic field between 100mT and 0mT in the presence of a steady DC magnetic field of 0.1mT and SIRM was applied at a field of 325 mT (determined through IRM acquisition).

3.2.3 Data Processing

Rock magnetic data sets (ARM, X, ARM/X, SIRM, SIRM/X) along with lithofacies data sets (grain size, bed thickness) were analyzed for dominant spectral frequencies. These data were stratigraphically corrected for the effects of differential compaction based on the measured section and results from AAR. Each bed of a particular lithology was assigned an increase in thickness equal to the amount of volume loss determined by AAR (i.e. 20% volume loss = 20% increase in bed thickness). A pointer series was generated to re-scale the stratigraphic position of each sample to the decompacted section. The data sets were then fit with a 4^{th} or 5^{th} order polynomial and the residuals from the polynomial curve were preserved, thereby removing any long-term variations at under-sampled low frequencies. Some data were scaled to time using

magnetostratigraphy (Pares et al., 2006). A pointer series was generated using polarity reversal locations (also re-scaled to the decompacted section) with associated Chron boundary ages (Cande and Kent, 1995; Palike et al., 2001; Gradstein et al., 2004) and applied to the relevant data sets, effectively converting stratigraphic distance into time.

Data was processed for spectral analysis in Analyseries 1.2 and Analyseries 2.0 (Paillard et al., 1996). Data was re-sampled evenly using simple interpolation and a linear function for distance-series every 0.1 m and for time-series every 1 kyr. Spectral analysis was done using the multitaper method (MTM) with a 3π window. Harmonic F-tests were used to determine which sinusoidal components have >90% significant contributions to spectral power. F-tests are generated as a ratio of spectral power at a particular frequency to spectral power of surrounding frequencies. False positives can occur where the power of a particular frequency is low but the surrounding power is extremely low. False negatives can occur where the power of a particular frequency is high but the power of surrounding frequencies is also high. F-tests should be used as a guide to identify dominant frequencies, not as an absolute rule for the presence or absence of dominant frequencies.

4. Results

4.1 Rock Magnetism

4.1.1 Compaction Correction

AAR was measured to identify differential compaction fabrics in each principal lithology identified in the Arguis measured section. Stereographic projections of the site anisotropy averages (fig. 4.1a) show characteristic compaction fabrics with Kmin perpendicular to bedding and Kmax and Kint distributed perpendicular to bedding for the four finer grain sizes. Most lithologies have an oblate magnetic anisotropy fabric (fig. 4.1b), with finer grain sizes having more oblate fabrics and the coarsest grain size having a slightly prolate fabric.

Volume loss for each lithology is summarized in table 4.1. For lithologies with depositional fabrics, volume loss ranges from ~43%-20%, indicating twice as much vertical shortening (compaction) for the finest grained lithology than for the coarsest grained lithology. The percent volume loss values were applied to the stratigraphic column and a de-compacted pointer series representing a new thickness for each bed was used to re-scale the depth-series ARM, MS, ARM/MS, and grain size data sets, and to apply new bedding thicknesses for the thickness data set. The 200-500 m section, originally 300 m thick, is decompacted to a thickness of 376 m.

4.1.2 Magnetic Mineralogy

Results from detailed IRM acquisition modeling from two samples for each lithology are summarized with characteristic results from modeling shown in figure 4.2a. Most IRM acquisition curves are modeled best with two overlapping low coercivity components and one to two high coercivity components. The two modeled low

coercivity components represent two different magnetic minerals with overlapping coercivities. The low coercivity components contribute ~90% to the overall SIRM and become saturated by 325mT. The high coercivity components in general contribute much less (~10%) to the SIRM than the low coercivity components. The highest coercivity component has an average coercivity of ~2T, does not begin to contribute to the IRM until ~1T, and saturates usually >5T.

Thermal demagnetization of a 3-component IRM (Lowrie, 1990) can provide information about magnetic mineralogy using coercivity and unblocking temperature (fig. 4.3). All samples become essentially demagnetized by 600°C, characteristic of magnetite (Tc=580°C). In many of the finer grained lithologies, a drop in remanence is observed between 300-400°C for both the soft (<0.1T) and intermediate (<0.6T) components, characteristic of magnetic sulfides. Very little magnetism was observed in the hard (1.2-0.6T) component. Two samples were re-magnetized in the same orientation after thermal demagnetization and measured. An increase in magnetization of approximately three orders of magnitude was observed for each component, suggesting a possible oxidation to magnetite of an originally non-magnetic material, likely pyrite. The increase in remanence following heating also suggests that the low-coercivity phase unblocked between 300 and 400°C is not maghemite (Dunlop and Ozdemir, 1997).

IRM was measured for samples with an induced field of 325mT in order to saturate the low coercivity components without activating the high coercivity components following the IRM acquisition results. The ratio of SIRM to magnetic susceptibility ranges from 0.48 to 1.16 kA/m. When compared with experimental results for magnetic minerals summarized in Peters and Dekkers (2003), the SIRM/χ ratio falls into the

magnetite/titanomagnetite range, well below the ratio expected for magnetic sulfides (pyrrhotite/greigite).

4.2 Cyclostratigraphy

Data sets including ARM, χ, ARM/χ, SIRM, SIRM/χ, grain size, and bed thickness were collected throughout the measured Arguis section (plate 4.1). Magnetic susceptibility values range from 1.5 E-8 to 7.8 E-8 m^3/kg; ARM values range from 1.1 E-6 to 1.0 E-5 Am^2/kg; and ARM/χ ratio values range from 30.2 to 185.6 A/m. SIRM values range from 2.4 E-5 to 5.8 E-5 Am^2/kg and SIRM/χ ratio values range from 0.49 to 1.16 kA/m. Grain sizes range from silt to coarse sand and bed thicknesses range from 0.1 to over 10 m. ARM, χ, and grain size raw data (fig. 4.4) from the section representing 200 to 500 m from the base of the Arguis section were de-trended, evenly re-sampled, and analyzed for spectral power (fig. 4.5). Each data set was then corrected for differential lithologic compaction, re-sampled, and analyzed for spectral power (fig. 4.6).

4.2.1 ARM

A detailed magnetostratigraphy along the sample transect was constructed by Pares et al. (2006). The magnetostratigraphy suggests that the 200-500 m section begins in chron C18n.1n and ends in C17n.2n, containing four chron boundaries with which to constrain absolute age. Three different absolute ages were recently suggested for each of the chron boundaries (Cande and Kent, 1995; Palike et al., 2001; and Gradstein et al.,

2004) (table 4.1). Pointer series were generated using chron boundary locations with associated ages from each of the three different sources and were applied as age-scales to the decompacted ARM data set. Spectral analysis was performed on each of the three magnetostratigraphy scaled decompacted ARM data sets according to standard procedures (fig. 4.7).

An evolutionary power spectrum (spectrogram) was generated using the ARM data scaled to the Palike et al. (2001) chron ages to identify migration of spectral power through time (fig. 4.8). Power exists near expected Milankovitch frequencies, but migration through time of spectral power in the precession band is observed. In order to refine age controls on the Arguis section, a precessional tune was conducted on the ARM data set. The precessional band was isolated using a Gaussian filter centered at a frequency of 0.048 ± 0.01 cycles/kyr applied to the ARM data (fig. 4.9a), encompassing the frequencies over which precession was observed to migrate (fig. 4.8). The filtered data was targeted to a portion of the Eocene modeled precession (Laskar et al., 2004) for exactly the same time period as predicted by the magnetostratigraphy age-scale (fig. 4.9b). To tune the data, each precessional peak and trough were matched and the filtered ARM data was scaled to match the precessional modeling using two pointers for each precessional wavelength (~10 kyr). A power spectrum and spectrogram were generated using the decompacted ARM data scaled to magnetostratigraphy and tuned to precession (fig. 4.9c&d). The precessional tune achieved an increase in spectral power and an alignment of significance at expected Milankovitch frequencies, including obliquity and eccentricity, along with an improvement in stability of spectral power at all expected Milankovitch frequencies.

4.2.2 Grain Size

The grain size data set was generated as a step function according to stratigraphic bed boundaries and grain diameter values from field estimations (plate 4.1). The grain size data from 200-500 m from the base of the Arguis Formation was analyzed for spectral power following a de-compaction and a stratigraphic scale to the magnetostratigraphy ages of Palike et al. (2001). The scaling technique applied to the grain size data set follows the same procedure as that used for the ARM data. Spectral power is observed at exected Milankovitch frequencies (fig. 4.10), in particular the long eccentricity (404 kyr) and obliquity (41 kyr) periods. The relative power of different Milankovitch frequencies varies between the grain size power spectrum and the ARM power spectrum.

5. Discussion

5.1 Magnetic Mineralogy

The ratio of SIRM/χ can be used as identify magnetic mineral contributions to remanence. SIRM/χ values for the Arguis formation range from 0.48 to 1.16 kA/m, well within the range reported for magnetite/titanomagnetite and below the range reported for magnetic sulfides pyrrhotite or greigite (Peters and Dekkers, 2003, and references

therein). This ratio must be used with caution, as susceptibility measures not only ferromagnetic minerals but also paramagnetic and diamagnetic minerals. The Arguis formation is composed of mainly quartz and calcite, both diamagnetic minerals. If these minerals were to contribute significantly to susceptibility, one would expect susceptibility values to be low and the SIRM/χ ratio high. Despite the presence of diamagnetic minerals, the SIRM/χ is low, so the impact of diamagnetic minerals could not have lowered the SIRM/χ and masked the contribution of sulfides to the remanence.

Thermal demagnetization of a 3-component IRM indicates the presence of two different magnetic phases present in both the low- (< 0.1 mT) and intermediate- (between 0.1 and 0.6 T) coercivity ranges (fig. 4.3). One phase has a characteristic unblocking temperature (Tc) between 300-400°C while another phase loses its remanence completely from 550-600°C. These results argue for the presence of both magnetite and pyrrhotite/greigite in all of the lithologies of the Arguis Formation.

IRM acquisition modeling (Kruiver, 2001) indicates the presence of a high-coercivity magnetic phase present in many of the samples to varying degrees. This magnetic phase appears to have a coercivity of ~1.8 T and does not saturate below 5 T. This magnetic phase either represents goethite or hematite. IRM acquisition modeling indicates the presence of a dominant low-coercivity phase (~40 mT) that on average contributes ~70% of the saturation remanence. Another low-coercivity phase is modeled with a coercivity of ~80 mT and an average contribution to saturation remanence of ~20%. Based on overwhelming evidence from rock magnetic analyses, the magnetic mineralogy of the Arguis Formation is composed of three different magnetic minerals. The high-coercivity magnetic mineral present in many samples from the Arguis

Formation, generally in small amounts, is goethite. IRM acquisition results support this based on modeled coercivity. The coercivity (~1.8 T) could also represent hematite, but this is unlikely because 1) hematite usually has a slightly lower coercivity (<1 T); 2) thermal demagnetization shows the loss of remanence by 600°C, which is well below the Tc for hematite (680°C); and 3) thermal demagnetization for magnetostratigraphy indicates occasional relatively sharp decrease in intensity below 200°C (Pares, written communication).

There are two low-coercivity magnetic minerals with overlapping coercivity spectra. IRM acquisition modeling indicates that the dominant phase, comprising ~70% of the total remanence, has a coercivity of ~40 mT. This phase is interpreted to be magnetite. The SIRM/χ ratio indicates that magnetite is the dominant magnetic mineral, therefore it is logical to assume that the most dominant magnetic phase modeled by IRM acquisition is also magnetite. A coercivity of 40 mT for magnetite is well within reasonable expected coercivities for magnetite (Peters and Dekkers, 2003).

The second low-coercivity magnetic mineral is interpreted to be pyrrhotite. IRM acquisition modeling requires the presence of another, slightly higher coercivity (~80 mT) component besides magnetite. A coercivity of ~80 mT is very consistent with coercivities expected from pyrrhotite (Peters and Dekkers, 2003). Thermal demagnetization results also indicate the presence of a low- or intermediate-coercivity magnetic mineral with a Tc between 300-400°C, consistent with pyrrhotite. The presence of sulfides is also implied by a 3-order of magnitude increase in remanence following an applied IRM on a thermally demagnetized sample. It is likely that a non-magnetic iron

sulfide (i.e. pyrite) became oxidized at higher temperatures and formed magnetite. The average contribution to remanence of the pyrrhotite is only ~20%.

A rock magnetic study performed on a more distal contemporary facies, the Pamplona Marls, also observes the presence of magnetite and pyrrhotite (Larrasoana et al., 2003). Larrasoana et al. (2003) suggest that both magnetite and pyrrhotite carry a primary remanence based on a fold test. Larrasoana et al. (2003) rule out greigite as the magnetic iron sulfide in the Pamplona-Arguis Marls based on low-temperature magnetic behavior along with well-documented instability of greigite over long time periods. The results reported in this study do not rule out the presence of greigite, but based on the results of Larrasoana et al. (2003) it is probable that the magnetic iron sulfide in the Arguis Formation is pyrrhotite.

The results of rock magnetic analysis indicate the presence of three magnetic minerals contributing to the remanence of the Arguis Formation. These minerals are magnetite, pyrrhotite, and goethite and they contribute ~70%, ~20%, and ~10% respectively to the total saturation remanence.

5.2 ARM

The concentration of low-coercivity magnetic grains as measured by ARM in the Arguis Formation is influenced by climate variations that modulate at expected Milankovitch frequencies. ARM reported in this study measures the remanent magnetization of magnetite and pyrrhotite grains with coercivities less than or equal to

100 mT. Magnetic mineralogy evidence indicates that magnetite grains are the primary contributor to ARM.

The presence of spectral power at expected Milankovitch frequencies in the raw ARM data set is cryptic (fig. 5.2a). Spectral power at low frequencies are more consistent than power at high frequencies. Significant improvement occurs when the ARM data set is corrected for expected differential lithologic compaction, indicating that this data set has spectral power at frequencies consistent with expected Milankovitch frequencies (figure 5.2b). The frequency of this power spectrum is reported in cycles/m, so the important observation with regard to Milankovitch frequencies involves identifying ratios for expected frequencies. The power observed near frequencies of 0.2 and 0.25 in the ARM power spectrum likely indicate power in the precessional band at 23 and 19 kyr respectively. Assuming these frequencies represent the precessional band, one would expect power from obliquity near a frequency of 0.12 cycles/m and power from the eccentricity band for 400 and 100 kyr near frequencies of 0.012 and 0.048, respectively. Power in the decompacted ARM spectrum appears at frequencies consistent with these Milankovitch frequencies.

Further adjustments can be made to improve the spectral power observed in the decompacted ARM data set by scaling the stratigraphic distance to absolute time using magnetostratigraphy. The power spectra reported in cycles/kyr allow a direct observation of the presence or absence of power at expected Milankovitch frequencies. A companion magnetostratigraphic study was conducted to provide magnetochron boundary constraints throughout the Arguis section (Pares et al., 2006). This study allows for the magnetostratigraphy of the Arguis section to be linked with the Geomagnetic Polarity

Time Scale (GPTS) and absolute ages to be assigned to magnetochron boundaries known throughout the Arguis section with up to 3 m precision. By applying an age-scale to the Arguis section using the stratigraphic position of Chron boundaries and the associated Chron boundary ages, stratigraphic distance can be converted into time. Three age models have been reported for magnetochron boundaries in the Eocene (Cande and Kent, 1995; Palike et al., 2001; Gradstein and Ogg, 2004) (table 4.1). Gradstein and Ogg (2004) and Cande and Kent (1995) base age determinations on a constant sea floor spreading rate model between radiometric dates, whereas Palike et al. (2001) utilize more absolute ages and multi-proxy climate models to determine chron boundary ages. An age-scale using each of these age determinations was applied to the ARM data and spectral analysis was performed to identify the age-scale that best preserved power at expected Milankovitch frequencies in the ARM data (figure 4.8). Spectral power of the decompacted ARM data scaled to the Chron boundary ages suggested by Palike et al. (2001) is the most consistent with frequencies expected for Milankovitch rhythms (fig. 5.2c).

Further refinement of the decompacted ARM data set is accomplished by a precessional tune (fig. 5.2d). Migration of the precessional band in the evolutionary spectrum from the Palike et al. (2001) magnetostratigraphic scale (fig. 4.8) is most likely the result of variable accumulation rates between chron boundaries. To account for this variability, we tune the ARM data set to modeled precession in the Eocene (Laskar, 2004) for a finer scale tuning. This tuning procedure should inevitably improve spectral power in the precessional band, as is evident in figure 4.10, but the goal and true test of the presence of Milankovitch frequencies in the data set is the refinement of spectral

power at other expected Milankovitch frequencies such as obliquity and eccentricity. Spectral power does indeed improve in the obliquity band (41 kyr) as an increase in power is observed at this frequency. Spectral power improves over the short eccentricity frequency (97 and 127 kyr) as well as power observed at long eccentricity (404 kyr).

Each successive step used to scale the ARM data set (decompaction, magnetostratigraphy scale, precessional tune) serves to improve spectral power at expected Milankovitch frequencies. A caveat that should be introduced here is that one should be careful not to introduce a bias by the manipulation of a data set that would produce spectral power at frequencies where none exist, in this case forcing power at expected Milankovitch frequencies. However, the only step used to scale the ARM data set that implicitly assumed the presence of Milankovitch frequencies was the final precessional tune, in which the ARM data was scaled to fit modeled precession. This was the final step and was only used to refine age resolution at the precessional time scale. Throughout the scaling process that frequencies expected from Milankovitch rhythms predominate the ARM spectral power prior to the precessional tune. By progressively scaling the ARM data set, time can be determined throughout the 200-500 m portion of the Arguis Formation with a precision as good as 10 kyr. A high-resolution age map is created for ages constrained every ~10 kyr (fig. 5.1) for the Arguis section.

5.3 Climate Encoding

Frequencies consistent with climate variations at orbital time scales are observed to have dominance and significance in ARM fluctuations in the Arguis Formation.

Results from IRM acquisition modeling indicate that two magnetic minerals contribute to the ARM measurement, magnetite and pyrrhotite, with magnetite being the dominant mineral. The magnetite carries a primary remanence as observed by reliable magnetostratigraphy results for both normal and reversed Chrons throughout the Arguis Formation (Pueyo et al., 2002; Pares et al., 2006).

The magnetite in the Arguis Formation likely originated from a detrital source for a number of reasons. 1) Grain size data from the same section of the Arguis Formation as the ARM data set (200-500 m) also exhibits spectral power at expected orbital frequencies (figure 4.11). The grain size data represents a depositional cyclicity with frequencies consistent with ARM cyclicity, implying that a depositional process is responsible for grain size variations as well as ARM (magnetite concentration) variations. 2) Anisotropy of ARM results from grain sizes within the section analyzed for ARM exhibit a characteristic depositional fabric with minimum anisotropy axes perpendicular to bedding (figure 4.1). 3) Evidence from low-temperature measurements and hysteresis on the Pamplona-Arguis Formation excludes the possibility of bacterial magnetite formation and burial conditions were not conducive to the thermal conditions needed for magnetite formation through diagenesis under standard geothermal gradients (Larrasoana, 2003). We conclude that the dominant magnetic mineral contributing to ARM in the Arguis Formation is primary detrital magnetite.

IRM acquisition modeling (fig. 4.4) indicates that pyrrhotite also contributes approximately 20% to ARM. The presence of pyrrhotite is also supported by results from thermal demagnetization of a 3-component IRM (fig. 4.5). A decrease in remanence is observed between 300-400°C for a majority of samples. The presence of

opaque framboids preferentially located in the vicinity of organic material (i.e. fossils, fig. 5.3a) observed in thin section analysis also supports the presence of pyrrhotite.

Iron sulfide minerals form in many marine sediments under anoxic, sulfate reducing conditions through a process known as pyritization (fig. 5.3b). Oxic bacteria consume all available O_2 near the sediment/water interface, creating anoxic conditions necessary for bacterial sulfate reduction just a few centimeters below the sediment/water interface. Three major factors control the amount and speed of iron sulfide formation (Berner, 1984), these factors are 1) The quantity and reactivity of organic material, 2) The availability of dissolved sulfate, and 3) The quantity of reactive iron minerals in the sediment. In most marine sediments, conditions favorable for iron sulfide formation exist from a few centimeters beneath the sediment/water interface once oxic bacteria create sufficiently anoxic conditions to one meter beneath the sediment/water interface where the materials required for iron sulfide production are progressively depleted by the process of pyritization (Westrich and Berner, 1984; Canfield and Berner, 1987; Roberts and Turner, 1993). Magnetic iron sulfides are metastable minerals formed as an intermediate step in pyritization prior to the formation of the non-magnetic mineral pyrite (FeS2) and are preserved only when the pyritization process is arrested and prevented from reacting to completion.

The Arguis Formation was deposited under conditions that were conducive to magnetic iron sulfide formation. Organic material is known to have been abundant based on high degrees of bioturbation and fossil preservation throughout the Arguis section (fig. 2.2). The presence of magnetite in the Arguis Formation is evidenced throughout the rock magnetic analysis and suggests that sufficient iron was available for dissolution

during pyritization. The availability of dissolved sulfate can be assumed because sulfate is generally present in marine waters and the Jaca Basin and External Sierras bedrock contains abundant evaporite deposits, including gypsum and anhydrite (Anastasio, 1992). The arrest of pyritization can be attributed to relatively rapid sedimentation rates (~0.2 m/kyr), causing reactive magnetite to pass through the zone of sulfate-rich pore fluid quickly and preventing the pyritization process from reacting to completion.

Cyclicity in the ARM record of the Arguis formation is consistent with known Milankovitch rhythm periodicities and suggests the encoding of climate variations in the concentration of magnetic minerals. Two climate-forcing mechanisms to explain variations in ARM seem plausible. The influx of magnetite into the sediment column could be controlled by runoff and aeolian variations associated with climate change in the form of rainfall fluctuations, chemical or physical weathering conditions, and aridity. Runoff variations have been attributed to orbital climate change at precessional frequencies for regions of the Atlantic Ocean and western Europe in the Eocene (Sloan and Huber, 2001). Aeolian deposition of magnetite grains has also been attributed to climate change on orbital scales (Latta et al., 2006). Another plausible mechanism for the encoding of climate change in rock magnetic concentration cyclicity is climatically induced variability in oceanic conditions affecting the pyritization process. This mechanism would assume an essentially steady magnetite input with variations in the degree of pyritization through time consistent with Milankovitch periodicities. The climatically induced variability could come in the form of availability of dissolved sulfate, quantity of organic material needed to drive the sulfate reduction process, or pace of sedimentation driven by sea-level change and proximity to source sediment.

Primary detrital magnetite dominates the ARM signal and records variable climate affecting fluvial and aeolian transport modulating at Milankovitch frequencies. Authigenic processes can also affect the abundance of ferromagnetic materials in sedimentary rocks. The anoxic dissolution of magnetite and formation of iron sulfides has been observed in marine rocks (Leslie et al., 1990; Roberts and Turner, 1993). It is possible that the interaction between both variability in runoff and oceanic pyritization conditions could operate concurrently to produce cyclicity in magnetic concentrations consistent with orbital periodicities. Much of the organic matter in the Jaca basin is humic terrestrial material that should be sensitive to runoff variability. Higher concentrations of magnetic material could result from an increase in runoff, increasing the detrital magnetite input, organic input, rate of burial, and the arrest of pyritization as sediment will pass more quickly through the diagenetic zone where sulfate rich pore waters are sufficiently available for reaction (Berner et al., 1984). The data for the Arguis Formation argue that detrital input is the dominant mechanism here; however, the relative importance between detrital input and pyritization could vary both temporally and spatially in this basin and in other similar basins. Detailed rock magnetic studies should always be conducted to determine the relative importance of primary and secondary magnetic minerals in the record.

5.4 Decompaction

A novel procedure of using experimental compaction data to account for differential lithologic compaction through the use of ARM anisotropy (AAR) is presented

here. This procedure allows for differential decompaction of lithologic units on a bed-to-bed scale. It has been shown in this study that differential lithologic de-compaction improves the identification of Milankovitch frequencies to as high as the precessional band (20 kyr). Other techniques used to correct for differential compaction require averaging lithologic porosity for a unit of rock (Sclater and Christie, 1980), lacking the resolution to assist in the identication of high frequency Milankovitch rhythms in most cases. Sufficient data exists for marine sedimentary rocks for this method to be applied generally (Kodama et al., in prep.).

6. Conclusions

A combination of rock magnetic analysis allows for the identification of magnetic mineralogy in the Arguis Formation and an assessment of relative magnetic mineral quantities. Magnetite, pyrrhotite, and goethite contribute to the saturation remanence, while only magnetite and pyrrhotite contribute to the ARM analyzed for cyclicity. Periodicity observed in ARM time series analysis is consistent with expected Milankovitch rhythm frequencies. Techniques including decompaction, magneto-stratigraphic scaling, and precessional tuning can be used to refine Milankovitch rhythm resolution by accounting for variable accumulation rates, and thereby generate high-resolution age constraints throughout a stratigraphic section. ARM serves as a proxy for climate change by recording Milankovitch cyclicity in magnetic mineral concentration. Climate forcing mechanisms, including runoff variability and changes in oceanic

pyritization conditions, have been proposed to explain the encoding of orbital climate change in magnetic mineral concentration variability.

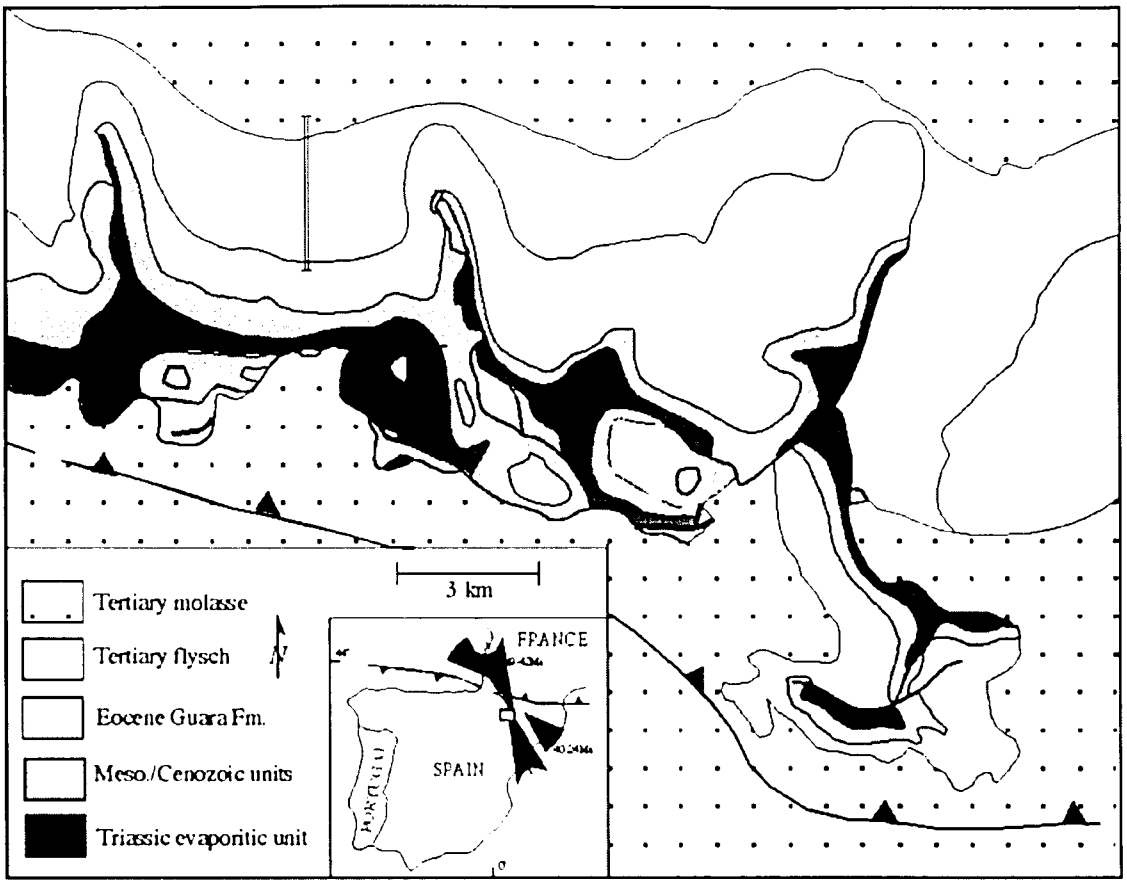

Figure 2.1. Location map of a portion of the External Sierra and the southern margin of the Jaca Basin. The measured section is located in the Arguis syncline, adjacent to the Pico del Aguila anticline to the east (after Anastasio and Holl, 2001).

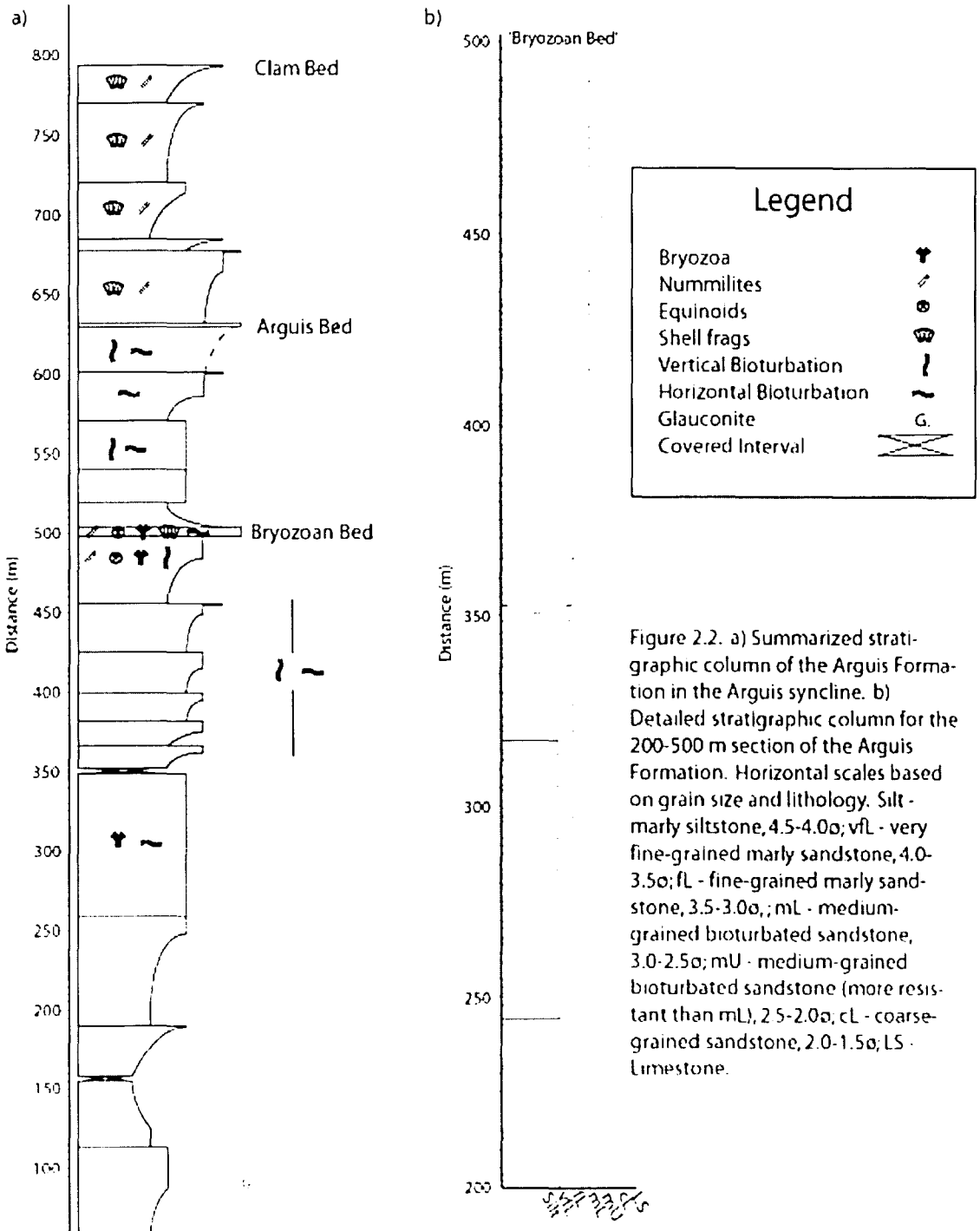

Figure 2.2. a) Summarized stratigraphic column of the Arguis Formation in the Arguis syncline. b) Detailed stratigraphic column for the 200-500 m section of the Arguis Formation. Horizontal scales based on grain size and lithology. Silt - marly siltstone, 4.5-4.0ø; vfL - very fine-grained marly sandstone, 4.0-3.5ø; fL - fine-grained marly sandstone, 3.5-3.0ø,; mL - medium-grained bioturbated sandstone, 3.0-2.5ø; mU - medium-grained bioturbated sandstone (more resistant than mL), 2.5-2.0ø; cL - coarse-grained sandstone, 2.0-1.5ø; LS - Limestone.

Lithology	Kmin	Kmax	tanIo/tanIc	% Volume Loss
Silt	0.3202	0.3413	1.301	43.13
vfl	0.3238	0.3388	1.203	32.95
fl	0.3261	0.3393	1.173	29.26
mL&mU	0.3283	0.3369	1.110	20.34
cL	0.3293	0.3383	1.113	20.88

Table 4.1. Table outlining important values for each lithology in calculating the compaction correction. Lithology - see figure 2.2; Kmax - normalized maximum anisotropy axis eigenvalue; Kmin - normalized minimum anisotropy axis eigenvalue; tanIo/tanIc - see text for calculation; % Volume loss - volume loss calculated by the curve fit in figure 4.1c.

Chron	Distance (m)	Cande & Kent, 1995 (Ma)	Palike et al., 2001 (Ma)	Gradstein & Ogg, 2004 (Ma)
C18n.2n	39.6	40.13	39.828	39.464
C18n.1r	75.4	39.631	39.486	39.041
C18n.1n	86.075	39.552	39.441	38.975
C17r	321.15	38.426	38.186	38.032
C17n.3n	370.25	38.113	37.897	37.771
C17n.2r	468.55	37.92	37.692	37.61
C17n.2n	487.65	37.848	37.618	37.549
C17n.1r	515.65	37.604	37.399	37.345
C17n.1n	563.7	37.473	37.3	37.235

Table 4.2. Reported ages for magnetostratigraphy throughout the Arguis section provided by three recent chron boundary age determinations (Cande and Kent, 1995; Palike et al., 2001; Gradstein and Ogg, 2004). Ages and distance are reported for the base of each chron listed. Distance is reported as the midpoint between a normal and reversed sample, sample spacing is generally a few meters.

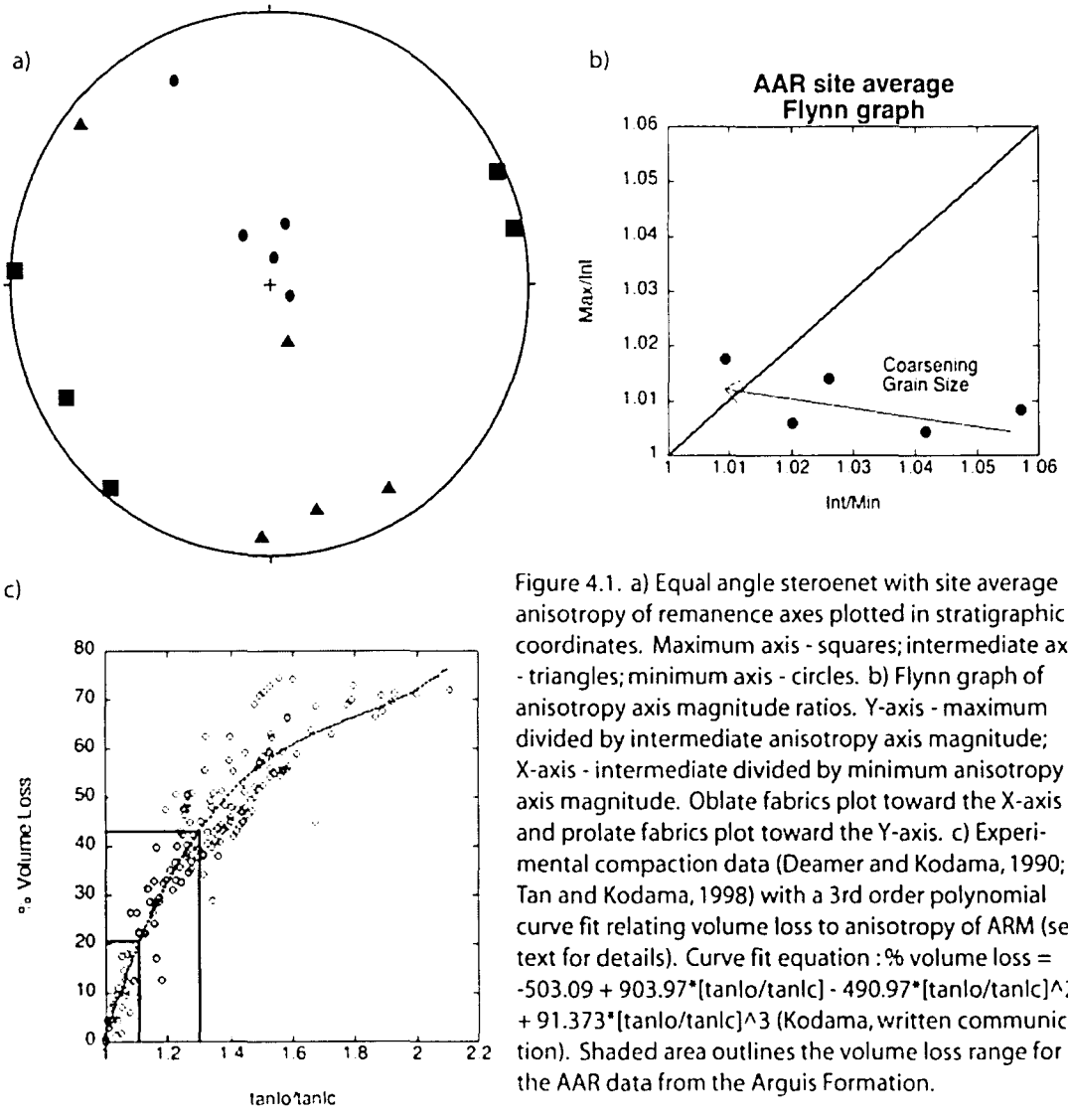

Figure 4.1. a) Equal angle steroenet with site average anisotropy of remanence axes plotted in stratigraphic coordinates. Maximum axis - squares; intermediate axis - triangles; minimum axis - circles. b) Flynn graph of anisotropy axis magnitude ratios. Y-axis - maximum divided by intermediate anisotropy axis magnitude; X-axis - intermediate divided by minimum anisotropy axis magnitude. Oblate fabrics plot toward the X-axis and prolate fabrics plot toward the Y-axis. c) Experimental compaction data (Deamer and Kodama, 1990; Tan and Kodama, 1998) with a 3rd order polynomial curve fit relating volume loss to anisotropy of ARM (see text for details). Curve fit equation : % volume loss = -503.09 + 903.97*[tanlo/tanlc] - 490.97*[tanlo/tanlc]^2 + 91.373*[tanlo/tanlc]^3 (Kodama, written communication). Shaded area outlines the volume loss range for the AAR data from the Arguis Formation.

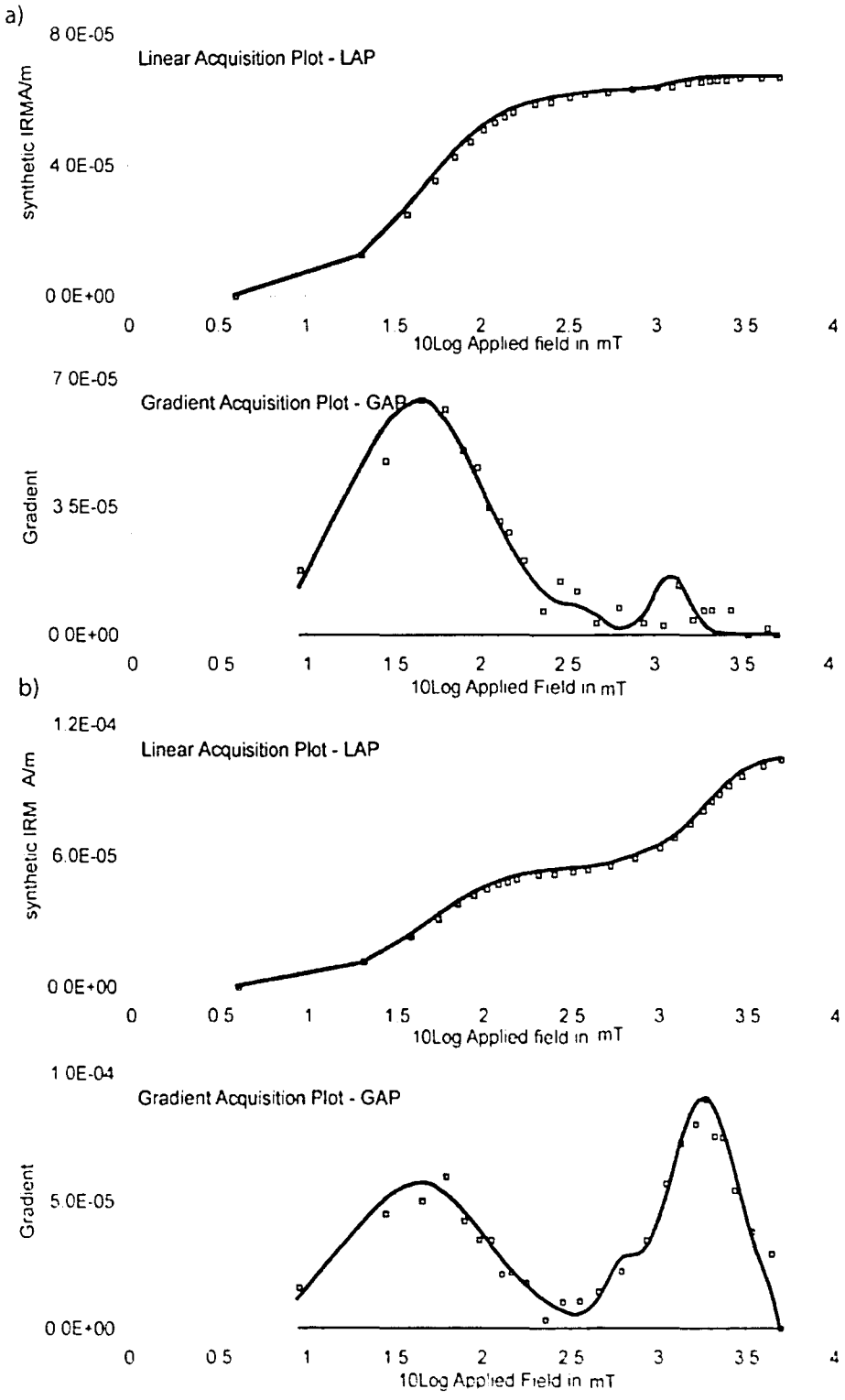

Figure 4.2. Two IRM acquisition models (Kruiver et al., 2001) for samples a) fl9 (a fine grained marly sandstone), characteristic of IRM acquisition models and b) bio3 (a bioturbated medium grained sandstone), uncharacteristic but shows the potential for large quantities of high-coercivity minerals.. LAP- Linear IRM acquisition plot. GAP- The derivative of the LAP. Shaded area represents coercivities activated by ARM.

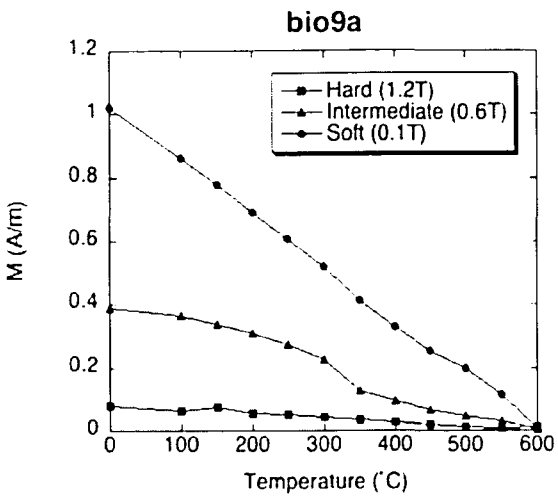

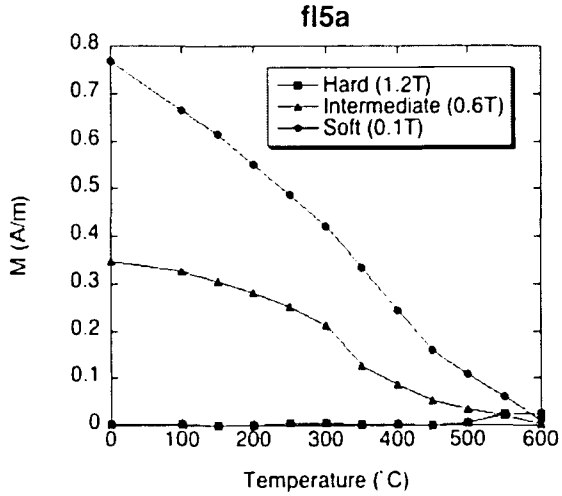

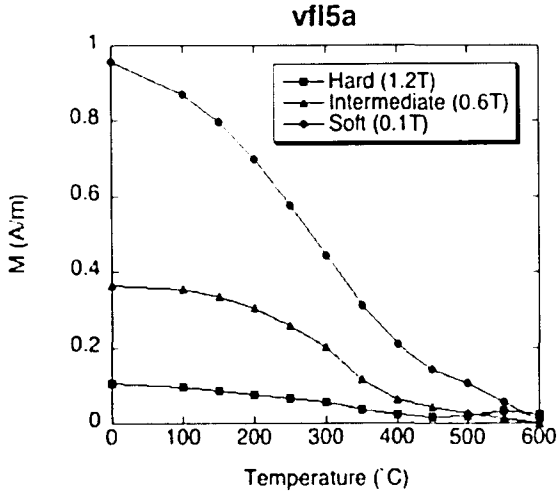

Figure 4.3. Characteristic 3-component IRM thermal demagnetization plots following the method of Lowrie (1990). a) bio9a - medium-grained bioturbated marly sandstone; b) fl5a - fine-grained marly sandstone; c) vfl5a - very fine-grained marly sandstone..

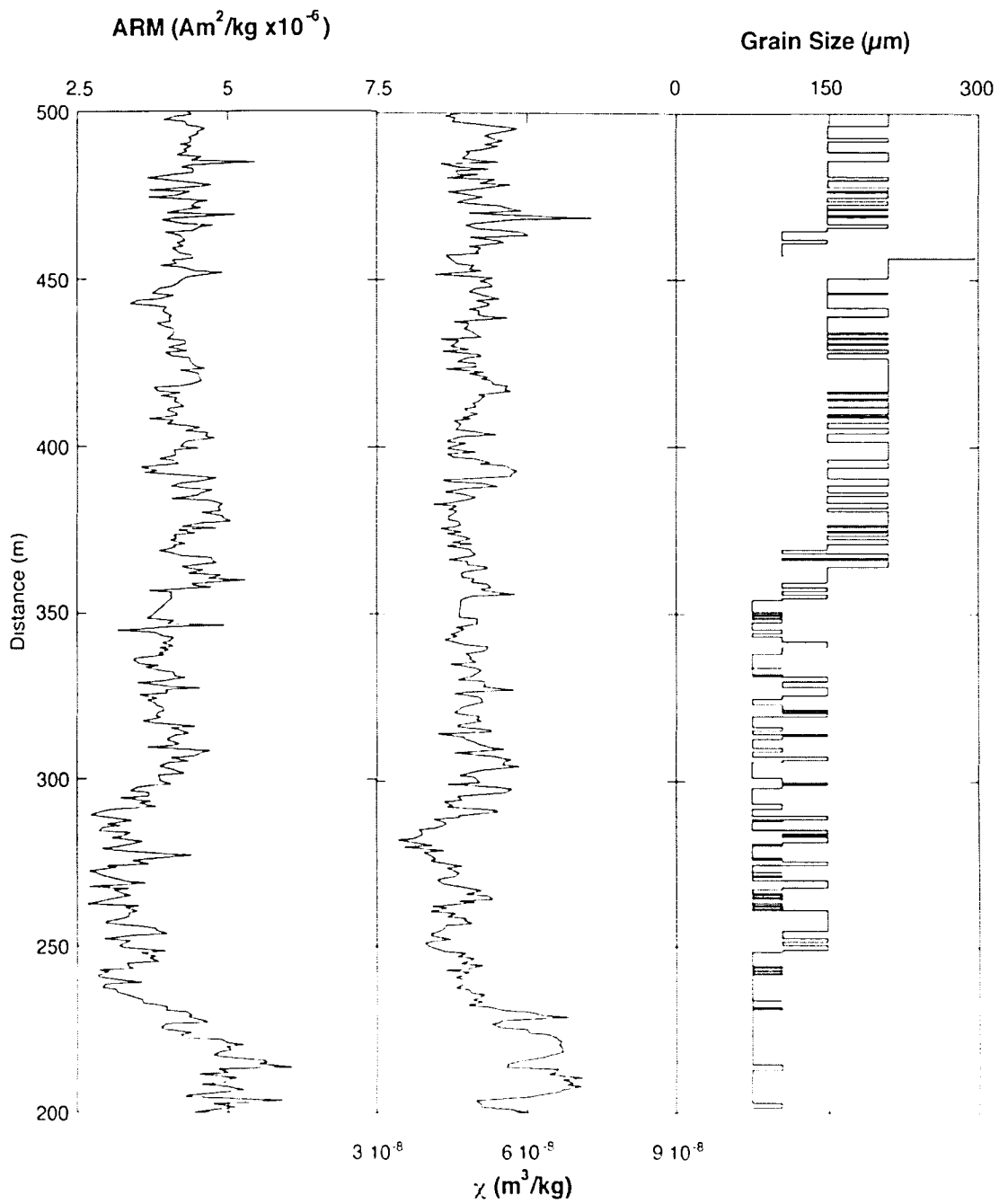

Figure 4.4. Raw ARM, χ, and Grain Size data from 200-500 m from the base of the Arguis section.

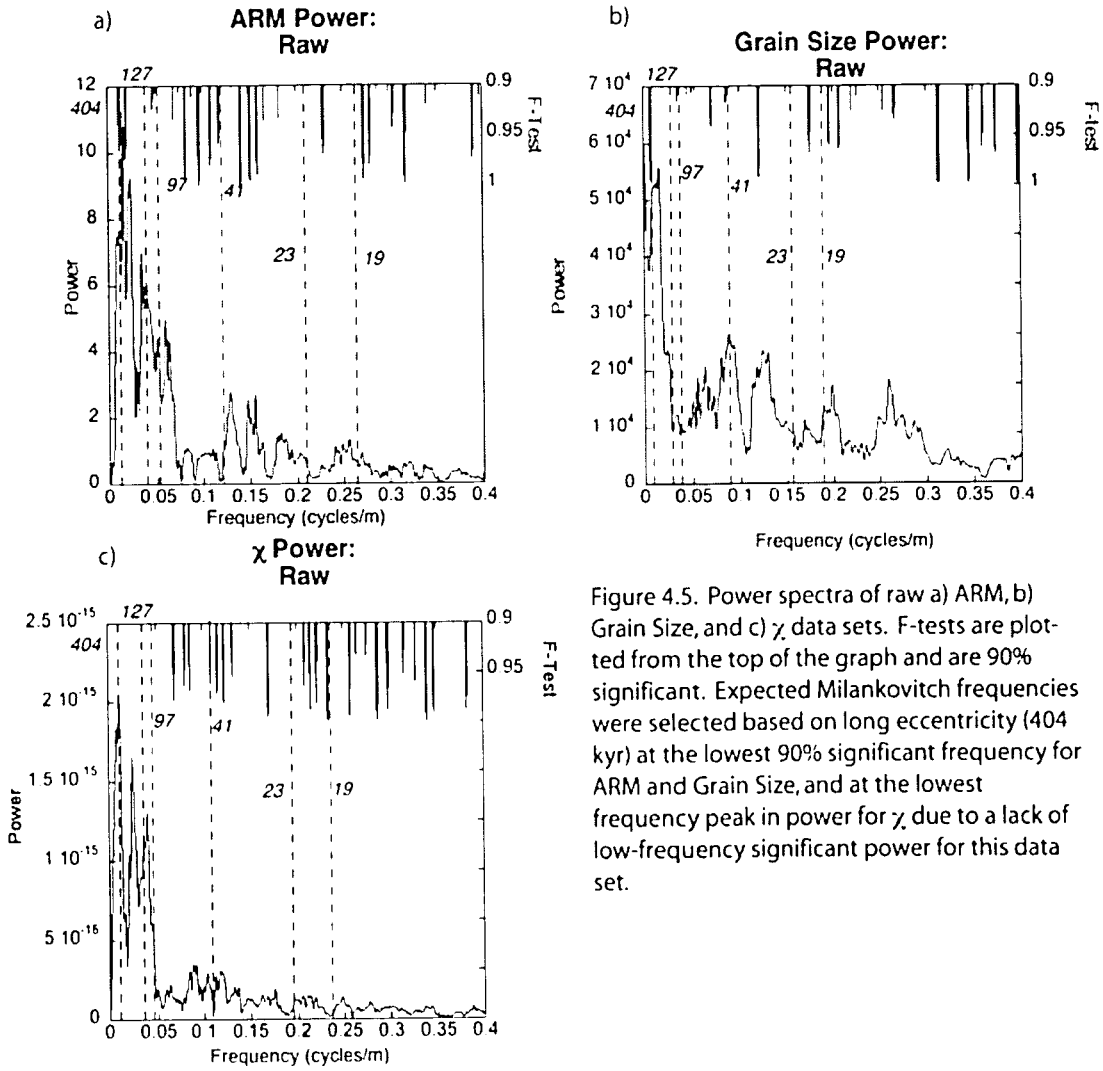

Figure 4.5. Power spectra of raw a) ARM, b) Grain Size, and c) χ data sets. F-tests are plotted from the top of the graph and are 90% significant. Expected Milankovitch frequencies were selected based on long eccentricity (404 kyr) at the lowest 90% significant frequency for ARM and Grain Size, and at the lowest frequency peak in power for χ due to a lack of low-frequency significant power for this data set.

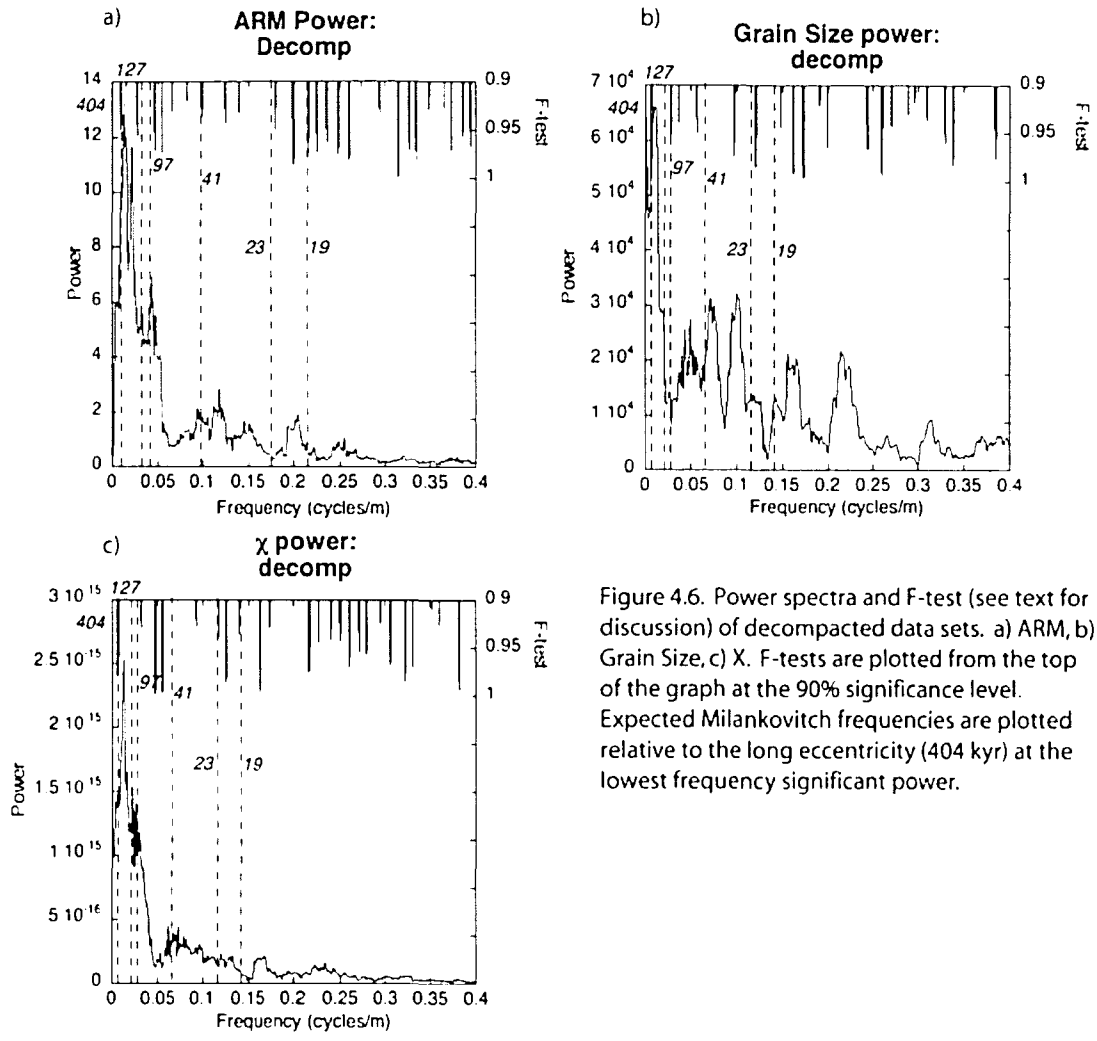

Figure 4.6. Power spectra and F-test (see text for discussion) of decompacted data sets. a) ARM, b) Grain Size, c) X. F-tests are plotted from the top of the graph at the 90% significance level. Expected Milankovitch frequencies are plotted relative to the long eccentricity (404 kyr) at the lowest frequency significant power.

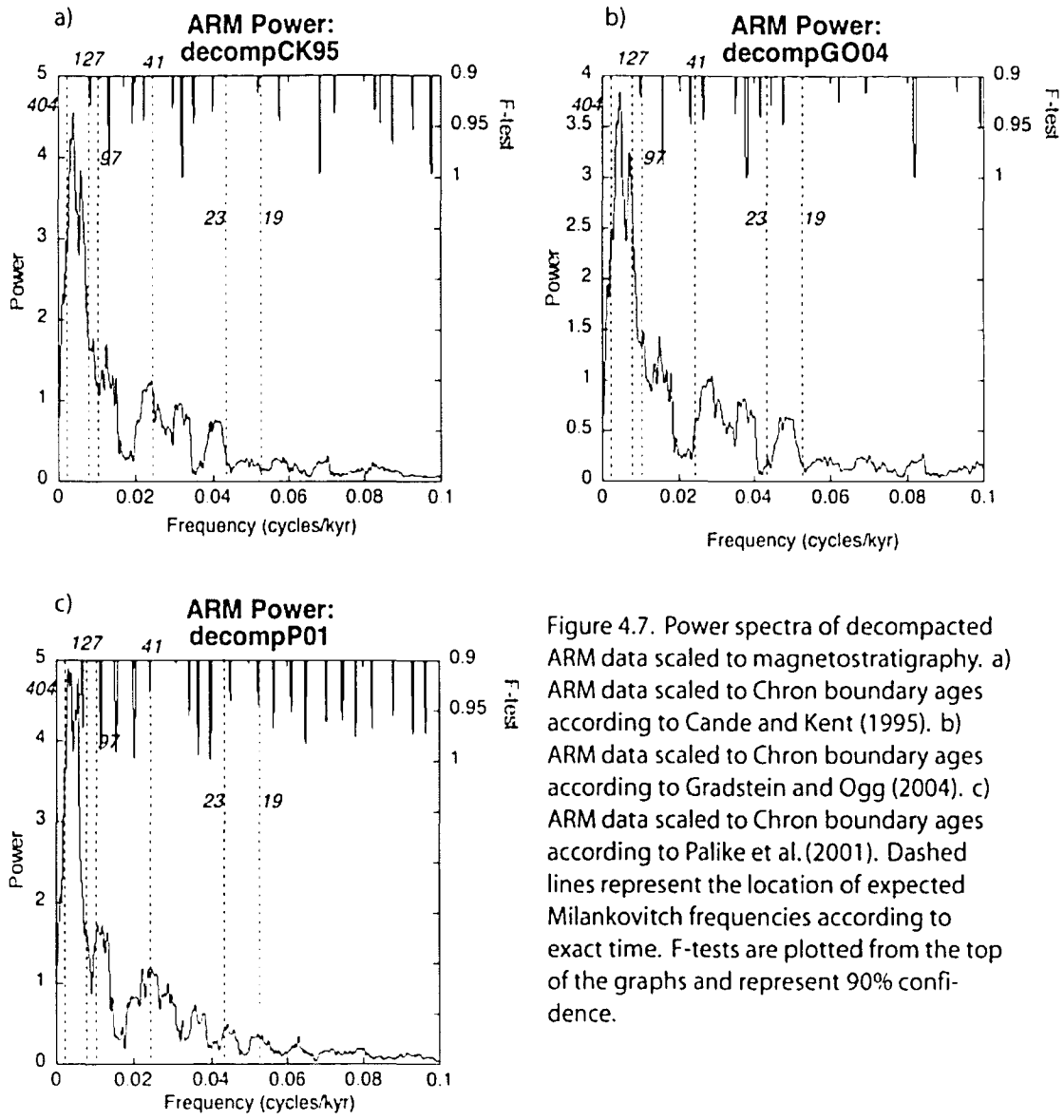

Figure 4.7. Power spectra of decompacted ARM data scaled to magnetostratigraphy. a) ARM data scaled to Chron boundary ages according to Cande and Kent (1995). b) ARM data scaled to Chron boundary ages according to Gradstein and Ogg (2004). c) ARM data scaled to Chron boundary ages according to Palike et al.(2001). Dashed lines represent the location of expected Milankovitch frequencies according to exact time. F-tests are plotted from the top of the graphs and represent 90% confidence.

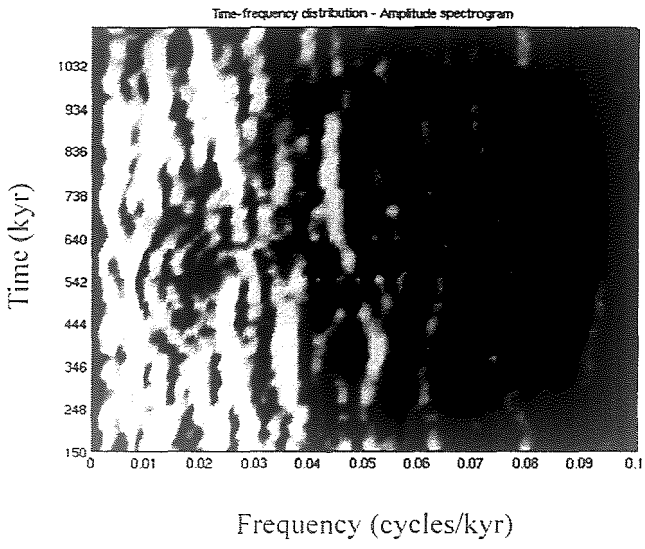

Figure 4.8. Evolutionary power spectrum of the decompacted ARM data set scaled to magneto-stratigraphy of Palike et al. (2001). Lighter colors represent higher power. Time is reported in thousands of years from the beginning of the section (38821 kybp).

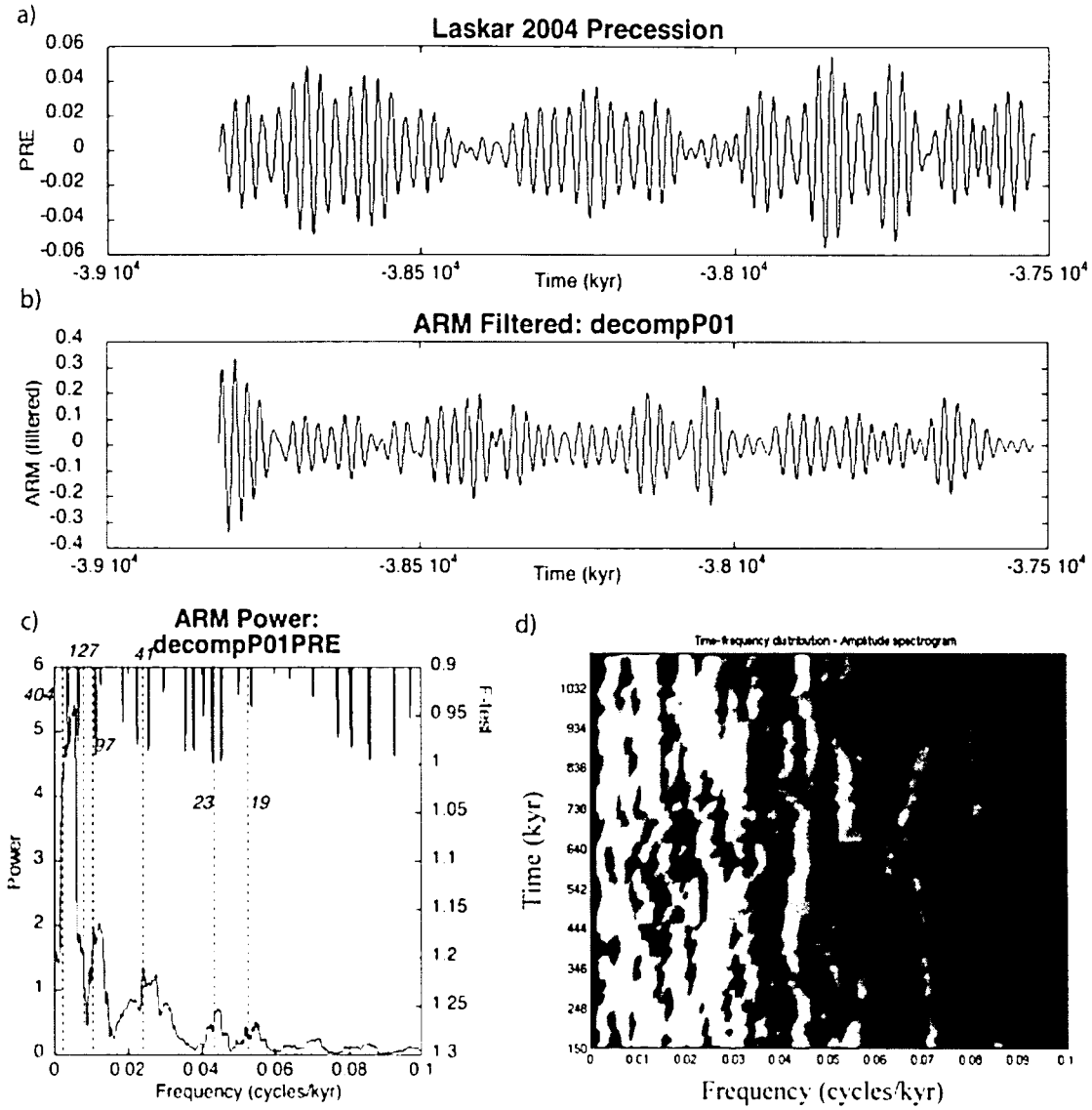

Figure 4.9. a) modeled precession. b) Bandpass filter of decompacted ARM data scaled to the magnetostratigraphy of Palike et al. (2001). c) Power spectrum of decompacted ARM data scaled to magnetostratigraphy and tuned to modeled precession by correlating each precessional peak and trough. Dashed lines represent expected Milankovitch frequencies. d) Evolutionary power spectrum of the decompacted ARM data set scaled to magnetostratigraphy of Palike et al. (2001) and tuned to Precession. Lighter colors represent higher power. Time is reported in thousands of years from the beginning of the section (38821 kybp).

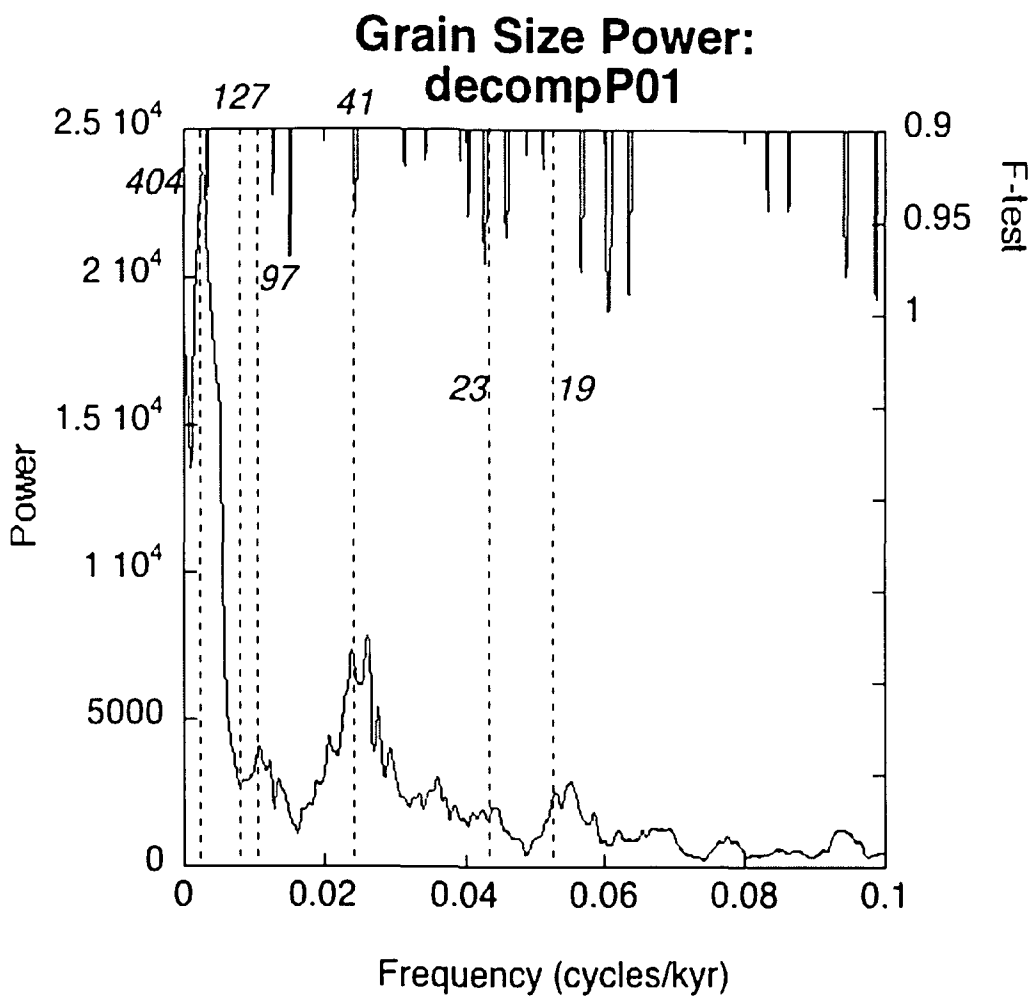

Figure 4.10. Power spectrum of the decompacted Grain Size data set scaled to magnetostratigraphy ages suggested by Palike et al. (2001). Dashed lines represent represent expected Milankovitch frequencies. F-tests plotted from the top of the graph are significant to the 90% confidnece limit.

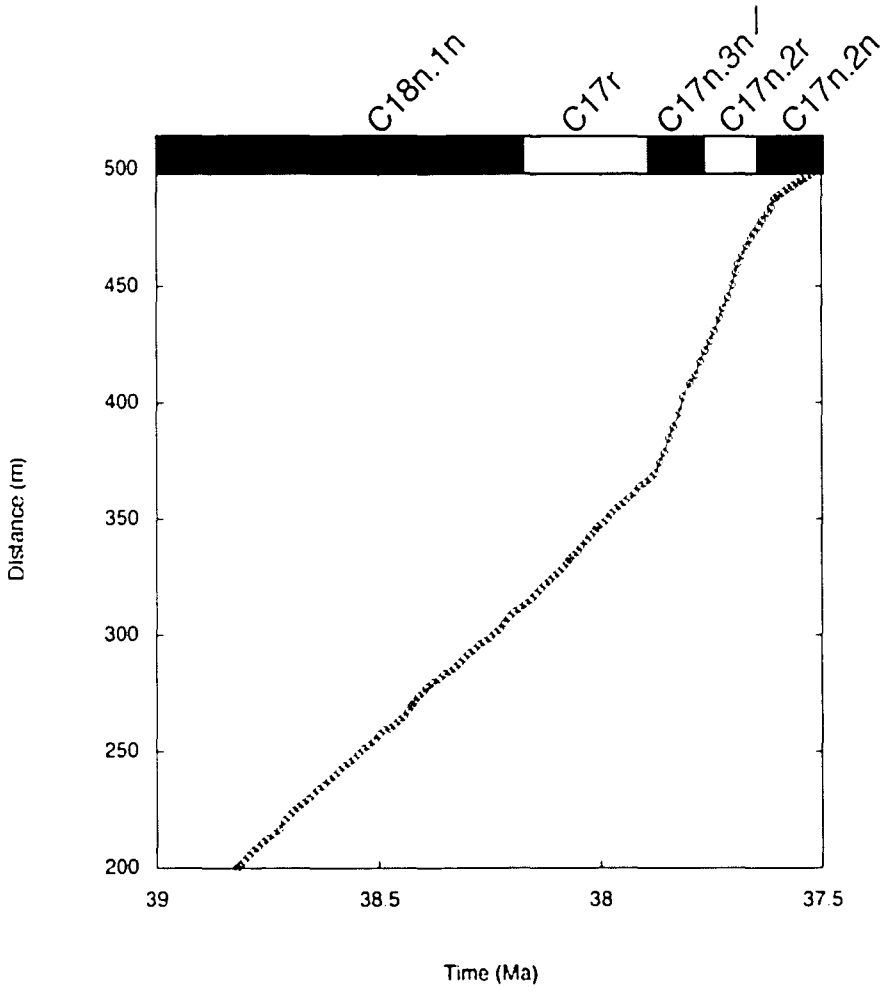

Figure 5.1. Agemap for the section from 200 to 500 m from the base of the Arguis Formation. Each point represents a correlated peak or trough from the bandpassed ARM data to modeled precession (Laskar, 2004). Chron boundary ages of Palike et al. (2001).

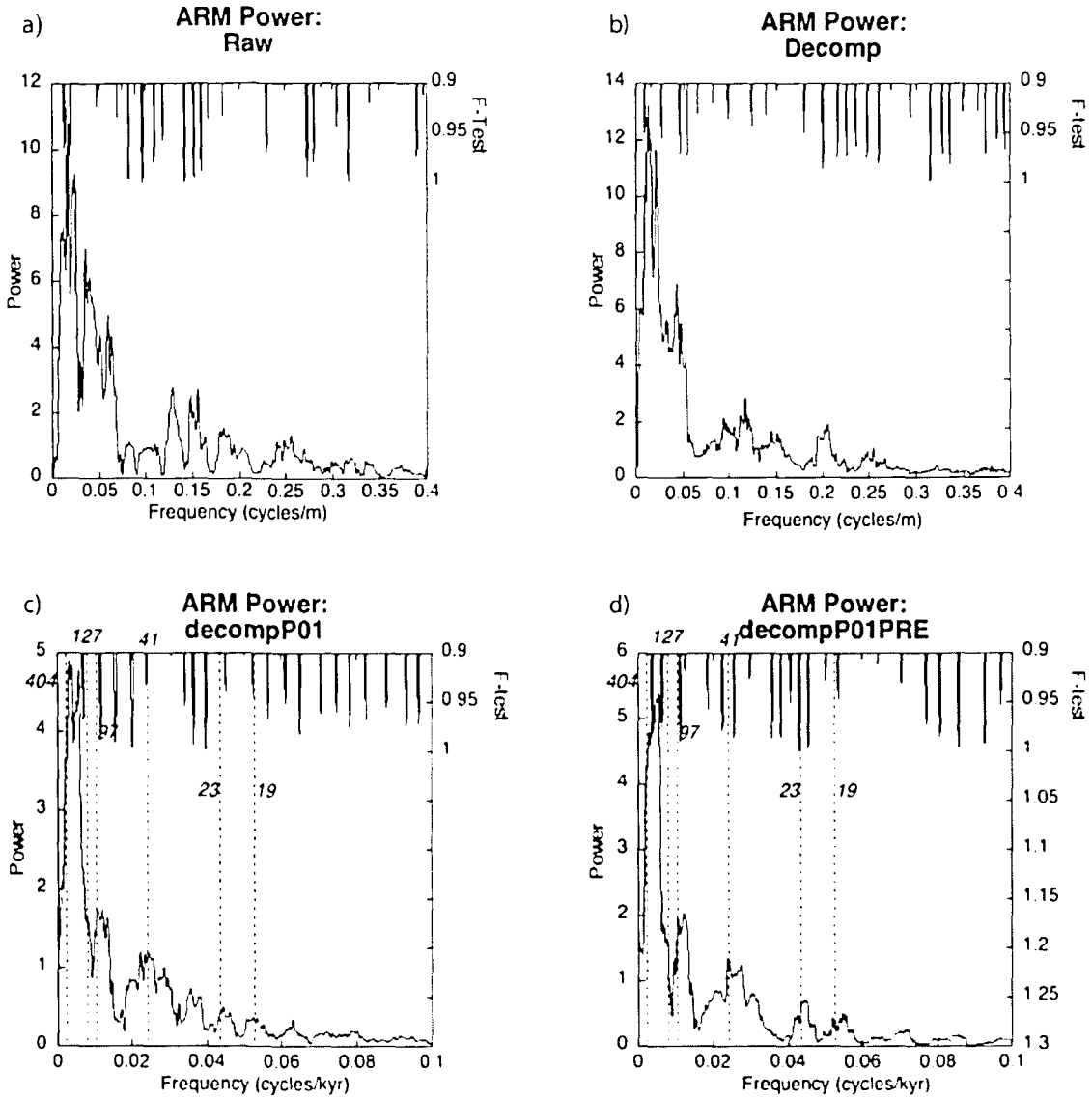

Figure 5.2. Power spectra of the ARM data set illustrating progressive improvement in spectral power at expected Milankovitch frequencies due to the application of scaling and tuning techniques. a) Raw ARM 3π power spectrum. b) De-compacted ARM 3π power spectrum. c) De-compacted ARM scaled to magnetostratigraphy ages of Palike et al. (2001) 3π power spectrum. d) De-compacted ARM scaled to magnetostratigraphy ages of Palike et al. (2001) and tuned to modeled precession (Laskar, 2004) 3π power spectrum.

a)

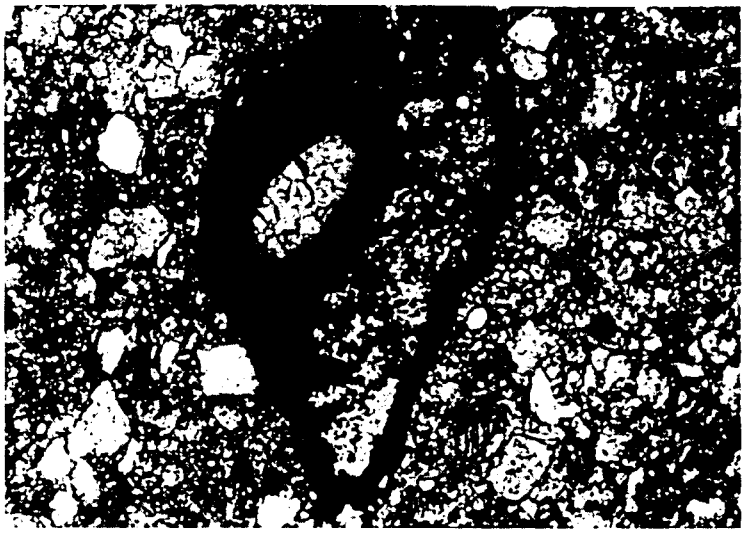

b)

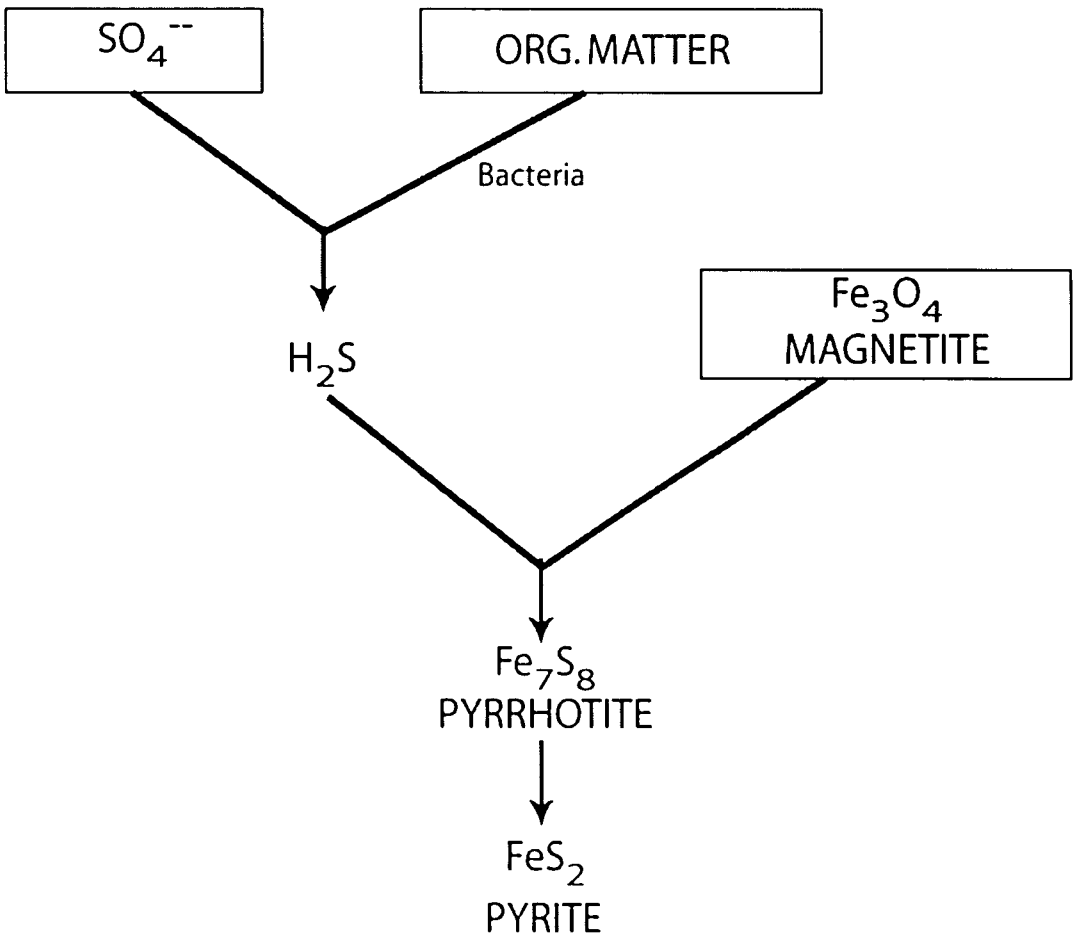

Figure 5.3. a) thin section image of framboidal opaque minerals formed within fossils, a source of organic matter. b) Diagram representing the general steps in the process of pyritization (after Berner, 1972). Boxes surround the three major inputs to the pyritization system.

References

Anastasio, D. J. (1992), Structural Evolution of the External Sierra, Spanish Pyrenees, in *The Structural Geology of Fold and Thrust Belts*, edited by S. Mitra, and G. W. Fisher, pp. 239-251, Johns Hopkins University Press, Baltimore.

Anastasio, D.J., and J.E. Holl (2001), Transverse fold evolution in the External Sierra, southern Pyrenees, Spain, *Journal of Structural Geology, 23*, 379-392.

Berger, A., M-F. Loutre, and C. Tricot (1993), Insolation and Earth's orbital periods, *J. Geophys. Res., 98*(D6), 10341-10362.

Berner, R. A. (1972), Sulfate reduction, pyrite formation, and the oceanic sulfur budget, in *The Changing Chemistry of the Oceans: Nobel Symposium 20*, edited by D. Dyrssen and D. Jagner, Almqvist and Wiksell, 347-361.

Berner, R. A. (1984), Sedimentary pyrite formation: an update, *Geochim. Cosmochim. Acta, 48*, 605-615.

Bloemendal, J., B. Lamb, and J. King (1988), Paleoenvironmental implications of rock-magnetic properties of late Quaternary sediment cores from the eastern Equatorial Atlantic, *Paleoceanography, 3*, 61-87.

Cande, S. C., and D. V. Kent (1995), Revised calibration of the geomagnetic polarity timescale for the Late Cretaceous and Cenozoic, Journal of Geophysical Research Solid Earth, 100, 6093-6095.

Canfield, D. E., and R. A. Berner (1987), Dissolution and pyritization of magnetite in anoxic marine sediments, *Geochim. Cosmochim. Acta, 51*, 645-659.

Canudo, J. I. (1990), Los foraminiferos planctonicos del Paleoceno-Eocene del Prepirineo oscense en el sector de Arguis, 435 pp., Thesis Doctoral, Univ. de Zaragoza, Spain.

Canudo, J. I., J. Malagon, A. Melendez, H. Millan, E. Molina, and J. J. Navarro (1991), Las secuencias deposicionales del Eoceno medio y superior de las Sierras exteriors (Prepirineo meridional aragones), *Geogaceta, 9*, 81-84.

Castelltort, S., F. Guillocheau, C. Robin, D. Rouby, T. Nalpas, F. Lafont, and R. Eschard (2003), Fold control on the stratigraphic record: a quantified sequence stratigraphic study of the Pico del Aguila anticline in the south-western Pyrenees (Spain), *Basin Research, 15*, 527-551.

Curtis, J. H., D. A. Hodell, and M. Brenner (1996), Climate Variability on the Yucatan Peninsula (Mexico) during the Past 3500 Years, and Implications for Maya Cultural Evolution, *Quaternary Research, 46*, 37-47.

Dansgaard, W., S. J. Johnsen, H. B. Clausen, D. Dahl-Jensen, N. S. Gundestrup, C. U. Hammer, C. S. Hvidberg, J. P. Steffensen, A. E. Sveinbjornsdottir, J. Jouzel, and G. Bond (1993), Evidence for geoneral instability of past climate from a 250-kyr ice-core record, *Nature, 364*, 218-220.

Deamer, G. A., and K. P. Kodama (1990), Compaction-induced inclination shallowing in synthetic natural clay-rich sediments, *Journal of Geophysical Research, 95*, 4511-4529.

DePaor, D.G., and D.J. Anastasio (1987), The External Sierra; A Case History in the Advance and Retreat of Mountains, *National Geographic Research, 3*, 199-209.

Dunlop, D., and O. Ozdemir (1997), *Rock Magnetism: Fundamentals and Frontiers*, 573 pp., Cambridge University Press.

Fischer, A. G. (1991), Orbital cyclicity in Mesozoic strata, in *Cycles and Events in Stratigraphy*, edited by G. Einsele et al., pp. 48-62, Berlin: Springer-Verlag

Gradstein, F. M., J. G. Ogg, A. G. Smith, F. P. Agterberg, W. Bleeker, R. A. Cooper, V.

Davydov, P. Gibbard, L. Hinnov, M. R. House, L. Lourens, H. P. Luterbacher, J. McArthur, M. J. Melchin, L. J. Robb, J. Shergold, M. Villeneuve, B. R. Wardlaw, J. Ali, H. Brinkhuis, F. J. Hilgen, J. Hooker, R. J. Howarth, A. H. Knoll, J. Laskar, S. Monechi, J. Powell, K. A. Plumb, I. Raffi, U. Röhl, A. Sanfilippo, B. Schmitz, N. J. Shackleton, G. A. Shields, H. Strauss, J. Van Dam, J. Veizer, Th. van Kolfschoten, and D. Wilson (2004), *A Geologic Time Scale 2004*, ~ 500 pp., Cambridge University Press.

Grimm, E. C., G. L. Jacobson Jr., W. A. Watts, B. C. S. Hansen, and K. A. Maasch (1993), A 50,000-Year Record of Climate Oscilations from Florita and Its Temporal Correlation with the Heinrich Events, *Science, 261*, 198-200.

Hays, J. D., J. Imbrie, and N. J. Shackleton (1976), Variations in Earth's orbit: pacemaker of the ice ages, *Science, 194*, 1121-1132.

Hodell, D. A., M. Brenner, J. H. Curtis, and T. Guilderson (2001), Solar Forcing of Drought Frequency in the Maya Lowlands, *Science, 292*, 1367-1370.

Hogan, P. J. (1993), Geochronologic, tectonic, and stratigraphic evolution of the southwest Pyrenean foreland basin, northern Spain, 220 pp., PhD. dissertation , University of Southern California.

Hogan, P. J., and D. W. Burbank (1996), Evolution of the Jaca piggyback basin and emergence of the external Sierra, southern Pyrenees, in *Tertiary Basins of Spain the stratigraphic record of crustal kinematics*, edited by P.F. Friend and C.J. Dabrio, pp. 153-160, Cambridge University Press, New York.

Jackson, M. J., S. K. Banerjee, J. A. Marvin, R. Lu, and W.Gruber (1991), Detrital remanence, inclination errors, and anhysteretic remanence anisotropy: Quantitative model and experimental results, *Geophysical Journal International, 104*, 95-103.

Kodama, K. P., and J. M. Davi (1995), A compaction correction for the paleomagnetism of the Cretaceous Pigeon Point Formation of California, *Tectonics, 14*, 1153-1164.

Kruiver, P. P., M. J. Dekkers, and D. Heslop (2001), Quantification of magnetic coercivity by the analysis of acquisition curves of isothermal remanent magnetization, *Earth and Planetary Science Letters, 189*, 269-276.

Larrasoana, J. C., J. M. Pares, and E. L. Pueyo (2003), Stable Eocene magnetization carried by magnetite and iron sulphides in marine marls (Pamolona-Arguis Formation, southern Pyrenees, northern Spain), *Stud. Geophys. Geod., 47*, 237-254.

Laskar, J., P. Robutel, F. Joutel, M. Gastineau, A. C. M. Correia, B. Levrard (2004), A long term numerical solution for the insolation quantities of the Earth, *Astronomy and Astrophysics, 428*, 261-285, doi:10.1051/0004-6361:20041335.

Latta, D.K., D.J. Anastasio, L.A. Hinnov, M. Elrick, and K.P. Kodama (2006), Magnetic record of Milankovitch rhythms in lithologically non-cyclic marine carbonates, *Geology, 34*(1), 29-32.

Leslie, B.W., S.P. Lund, and D.E. Hammond (1990), Rock Magnetic Evidence for the Dissolution and Authigenic Growth of Magnetic Minerals Within Anoxic Marine Sediments of the California Continental Borderland, *Journal of Geophysical Research, 95*(B4), 4437-4452.

Lowrie, W. (1990), Identification of ferromagnetic minerals in a rock by coercivity and unblocking temperature properties, *Geophysical Research Letters, 17* (2), 159-162.

Mayer, H., and E. Appel (1999), Milankovitch cyclicity and rock-magnetic signatures of paleoclimatic change in the Early Cretaceous Biancone Formation of the Southern Alps, Italy, *Cretaceous Research, 20*, 189-214.

McCabe, C., M. Jackson, and B. B. Ellwood (1985), Magnetic anisotropy in the Trenton limestone: Results of a new technique, anisotropy of anhysteretic susceptibility, *Geophysical Research Letters, 12*, 333-336.

Millan, H., M. Aurell, and A. Melendez (1994), Synchronous detachment folds and coeval sedimentation in the Pre-pyrenean External Sierras (Spain); a case study for a tectonic origin of sequences and system tracts, *Sedimentology, 41*, 1001-1024.

Paillard, D., L. Labeyrie, and P. Yiou (1996), Macintosh program performs time-series analysis, *Eos Transactions American Geophysical Union, 77*, 379.

Palike, H., N. J. Shackleton, and U. Rohl (2001), Astronomical forcing in Late Eocene marine sediments, *EPSL, 193*, 589-602.

Pares, J.M., K.P. Kodama, D.J. Anastasio, and M.L. Newton (2006), Magnetic reversal stratigraphy of Eocene growth strata, South Pyrenean fold-and-thrust belt, *Eos Trans. AGU, 87*(36), Jt. Assem. Suppl., Abstract GP41B-03.

Peters, C., and M. J. Dekkers (2003), Selected room temperature magnetic parameters as a function of mineralogy, concentration and grain size, *Physics and Chemistry of the Earth, 28*, 659-667.

Poblet, J., and S. Hardy (1995), Reverse modeling of detachment folds; application to the Pico del Aguila anticline in the South Central Pyrenees (Spain), *Journal of Structural Geology, 17* (12), 1707-1724.

Preto, N., L. A. Hinnov, L. A. Hardie, and V. De Zanche (2001), Middle Triassic orbital signature recorded in the shallow-marine Latemar carbonate buildup (Dolomites, Italy), *Geology, 29*, 1123-1126.

Pueyo, E. L., H. Millån, and A. Pocovî (2002), Rotation velocity of a thrust; a paleomagnetic study in the External Sierras (Southern Pyrenees): *Sedimentary Geology, 146*, 191-208.

Puigdefabregas, C. T. (1975), La sedimentation Molasica en la cuenca de Jaca, *Monografias del instituto de estudion Pirenaicos*, 104.

Roberts, A. P., and G. M. Turner (1993), Diagenetic formation of ferromagnetic iron sulphide minerals in rapidly deposited marine sediments, South Island, New Zealand, *Earth and Planetary Science Letters, 115*, 257-273.

Rodbell, D. T., G. O. Seltzer, D. M. Anderson, M. B. Abbott, D. B. Enfield, and J. H. Newman (1999), An ~15,000-Year Record of El Nino-Driven Alluviation in Southwestern Ecuador, *Science, 283*, 516-520.

Sclatar, J. G., and P. A. F. Christie (1980), Continental stretching: an explanation of the mid-Cretaceous subsidence of the Central North Sea Basin, *Journal of Geophysical Research, 85*, 3711-3739.

Shackleton, N. J., S. J. Crowhurst, G. P. Weedon, and J. Laskar (1999), Astronomical calibration of Oligocene-Miocene time, *Phil. Trans. R. Soc. Lond., 357*, 1907-1929.

Sloan, L. C., and M. Huber (2001), Eocene Oceanic Responses to Orbital Forcing on Precessional Time Scales, *Paleoceanography, 16*(01), 101-111.

Tan, X., and K. P. Kodama, Compaction-corrected inclinations from southern California Cretaceous marine sedimentary rocks indicate no paleolatitudinal offset for the Peninsular Ranges terrane, *Journal of Geophysical Research, 103* (B11), 27169-27192.

Tauxe, L. (1998), Paleomagnetic principles and Practice, Kluwer Academic Publishers.

Tiedemann, R., M. Sarnthein, and N. J. Shackleton (1994), Astronomic timescale for the Pliocene Atlantic δ18O and dust flux records of Ocean Drilling Program site 659, *Paleoceanography, 9*(4), 619-638.

Westrich, J. T., and R. A. Berner (1984), The role of sedimentary organic matter in bacterial sulfate reduction: the G model tested, *Limnol. Oceanogr., 29*, 236-249.

Wu, G., B. Pan, Q. Guan, and D. Xia (2005), Terminations and their correlation with solar insolation in the Northern Hemisphere: a record from a loess section in Northwest China, *Paleogeography, Paleoclimatology, Paleoecology, 216*, 267-277.

Appendix 1: Data Table

Label	#	Strat. Pos.	MS (m^3/kg)	ARM (Am^2/kg)	ARM/X (A/m)	Gr. Rank	SIRM (Am^2/kg)	SIRM/X (kA/m)
A2a	0	2.8	4.77E-08	2.37E-06	49.56	4		
A2a	0.2	3	4.80E-08	2.29E-06	47.78	4		
A2a	0.4	3.2	4.85E-08	2.20E-06	45.26	5		
A2a	0.6	3.4	4.76E-08	2.25E-06	47.29	4		
A2a	0.8	3.6	4.57E-08	2.13E-06	46.56	4		
A2a	1	3.8	4.76E-08	2.15E-06	45.18	4		
A2a	1.2	4	4.77E-08	2.32E-06	48.72	4		
A2a	1.4	4.2	4.79E-08	2.45E-06	51.19	5		
A2a	1.6	4.4	4.00E-08	2.02E-06	50.40	4		
A2a	1.8	4.6	4.53E-08	1.93E-06	42.62	4		
A2a	2	4.8	4.35E-08	2.38E-06	54.82	4		
A2a	2.2	5	4.38E-08	2.42E-06	55.23	4		
A2a	2.4	5.2	4.25E-08	2.36E-06	55.47	5		
A2a	2.6	5.4	4.72E-08	2.50E-06	53.03	4		
A2a	2.8	5.6	4.30E-08	2.44E-06	56.76	5		
A2a	3	5.8	4.41E-08	2.52E-06	57.19	4		
A2a	3.2	6	4.21E-08	2.01E-06	47.67	5		
A2a	3.4	6.2	4.41E-08	2.43E-06	55.06	4		
A2a	3.6	6.4	4.44E-08	2.61E-06	58.65	4		
A2a	3.8	6.6	4.71E-08	2.49E-06	52.78	4		
A2a	4	6.8	4.06E-08	2.35E-06	57.94	4		
A2a	4.2	7	4.86E-08	2.57E-06	52.80	5		
A2a	4.4	7.2	4.31E-08	2.66E-06	61.84	5		
A2a	4.6	7.4	4.60E-08	2.69E-06	58.56	4		
A2a	4.8	7.6	4.38E-08	2.82E-06	64.36	4		

A2a	5	7.8	4.60E-08	3.41E-06	74.23	4
A2a	5.2	8	4.49E-08	2.70E-06	60.18	5
A2a	5.4	8.2	4.39E-08	2.95E-06	67.23	4
A2a	5.6	8.4	4.34E-08	3.11E-06	71.64	4
A2a	5.8	8.6	4.48E-08	2.84E-06	63.51	5
A2a	6	8.8	4.40E-08	2.94E-06	66.83	5
A2a	6.2	9	4.56E-08	2.95E-06	64.77	4
A2a	6.4	9.2	4.57E-08	3.02E-06	66.02	4
A2a	6.6	9.4	4.41E-08	2.93E-06	66.37	5
A2a	6.8	9.6	4.31E-08	2.71E-06	62.89	5
A2a	7	9.8	4.15E-08	2.81E-06	67.72	4
A2a	7.2	10	4.46E-08	2.67E-06	59.91	4
A2a	7.4	10.2	4.23E-08	2.63E-06	62.14	4
A2a	7.6	10.4	4.33E-08	2.59E-06	59.84	5
A2a	7.8	10.6	4.42E-08	2.55E-06	57.71	4
A2a	8	10.8	4.63E-08	2.61E-06	56.33	5
A2a	8.2	11	4.64E-08	2.65E-06	57.13	4
A2a	8.4	11.2	4.51E-08	2.64E-06	58.63	4
A2a	8.6	11.4	4.71E-08	2.62E-06	55.68	4
A2a	8.8	11.6	4.39E-08	2.66E-06	60.55	4
A2a	9	11.8	4.35E-08	2.54E-06	58.32	4
A2a	9.2	12	4.39E-08	2.58E-06	58.84	4
A2a	9.4	12.2	4.55E-08	2.36E-06	51.81	4
A2a	9.6	12.4	4.73E-08	2.59E-06	54.71	4
A2a	9.8	12.6	4.75E-08	2.41E-06	50.82	4
A2a	10	12.8	4.43E-08	2.60E-06	58.72	4
A2a	10.2	13	4.49E-08	2.55E-06	56.91	4

A2a	10.4	13.2	4.84E-08	2.40E-06	49.61	4
A2a	10.6	13.4	4.24E-08	2.64E-06	62.19	4
A2a	10.8	13.6	4.58E-08	2.52E-06	55.14	4
A2a	11	13.8	4.31E-08	2.36E-06	54.66	4
A2a	11.2	14	4.75E-08	2.31E-06	48.57	4
A2a	11.4	14.2	4.56E-08	2.52E-06	55.22	4
A2a	11.6	14.4	4.59E-08	2.50E-06	54.36	5
A2a	11.8	14.6	4.58E-08	2.46E-06	53.82	5
A2a	12	14.8	4.46E-08	2.45E-06	54.81	4
A2a	12.2	15	4.58E-08	2.39E-06	52.20	5
A2a	12.4	15.2	4.43E-08	2.56E-06	57.77	5
A2a	12.6	15.4	4.54E-08	2.45E-06	53.88	4
A2a	12.8	15.6	4.39E-08	2.39E-06	54.40	4
A2a	13	15.8	4.53E-08	2.45E-06	54.02	5
A2a	13.2	16	4.62E-08	2.32E-06	50.21	5
A2a	13.4	16.2	4.59E-08	2.52E-06	54.84	5
A2a	13.6	16.4	4.50E-08	2.42E-06	53.61	5
A2a	13.8	16.6	4.69E-08	2.42E-06	51.49	5
A2a	14	16.8	4.31E-08	2.40E-06	55.54	5
A2a	14.2	17	4.30E-08	2.42E-06	56.23	5
A2a	14.4	17.2	4.81E-08	2.30E-06	47.90	5
A2a	14.6	17.4	4.79E-08	2.30E-06	47.88	5
A2a	14.8	17.6	4.49E-08	2.40E-06	53.37	5
A2a	15	17.8	4.24E-08	2.47E-06	58.28	5
A2a	15.2	18	4.43E-08	2.50E-06	56.44	4
A2a	15.4	18.2	4.39E-08	2.16E-06	49.21	5
A2a	15.6	18.4	4.09E-08	2.08E-06	50.96	4

A2a	15.8	18.6	4.29E-08	2.22E-06	51.82	4
A2a	16	18.8	3.59E-08	2.17E-06	60.42	5
A2a	16.2	19	3.64E-08	2.14E-06	58.81	5
A2a	16.4	19.2	3.92E-08	2.20E-06	56.01	4
A2a	16.6	19.4	3.69E-08	2.20E-06	59.60	4
A2a	16.8	19.6	4.22E-08	2.09E-06	49.45	4
A2a	17	19.8	4.18E-08	2.21E-06	52.96	5
A2a	17.2	20	4.20E-08	2.21E-06	52.55	5
A2a	17.4	20.2	4.83E-08	2.01E-06	41.55	4
A2a	17.6	20.4	4.48E-08	2.09E-06	46.62	5
A2a	17.8	20.6	4.06E-08	2.16E-06	53.31	4
A2a	18	20.8	4.76E-08	2.16E-06	45.34	4
A2a	18.2	21	4.51E-08	1.97E-06	43.72	5
A2a	18.4	21.2	4.67E-08	2.05E-06	43.85	5
A2a	18.6	21.4	4.37E-08	2.03E-06	46.40	4
A2a	18.8	21.6	4.12E-08	1.63E-06	39.53	4
A2a	19	21.8	4.08E-08	1.60E-06	39.21	4
A2a	19.2	22	4.12E-08	1.82E-06	44.33	4
A2a	19.4	22.2	4.12E-08	1.96E-06	47.58	4
A2a	19.6	22.4	4.37E-08	2.18E-06	49.86	4
A2a	19.8	22.6	4.18E-08	2.03E-06	48.51	4
A2a	20	22.8	4.19E-08	2.21E-06	52.71	5
A2a	20.2	23	4.24E-08	2.32E-06	54.83	5
A2a	20.4	23.2	4.39E-08	2.27E-06	51.71	4
A2a	20.6	23.4	4.51E-08	2.53E-06	56.04	4
A2a	20.8	23.6	4.44E-08	2.46E-06	55.41	4
A2a	21	23.8	4.70E-08	2.51E-06	53.36	4

A2a	21.2	24	4.83E-08	2.61E-06	54.00	4
A2a	21.4	24.2	4.74E-08	2.71E-06	57.27	4
A2a	21.6	24.4	4.50E-08	2.45E-06	54.53	4
A2a	21.8	24.6	4.67E-08	2.42E-06	51.80	4
A2a	22	24.8	4.58E-08	2.51E-06	54.73	4
A2a	22.2	25	4.08E-08	2.36E-06	57.77	5
A2a	22.4	25.2	4.17E-08	2.37E-06	56.82	5
A2a	22.6	25.4	4.85E-08	2.51E-06	51.68	4
A2a	22.8	25.6	4.75E-08	2.52E-06	52.99	4
A2a	23	25.8	4.60E-08	2.54E-06	55.23	4
A2a	23.2	26	4.58E-08	2.52E-06	54.95	4
A2a	23.4	26.2	4.62E-08	2.41E-06	52.11	4
A2a	23.6	26.4	4.44E-08	2.47E-06	55.54	5
A2a	23.8	26.6	4.28E-08	2.71E-06	63.15	5
A2a	24	26.8	4.39E-08	2.56E-06	58.35	5
A2a	24.2	27	4.34E-08	2.55E-06	58.81	5
A2a	24.4	27.2	4.18E-08	2.62E-06	62.65	4
A2a	24.6	27.4	3.90E-08	2.61E-06	66.83	4
A2a	24.8	27.6	4.34E-08	2.64E-06	60.80	4
A2a	25	27.8	4.21E-08	2.70E-06	64.10	5
A2a	25.2	28	3.82E-08	2.34E-06	61.13	5
A2a	25.4	28.2	4.27E-08	2.19E-06	51.19	4
A2a	25.6	28.4	4.75E-08	2.65E-06	55.91	4
A2a	25.8	28.6	4.05E-08	2.49E-06	61.30	5
A2a	26	28.8	4.47E-08	2.84E-06	63.50	4
A2a	26.2	29	4.30E-08	2.82E-06	65.50	4
A2a	26.4	29.2	4.49E-08	2.53E-06	56.19	4

A2a	26.6	29.4	4.49E-08	2.74E-06	61.00	4
A2a	26.8	29.6	4.20E-08	2.83E-06	67.38	4
A2a	27	29.8	4.15E-08	2.94E-06	70.95	5
A2a	27.2	30	4.65E-08	2.76E-06	59.36	5
A2a	27.4	30.2	4.25E-08	2.30E-06	54.11	5
A2a	27.6	30.4	4.39E-08	2.28E-06	52.00	5
A2a	27.8	30.6	4.62E-08	2.25E-06	48.69	5
A2a	28	30.8	4.61E-08	2.39E-06	51.95	5
A2a	28.2	31	4.25E-08	2.45E-06	57.60	5
A2a	28.4	31.2	4.45E-08	2.25E-06	50.61	5
A2a	28.6	31.4	4.00E-08	2.36E-06	59.01	5
A2a	28.8	31.6	4.00E-08	2.38E-06	59.39	5
A2b	29	31.8	3.67E-08	2.95E-06	80.37	4
A2b	29.2	32	3.56E-08	2.89E-06	81.13	4
A2b	29.4	32.2	3.86E-08	2.99E-06	77.56	4
A2b	29.6	32.4	4.12E-08	2.94E-06	71.37	4
A2b	29.8	32.6	3.91E-08	2.95E-06	75.56	4
A2b	30	32.8	3.79E-08	2.81E-06	74.06	4
A2b	30.2	33	3.58E-08	2.90E-06	80.95	4
A2b	30.4	33.2	3.49E-08	2.64E-06	75.65	4
A2b	30.6	33.4	3.78E-08	2.89E-06	76.59	4
A2b	30.8	33.6	3.63E-08	2.72E-06	74.81	4
A2b	31	33.8	4.15E-08	2.73E-06	65.76	4
A2b	31.2	34	4.23E-08	2.68E-06	63.28	4
A2b	31.4	34.2	4.21E-08	2.80E-06	66.60	4
A2b	31.6	34.4	4.13E-08	2.70E-06	65.53	4
A2b	31.8	34.6	3.92E-08	2.62E-06	66.87	4

A2b	32	34.8	3.85E-08	2.66E-06	68.98	4
A2b	32.2	35	3.64E-08	2.54E-06	69.63	4
A2b	32.4	35.2	4.09E-08	2.77E-06	67.61	4
A2b	32.6	35.4	3.79E-08	2.71E-06	71.62	4
A2b	32.8	35.6	3.82E-08	2.62E-06	68.52	4
A2b	33	35.8	3.82E-08	2.37E-06	61.94	4
A2b	33.2	36	4.08E-08	2.79E-06	68.43	4
A2b	33.4	36.2	4.10E-08	2.82E-06	68.81	4
A2b	33.6	36.4	4.23E-08	2.84E-06	67.29	4
A2b	33.8	36.6	4.16E-08	2.83E-06	68.11	4
A2b	34	36.8	4.51E-08	2.84E-06	63.02	4
A2b	34.2	37	3.61E-08	2.71E-06	75.17	4
A2b	34.4	37.2	4.31E-08	2.78E-06	64.53	4
A2b	34.6	37.4	3.83E-08	2.78E-06	72.56	4
A2b	34.8	37.6	3.55E-08	2.85E-06	80.22	4
A2b	35	37.8	3.69E-08	2.65E-06	71.95	4
A2b	35.2	38	3.97E-08	2.38E-06	60.00	4
A2b	35.4	38.2	4.20E-08	2.75E-06	65.37	5
A2b	35.6	38.4	4.15E-08	2.84E-06	68.27	5
A2b	35.8	38.6	3.80E-08	2.78E-06	73.13	5
A2b	36	38.8	4.29E-08	2.77E-06	64.54	5
A2b	36.2	39	3.99E-08	2.92E-06	73.13	5
A2b	36.4	39.2	4.30E-08	2.69E-06	62.48	5
A2b	36.6	39.4	4.59E-08	2.76E-06	60.04	5
A2b	36.8	39.6	4.04E-08	2.24E-06	55.50	5
A2b	37	39.8	3.98E-08	2.54E-06	63.79	5
A2b	37.2	40	4.01E-08	2.43E-06	60.55	4

A2b	37.4	40.2	4.25E-08	2.95E-06	69.42	4
A2b	37.6	40.4	4.46E-08	2.87E-06	64.33	4
A2b	37.8	40.6	4.02E-08	2.93E-06	72.72	4
A2b	38	40.8	4.02E-08	2.80E-06	69.48	4
A2b	38.2	41	4.30E-08	3.11E-06	72.35	5
A2b	38.4	41.2	3.98E-08	2.85E-06	71.76	5
A2b	38.6	41.4	3.99E-08	2.92E-06	73.25	5
A2b	38.8	41.6	4.19E-08	2.92E-06	69.83	4
A2b	39	41.8	3.88E-08	2.84E-06	73.18	4
A2b	39.2	42	4.15E-08	2.87E-06	69.13	4
A2b	39.4	42.2	3.87E-08	3.04E-06	78.59	4
A2b	39.6	42.4	4.17E-08	2.67E-06	63.97	5
A2b	39.8	42.6	4.22E-08	2.68E-06	63.57	5
A2b	40	42.8	4.55E-08	2.72E-06	59.67	5
A2b	40.2	43	4.24E-08	2.67E-06	62.87	5
A2b	40.4	43.2	4.16E-08	2.67E-06	64.12	4
A2b	40.6	43.4	4.52E-08	2.62E-06	57.81	4
A2b	40.8	43.6	4.79E-08	2.73E-06	56.97	4
A2b	41.4	44.2	5.10E-08	2.28E-06	44.81	4
A2b	41.6	44.4	5.05E-08	2.58E-06	51.11	5
A2b	41.8	44.6	5.10E-08	2.53E-06	49.63	5
A2b	42	44.8	4.80E-08	2.61E-06	54.30	5
A2b	42.2	45	4.62E-08	2.74E-06	59.38	5
A2b	42.4	45.2	4.25E-08	2.71E-06	63.86	5
A2b	42.6	45.4	4.53E-08	2.56E-06	56.43	5
A2b	42.8	45.6	4.39E-08	2.57E-06	58.45	4
A2b	43	45.8	4.29E-08	2.94E-06	68.64	4

A2b	43.2	46	4.56E-08	2.77E-06	60.85	4
A2b	43.4	46.2	4.02E-08	2.94E-06	73.08	4
A2b	43.6	46.4	4.57E-08	2.79E-06	61.16	4
A2b	43.8	46.6	4.54E-08	2.78E-06	61.35	4
A2b	44	46.8	4.63E-08	2.75E-06	59.27	4
A2b	44.2	47	5.39E-08	2.94E-06	54.60	4
A2b	44.4	47.2	5.56E-08	2.92E-06	52.48	4
A2b	44.6	47.4	4.97E-08	3.08E-06	61.91	4
A2b	44.8	47.6	4.75E-08	3.30E-06	69.60	4
A2b	45	47.8	4.68E-08	3.10E-06	66.32	4
A2b	45.2	48	4.50E-08	3.17E-06	70.53	4
A2b	45.4	48.2	4.79E-08	2.73E-06	57.04	4
A2b	45.6	48.4	4.72E-08	2.68E-06	56.84	4
A2b	45.8	48.6	4.97E-08	2.90E-06	58.28	5
A2b	46	48.8	4.68E-08	2.94E-06	62.84	5
A2b	46.2	49	4.50E-08	2.92E-06	65.05	5
A2b	46.4	49.2	4.32E-08	2.95E-06	68.33	5
A2b	46.6	49.4	4.42E-08	2.79E-06	63.20	5
A2b	46.8	49.6	4.92E-08	2.82E-06	57.36	4
A2b	47	49.8	4.85E-08	2.81E-06	58.06	4
A2b	47.2	50	4.77E-08	2.66E-06	55.69	4
A2b	47.4	50.2	4.86E-08	2.66E-06	54.78	4
A2b	47.6	50.4	4.95E-08	2.78E-06	56.16	4
A2b	47.8	50.6	5.13E-08	2.83E-06	55.13	4
A2b	48	50.8	3.93E-08	2.32E-06	58.95	5
A2b	48.2	51	3.52E-08	2.47E-06	70.27	5
A2b	48.4	51.2	3.78E-08	2.33E-06	61.64	4

A2b	48.6	51.4	3.93E-08	2.47E-06	62.85	4
A2b	48.8	51.6	3.65E-08	2.45E-06	67.06	4
A2b	49	51.8	3.80E-08	2.38E-06	62.72	4
A2b	49.2	52	4.02E-08	2.39E-06	59.44	4
A2b	49.4	52.2	4.26E-08	2.41E-06	56.53	4
A2b	49.6	52.4	4.41E-08	2.33E-06	52.88	4
A2b	49.8	52.6	4.24E-08	2.20E-06	51.90	4
A2b	50	52.8	4.60E-08	2.33E-06	50.75	4
A2b	50.2	53	4.24E-08	2.43E-06	57.29	4
A2b	50.4	53.2	4.51E-08	2.32E-06	51.50	4
A2b	50.6	53.4	4.56E-08	2.42E-06	53.19	4
A2b	50.8	53.6	4.91E-08	2.52E-06	51.23	4
A2b	51	53.8	4.48E-08	2.43E-06	54.35	4
A2b	51.2	54	4.85E-08	2.22E-06	45.76	4
A2b	51.4	54.2	4.84E-08	2.32E-06	47.88	4
A2b	51.6	54.4	5.08E-08	2.34E-06	46.05	5
A2b	51.8	54.6	4.85E-08	2.32E-06	47.79	4
A2b	52	54.8	4.76E-08	2.38E-06	50.02	4
A2b	52.2	55	4.85E-08	2.32E-06	47.93	4
A2b	52.4	55.2	4.94E-08	2.28E-06	46.15	4
A2b	52.6	55.4	5.29E-08	2.34E-06	44.35	5
A2b	52.8	55.6	5.15E-08	2.43E-06	47.27	4
A2b	53	55.8	4.95E-08	2.44E-06	49.37	4
A2b	53.2	56	5.23E-08	2.25E-06	42.95	4
A2b	53.4	56.2	5.13E-08	2.37E-06	46.25	5
A2b	53.6	56.4	5.24E-08	2.30E-06	43.99	5
A2b	53.8	56.6	5.03E-08	2.11E-06	41.82	4

A2b	54	56.8	5.32E-08	2.32E-06	43.72	4
A2b	54.2	57	5.32E-08	2.35E-06	44.19	4
A2b	54.4	57.2	5.39E-08	2.40E-06	44.62	4
A2b	54.6	57.4	5.28E-08	2.41E-06	45.65	4
A2b	54.8	57.6	5.48E-08	2.31E-06	42.13	4
A2b	55	57.8	5.30E-08	2.45E-06	46.25	4
A2b	55.2	58	5.31E-08	2.44E-06	46.05	4
A2b	55.4	58.2	5.48E-08	2.43E-06	44.35	4
A2b	55.6	58.4	5.56E-08	2.50E-06	44.91	4
A2b	55.8	58.6	5.80E-08	2.31E-06	39.74	4
A2b	56	58.8	5.82E-08	2.41E-06	41.45	4
A2b	56.2	59	5.98E-08	2.30E-06	38.43	4
A2b	56.4	59.2	5.85E-08	2.34E-06	40.07	4
A2b	56.6	59.4	5.77E-08	2.37E-06	41.14	4
A2b	56.8	59.6	5.74E-08	2.33E-06	40.55	4
A2b	57	59.8	5.92E-08	2.34E-06	39.55	4
A2b	57.2	60	5.89E-08	2.35E-06	39.95	4
A2b	57.4	60.2	5.87E-08	2.30E-06	39.15	4
A2b	57.6	60.4	6.49E-08	2.48E-06	38.23	4
A2b	57.8	60.6	6.99E-08	2.38E-06	33.99	4
A2b	58	60.8	7.01E-08	2.17E-06	31.01	4
A2b	58.2	61	6.78E-08	2.41E-06	35.60	4
A2b	58.4	61.2	6.84E-08	2.68E-06	39.16	4
A2b	58.6	61.4	6.69E-08	2.51E-06	37.58	4
A2b	58.8	61.6	6.54E-08	2.43E-06	37.12	4
A2b	59	61.8	6.31E-08	2.55E-06	40.45	4
A2b	59.2	62	6.77E-08	3.15E-06	46.49	4

A2b	59.4	62.2	6.61E-08	2.76E-06	41.78	4
A2b	59.6	62.4	6.71E-08	2.70E-06	40.24	4
A2b	59.8	62.6	6.75E-08	2.37E-06	35.17	4
A2b	60	62.8	6.87E-08	2.77E-06	40.31	4
A2b	60.2	63	7.02E-08	2.87E-06	40.85	4
A2b	60.4	63.2	7.05E-08	2.86E-06	40.51	4
A2b	60.6	63.4	7.23E-08	2.82E-06	39.00	4
A2b	60.8	63.6	7.09E-08	2.95E-06	41.59	4
A2b	61	63.8	6.57E-08	3.10E-06	47.08	4
A2b	61.2	64	6.32E-08	3.01E-06	47.60	4
A2b	61.4	64.2	6.23E-08	2.76E-06	44.20	4
A2b	61.6	64.4	6.23E-08	2.68E-06	43.04	4
A2b	61.8	64.6	6.58E-08	2.53E-06	38.44	4
A2b	62	64.8	6.14E-08	1.94E-06	31.52	4
A2b	62.2	65	6.45E-08	2.08E-06	32.26	4
A2b	62.4	65.2	6.17E-08	2.85E-06	46.16	4
A2b	62.6	65.4	5.47E-08	2.59E-06	47.34	4
A2b	62.8	65.6	5.68E-08	2.84E-06	50.00	4
A2b	63	65.8	5.75E-08	2.80E-06	48.70	4
A2b	63.2	66	5.83E-08	2.81E-06	48.24	4
A2b	63.4	66.2	5.67E-08	2.86E-06	50.45	4
A2b	63.6	66.4	5.66E-08	2.98E-06	52.76	4
A2b	63.8	66.6	5.72E-08	2.95E-06	51.60	4
A2b	64	66.8	5.64E-08	3.08E-06	54.60	4
A2b	64.2	67	5.37E-08	2.53E-06	47.14	4
A2b	64.4	67.2	5.07E-08	2.71E-06	53.42	4
A2b	64.6	67.4	4.92E-08	2.94E-06	59.87	4

A2b	64.8	67.6	5.13E-08	2.66E-06	51.78	5
A2b	65	67.8	5.34E-08	3.44E-06	64.30	4
A2b	65.2	68	5.15E-08	3.24E-06	62.94	4
A2b	65.4	68.2	5.43E-08	3.00E-06	55.21	4
A2b	65.6	68.4	5.28E-08	2.89E-06	54.78	5
A2b	65.8	68.6	5.50E-08	2.78E-06	50.67	4
A2b	66	68.8	5.12E-08	2.65E-06	51.70	4
A2b	66.2	69	5.58E-08	2.77E-06	49.61	4
A2b	66.4	69.2	5.57E-08	2.79E-06	50.05	4
A2b	66.6	69.4	5.70E-08	2.73E-06	47.83	4
A2b	66.8	69.6	5.50E-08	2.61E-06	47.39	4
A2b	67	69.8	5.79E-08	2.69E-06	46.49	4
A2b	67.2	70	5.66E-08	2.74E-06	48.42	4
A2b	67.4	70.2	5.65E-08	2.85E-06	50.57	4
A2b	67.6	70.4	5.48E-08	2.81E-06	51.24	4
A2b	67.8	70.6	5.50E-08	2.67E-06	48.57	4
A2b	68	70.8	5.78E-08	2.62E-06	45.31	4
A2b	68.2	71	5.81E-08	2.68E-06	46.21	4
A2b	68.4	71.2	5.53E-08	2.75E-06	49.70	4
A2b	68.6	71.4	5.60E-08	2.76E-06	49.34	4
A2b	68.8	71.6	5.55E-08	2.76E-06	49.81	4
A2b	69	71.8	5.73E-08	2.66E-06	46.47	4
A2b	69.2	72	5.49E-08	2.63E-06	47.99	4
A2b	69.4	72.2	5.62E-08	2.72E-06	48.44	4
A2b	69.6	72.4	5.24E-08	2.60E-06	49.59	5
A2b	69.8	72.6	5.31E-08	2.70E-06	50.81	5
A2b	70	72.8	5.46E-08	2.69E-06	49.22	5

A2b	70.2	73	4.43E-08	2.27E-06	51.21	5
A2b	70.4	73.2	5.07E-08	2.49E-06	49.18	5
A2b	70.6	73.4	5.02E-08	2.45E-06	48.71	5
A2b	70.8	73.6	5.00E-08	2.38E-06	47.62	5
A2b	71	73.8	4.82E-08	2.32E-06	48.13	5
A2b	71.2	74	4.76E-08	2.25E-06	47.22	5
A2b	71.4	74.2	4.91E-08	2.27E-06	46.15	5
A2b	71.6	74.4	5.08E-08	2.41E-06	47.55	5
A2b	71.8	74.6	5.56E-08	2.09E-06	37.61	4
A2b	72	74.8	5.47E-08	2.23E-06	40.81	4
A2b	72.2	75	5.53E-08	3.09E-06	55.94	4
A2b	72.4	75.2	5.09E-08	2.06E-06	40.51	4
A2b	72.6	75.4	5.08E-08	2.06E-06	40.48	4
A2b	72.8	75.6	5.17E-08	2.35E-06	45.37	4
A2b	73	75.8	5.17E-08	2.13E-06	41.27	4
A2b	73.2	76	5.40E-08	2.02E-06	37.47	4
A2b	73.4	76.2	5.38E-08	1.91E-06	35.62	4
A2b	73.6	76.4	5.21E-08	1.94E-06	37.14	5
A2b	73.8	76.6	5.24E-08	1.91E-06	36.44	5
A2b	74	76.8	5.39E-08	1.94E-06	35.90	4
A2b	74.2	77	5.54E-08	1.77E-06	31.99	4
A2b	74.4	77.2	5.41E-08	1.93E-06	35.62	4
A2b	74.6	77.4	5.59E-08	1.86E-06	33.33	4
A2b	74.8	77.6	5.62E-08	1.86E-06	33.04	4
A2b	75	77.8	5.52E-08	1.88E-06	34.04	4
A2b	75.2	78	5.13E-08	1.92E-06	37.41	4
A2b	75.4	78.2	5.41E-08	2.01E-06	37.06	4

A2b	75.6	78.4	5.65E-08	1.87E-06	33.05	4
A2b	75.8	78.6	5.76E-08	1.85E-06	32.17	4
A2b	76	78.8	5.91E-08	1.86E-06	31.51	4
A2b	76.2	79	5.84E-08	1.88E-06	32.19	4
A2b	76.4	79.2	5.65E-08	1.81E-06	32.07	4
A2b	76.6	79.4	5.86E-08	1.91E-06	32.64	4
A2b	76.8	79.6	5.96E-08	1.93E-06	32.45	4
A2b	77	79.8	5.50E-08	1.93E-06	35.13	4
A2b	77.2	80	5.68E-08	1.98E-06	34.79	4
A2b	77.4	80.2	5.82E-08	2.00E-06	34.38	4
A2b	77.6	80.4	5.86E-08	1.98E-06	33.76	4
A2b	77.8	80.6	5.57E-08	1.92E-06	34.50	4
A2b	78	80.8	5.28E-08	2.03E-06	38.41	4
A2b	78.2	81	5.35E-08	1.99E-06	37.24	4
A2b	78.4	81.2	5.66E-08	1.92E-06	33.89	4
A2b	78.6	81.4	5.03E-08	1.91E-06	38.02	4
A2b	78.8	81.6	5.48E-08	2.03E-06	37.05	4
A2b	79	81.8	5.26E-08	1.93E-06	36.65	4
A2b	79.2	82	5.34E-08	1.92E-06	36.04	4
A2b	79.4	82.2	5.70E-08	2.09E-06	36.62	4
A2b	79.6	82.4	5.87E-08	2.88E-06	49.03	4
A2b	79.8	82.6	5.75E-08	2.71E-06	47.14	4
A2b	80	82.8	6.06E-08	2.14E-06	35.41	4
A2b	80.2	83	6.23E-08	1.88E-06	30.18	4
A2b	80.4	83.2	5.26E-08	2.05E-06	38.94	4
A2b	80.6	83.4	4.92E-08	2.12E-06	43.06	4
A2b	80.8	83.6	4.74E-08	2.16E-06	45.54	5

A2b	81	83.8	4.56E-08	2.11E-06	46.21	5
A2b	81.2	84	4.44E-08	2.22E-06	49.99	5
A2b	81.4	84.2	4.61E-08	2.30E-06	49.84	5
A2b	81.6	84.4	5.37E-08	2.04E-06	38.06	5
A2b	81.8	84.6	4.70E-08	2.05E-06	43.74	5
A2b	82	84.8	4.84E-08	2.42E-06	49.90	4
A2b	82.2	85	4.81E-08	2.40E-06	49.86	4
A2b	82.4	85.2	4.81E-08	2.50E-06	52.05	4
A2b	82.6	85.4	4.62E-08	2.63E-06	56.89	4
A2b	82.8	85.6	4.43E-08	2.63E-06	59.40	4
A2b	83	85.8	4.34E-08	2.65E-06	61.10	4
A2b	83.2	86	4.58E-08	2.93E-06	63.94	4
A2b	83.4	86.2	4.63E-08	2.79E-06	60.22	4
A2b	83.6	86.4	4.76E-08	2.73E-06	57.38	4
A2b	83.8	86.6	5.58E-08	2.52E-06	45.15	4
A2b	84	86.8	5.40E-08	2.58E-06	47.75	4
A2b	84.2	87	5.40E-08	2.61E-06	48.32	4
A2b	84.4	87.2	5.34E-08	2.78E-06	52.11	4
A2b	84.6	87.4	5.26E-08	2.72E-06	51.85	4
A2b	84.8	87.6	5.21E-08	2.69E-06	51.65	4
A2b	85	87.8	5.28E-08	2.53E-06	47.96	5
A2b	85.2	88	5.21E-08	2.60E-06	49.92	5
A2b	85.4	88.2	5.27E-08	2.59E-06	49.18	5
A2b	85.6	88.4	5.29E-08	2.54E-06	48.04	5
A2b	85.8	88.6	5.29E-08	2.49E-06	47.07	5
A2b	86	88.8	5.09E-08	2.50E-06	49.03	5
A2b	86.2	89	5.16E-08	2.54E-06	49.21	5

A2b	86.4	89.2	5.67E-08	2.00E-06	35.18	5
A2b	86.6	89.4	5.18E-08	2.54E-06	48.99	5
A2b	86.8	89.6	5.48E-08	1.99E-06	36.24	5
A2b	87	89.8	5.16E-08	2.13E-06	41.27	5
A2b	87.2	90	5.05E-08	2.22E-06	43.90	5
A2b	87.4	90.2	4.95E-08	2.27E-06	45.87	5
A2b	87.6	90.4	4.96E-08	2.28E-06	46.02	5
A2b	87.8	90.6	4.66E-08	2.26E-06	48.60	5
A2b	88	90.8	4.49E-08	2.35E-06	52.29	5
A2b	88.2	91	5.43E-08	2.33E-06	42.94	5
A2b	88.4	91.2	5.41E-08	2.64E-06	48.85	5
A2b	88.6	91.4	5.04E-08	2.33E-06	46.28	5
A2b	88.8	91.6	4.91E-08	2.37E-06	48.25	5
A2b	89	91.8	4.56E-08	2.49E-06	54.73	5
A2b	89.2	92	4.73E-08	2.53E-06	53.37	5
A2b	89.4	92.2	4.81E-08	2.62E-06	54.47	5
A2b	89.6	92.4	4.74E-08	2.55E-06	53.80	5
A2b	89.8	92.6	3.95E-08	2.08E-06	52.64	5
A2b	90	92.8	3.83E-08	2.20E-06	57.34	5
A2b	90.2	93	3.86E-08	2.16E-06	55.93	5
A2c	0	93.2	5.37E-08	2.72E-06	50.62	4
A2c	0.75	93.95	5.64E-08	2.51E-06	44.47	5
A2c	1.5	94.7	5.35E-08	2.37E-06	44.29	5
A2c	2.25	95.45	5.15E-08	2.70E-06	52.36	4
A2c	3	96.2	4.86E-08	2.73E-06	56.20	4
A2c	3.75	96.95	4.97E-08	3.20E-06	64.41	4
A2c	4.5	97.7	4.55E-08	3.01E-06	66.18	4

A2c	5.25	98.45	4.44E-08	3.19E-06	71.79	4
A2c	6	99.2	3.91E-08	3.39E-06	86.53	4
A2c	6.75	99.95	4.29E-08	3.34E-06	77.86	4
A2c	7.5	100.7	4.17E-08	3.14E-06	75.47	4
A2c	8.25	101.45	4.36E-08	3.13E-06	71.82	4
A2c	9	102.2	4.00E-08	3.29E-06	82.34	4
A2c	9.75	102.95	4.24E-08	3.21E-06	75.75	4
A2c	10.5	103.7	4.10E-08	3.13E-06	76.22	4
A2c	11.25	104.45	4.30E-08	3.16E-06	73.46	4
A2c	12	105.2	4.36E-08	2.91E-06	66.77	5
A2c	12.75	105.95	4.42E-08	2.86E-06	64.70	4
A2c	13.5	106.7	4.49E-08	2.73E-06	60.92	4
A2c	14.25	107.45	4.56E-08	2.71E-06	59.46	5
A2c	15	108.2	4.95E-08	2.73E-06	55.15	5
A2c	15.75	108.95	4.72E-08	2.34E-06	49.53	4
A2c	16.5	109.7	4.65E-08	2.67E-06	57.44	4
A2c	17.25	110.45	4.63E-08	2.40E-06	51.79	4
A2c	18	111.2	4.86E-08	2.65E-06	54.54	4
A2c	18.75	111.95	4.61E-08	2.25E-06	48.84	5
A2c	19.5	112.7	4.49E-08	2.36E-06	52.64	4
A2c	20.25	113.45	4.49E-08	2.75E-06	61.18	5
A2c	21	114.2	4.77E-08	2.93E-06	61.41	4
A2c	21.75	114.95	4.47E-08	2.77E-06	62.02	4
A2c	24	117.2	5.47E-08	1.86E-06	33.99	4
A2c	24.75	117.95	5.67E-08	1.90E-06	33.48	4
A2c	25.5	118.7	5.45E-08	1.95E-06	35.80	4
A2c	26.25	119.45	5.40E-08	1.97E-06	36.46	4

A2c	27	120.2	5.44E-08	1.96E-06	36.09	4
A2c	27.75	120.95	5.63E-08	1.92E-06	34.14	4
A2c	28.5	121.7	5.55E-08	2.33E-06	41.92	4
A2c	29.25	122.45	5.60E-08	1.91E-06	34.16	4
A2c	30	123.2	5.17E-08	1.96E-06	37.80	4
A2c	30.75	123.95	4.95E-08	2.08E-06	41.99	5
A2c	31.5	124.7	4.67E-08	2.30E-06	49.21	5
A2c	32.25	125.45	5.14E-08	2.81E-06	54.64	3
A2c	33	126.2	5.27E-08	2.64E-06	50.16	4
A2c	33.75	126.95	5.66E-08	2.73E-06	48.25	3
A2c	34.5	127.7	5.69E-08	1.82E-06	32.03	3
A2c	35.25	128.45	5.59E-08	1.96E-06	35.00	3
A3a	36	129.2	6.81E-08	2.13E-06	31.35	3
A3a	36.75	129.95	7.50E-08	5.79E-06	77.26	3
A3a	37.5	130.7	6.87E-08	4.62E-06	67.33	3
A3a	38.25	131.45	6.66E-08	2.23E-06	33.49	3
A3a	38.8	132	7.21E-08	3.36E-06	46.67	3
A3a	39.75	132.95	7.18E-08	2.30E-06	32.11	3
A3a	40.5	133.7	7.38E-08	4.21E-06	57.00	3
A3a	41.25	134.45	6.81E-08	2.32E-06	34.01	3
A3a	42	135.2	5.53E-08	2.38E-06	43.05	4
A3a	42.75	135.95	5.55E-08	2.21E-06	39.79	3
A3a	43.5	136.7	5.65E-08	2.12E-06	37.46	3
A3a	44.25	137.45	5.96E-08	2.18E-06	36.62	3
A3a	45	138.2	6.00E-08	2.19E-06	36.49	3
A3a	45.75	138.95	6.13E-08	2.10E-06	34.34	3
A3a	46.5	139.7	5.87E-08	2.31E-06	39.28	3

A3a	47.25	140.45	6.04E-08	2.19E-06	36.20	3
A3a	48	141.2	6.04E-08	2.31E-06	38.30	4
A3a	48.75	141.95	6.14E-08	2.16E-06	35.20	3
A3a	49.5	142.7	6.34E-08	2.05E-06	32.35	3
A3a	50.25	143.45	5.97E-08	2.22E-06	37.11	3
A3a	51	144.2	5.91E-08	2.76E-06	46.70	3
A3a	51.75	144.95	4.85E-08	2.75E-06	56.68	4
A3a	52.5	145.7	4.93E-08	1.92E-06	38.89	3
A3a	53.25	146.45	5.38E-08	2.07E-06	38.54	4
A3a	54	147.2	4.75E-08	2.26E-06	47.56	4
A3a	54.75	147.95	4.20E-08	2.14E-06	50.92	4
A3a	55.5	148.7	4.86E-08	2.10E-06	43.13	4
A3a	56.25	149.45	5.23E-08	2.05E-06	39.23	4
A3a	57	150.2	4.65E-08	2.14E-06	46.05	4
A3a	57.75	150.95	4.79E-08	2.16E-06	45.01	3
A3a	58.5	151.7	3.79E-08	2.84E-06	74.87	4
A3a	59.25	152.45	4.11E-08	3.17E-06	77.14	4
A3a	60	153.2	4.08E-08	2.87E-06	70.43	4
A3a	60.75	153.95	4.51E-08	2.37E-06	52.63	3
A3b	61.5	154.7	6.02E-08	2.29E-06	38.05	3
A3b	62.25	155.45	6.23E-08	2.29E-06	36.80	3
A3b	63	156.2	5.74E-08	2.29E-06	39.87	3
A3b	66	159.2	5.58E-08	2.42E-06	43.44	3
A3b	66.75	159.95	5.54E-08	2.54E-06	45.94	4
A3b	67.5	160.7	4.43E-08	2.37E-06	53.39	4
A3b	68.25	161.45	5.01E-08	2.34E-06	46.69	3
A3b	69	162.2	5.00E-08	2.40E-06	47.97	3

A3b	69.75	162.95	5.07E-08	2.50E-06	49.21	3
A3b	70.5	163.7	4.58E-08	2.43E-06	53.06	4
A3b	71.25	164.45	3.51E-08	2.17E-06	62.01	4
A3b	72	165.2	4.65E-08	2.24E-06	48.11	4
A3b	72.75	165.95	4.29E-08	2.08E-06	48.45	4
A3b	73.5	166.7	5.13E-08	2.04E-06	39.75	4
A3b	74.25	167.45	3.60E-08	1.75E-06	48.56	4
A3b	75	168.2	3.34E-08	1.68E-06	50.40	4
A3b	75.75	168.95	4.68E-08	2.20E-06	46.99	4
A2d	5.25	169.45	5.22E-08	2.23E-06	42.73	4
A2d	6.75	170.95	5.53E-08	2.45E-06	44.32	4
A2d	7.5	171.7	4.95E-08	2.39E-06	48.18	4
A2d	8.25	172.45	3.94E-08	2.19E-06	55.50	4
A2d	9	173.2	4.26E-08	1.92E-06	45.10	4
A2d	9.75	173.95	4.39E-08	2.07E-06	47.23	5
A2d	10.5	174.7	5.30E-08	2.09E-06	39.51	4
A2d	11.25	175.45	5.75E-08	2.16E-06	37.61	4
A2d	12	176.2	5.36E-08	2.28E-06	42.48	4
A2d	12.75	176.95	6.10E-08	2.20E-06	36.04	4
A2d	13.5	177.7	4.41E-08	2.72E-06	61.67	5
A2d	14.25	178.45	3.86E-08	2.41E-06	62.46	5
A2d	15	179.2	4.50E-08	2.54E-06	56.44	5
A2d	15.75	179.95	4.81E-08	2.45E-06	51.02	4
A2d	16.5	180.7	4.61E-08	2.44E-06	52.95	4
A2d	17.25	181.45	4.85E-08	2.27E-06	46.80	4
A2d	18	182.2	4.73E-08	2.39E-06	50.61	4
A2d	18.75	182.95	5.63E-08	2.68E-06	47.60	5

A2d	19.5	183.7	5.00E-08	3.29E-06	65.76	5		
A2d	20.25	184.45	5.80E-08	4.25E-06	73.25	4		
A2d	21	185.2	6.09E-08	3.81E-06	62.63	4		
A2d	21.75	185.95	6.07E-08	5.95E-06	98.12	4		
A2d	22.5	186.7	5.42E-08	1.01E-05	185.58	4		
A2d	23.25	187.45	6.48E-08	4.78E-06	73.72	4		
A2d	24	188.2	5.84E-08	4.66E-06	79.80	4		
A2d	24.75	188.95	6.91E-08	5.04E-06	72.96	4		
A2d	25.5	189.7	5.87E-08	5.16E-06	87.87	6		
A2d	26.25	190.45	6.37E-08	4.48E-06	70.32	5		
A2d	27	191.2	7.38E-08	6.71E-06	90.96	5		
A2d	27.75	191.95	5.61E-08	8.71E-06	155.28	4		
A2d	28.5	192.7	6.68E-08	4.82E-06	72.18	4		
A2d	29.25	193.45	6.53E-08	4.70E-06	71.93	5		
A2d	30	194.2	5.79E-08	5.90E-06	101.82	5		
A2d	30.75	194.95	4.99E-08	4.83E-06	96.71	5		
A2d	31.5	195.7	4.83E-08	4.46E-06	92.46	5		
A2d	32.25	196.45	4.77E-08	6.32E-06	132.51	5		
A2d	33	197.2	5.53E-08	4.59E-06	82.91	4		
A2d	33.75	197.95	6.05E-08	4.70E-06	77.66	4		
A2d	34.5	198.7	6.33E-08	4.37E-06	69.03	4		
A2d	35.25	199.45	6.30E-08	4.48E-06	71.09	4		
A2d	36	200.2	5.97E-08	4.47E-06	74.84	4	3.45E-05	0.58
A2d	36.75	200.95	5.65E-08	4.87E-06	86.13	4	3.39E-05	0.60
A2d	37.5	201.7	5.11E-08	5.14E-06	100.54	5	3.69E-05	0.72
A2d	38.25	202.45	5.09E-08	4.75E-06	93.47	5	3.51E-05	0.69
A2d	39	203.2	5.02E-08	5.57E-06	110.93	4	3.81E-05	0.76

A2d	39.75	203.95	4.99E-08	5.96E-06	119.53	4	3.87E-05	0.78
A2d	40.5	204.7	6.04E-08	4.29E-06	71.01	4	3.44E-05	0.57
A2d	41.25	205.45	6.23E-08	4.37E-06	70.04	4	3.63E-05	0.58
A2d	42	206.2	6.68E-08	5.04E-06	75.46	4	4.27E-05	0.64
A2d	42.75	206.95	6.70E-08	5.30E-06	79.12	4	4.61E-05	0.69
A2d	43.5	207.7	7.09E-08	4.99E-06	70.33	4	4.58E-05	0.65
A2d	44.25	208.45	6.80E-08	4.58E-06	67.36	4	4.45E-05	0.65
A2d	45	209.2	6.94E-08	4.92E-06	70.89	4	4.43E-05	0.64
A2d	45.75	209.95	6.73E-08	5.02E-06	74.67	4	5.20E-05	0.77
A2d	46.5	210.7	7.14E-08	5.19E-06	72.69	4	5.18E-05	0.72
A2d	47.25	211.45	6.43E-08	4.52E-06	70.23	4	4.21E-05	0.65
A2d	48	212.2	6.53E-08	5.01E-06	76.75	4	4.53E-05	0.69
A2d	48.75	212.95	6.62E-08	4.85E-06	73.26	4	4.46E-05	0.67
A2d	49.5	213.7	5.61E-08	6.08E-06	108.50	5	4.50E-05	0.80
A2d	50.25	214.45	5.65E-08	5.54E-06	98.05	5	4.41E-05	0.78
A2d	51	215.2	5.81E-08	5.67E-06	97.56	4	4.30E-05	0.74
A2d	51.75	215.95	5.90E-08	5.65E-06	95.82	4	4.16E-05	0.70
A2d	52.5	216.7	6.33E-08	4.96E-06	78.37	4	3.90E-05	0.62
A2d	53.25	217.45	6.42E-08	4.77E-06	74.23	4	3.94E-05	0.61
A2d	54	218.2	6.74E-08	4.88E-06	72.46	4	4.30E-05	0.64
A2d	54.75	218.95	6.71E-08	5.06E-06	75.40	4	4.55E-05	0.68
A2d	55.5	219.7	6.69E-08	4.99E-06	74.54	4	4.40E-05	0.66
A2d	56.25	220.45	6.62E-08	5.29E-06	79.89	4	4.59E-05	0.69
A2d	57	221.2	6.71E-08	5.00E-06	74.54	4	4.06E-05	0.60
A2d	57.75	221.95	6.59E-08	4.90E-06	74.46	4	4.03E-05	0.61
A2d	58.5	222.7	6.60E-08	4.27E-06	64.74	4	3.61E-05	0.55
A2d	59.25	223.45	6.44E-08	4.22E-06	65.50	4	3.60E-05	0.56

A2d	60	224.2	6.05E-08	4.39E-06	72.63	4	3.48E-05	0.58
A2d	60.75	224.95	5.99E-08	3.94E-06	65.84	4	3.16E-05	0.53
A2d	61.5	225.7	5.50E-08	3.87E-06	70.38	4	3.16E-05	0.58
A2d	62.25	226.45	5.30E-08	3.96E-06	74.59	4	3.07E-05	0.58
A2d	63	227.2	5.47E-08	4.69E-06	85.68	4	3.59E-05	0.66
A2d	63.75	227.95	5.49E-08	4.59E-06	83.70	4	3.45E-05	0.63
A2d	64.5	228.7	6.83E-08	4.36E-06	63.85	4	3.56E-05	0.52
A2d	65.25	229.45	6.35E-08	4.41E-06	69.44	4	3.74E-05	0.59
A2d	66	230.2	6.06E-08	4.32E-06	71.26	4	3.73E-05	0.62
A2d	66.75	230.95	5.56E-08	3.96E-06	71.23	4	3.50E-05	0.63
A2d	67.5	231.7	5.24E-08	3.98E-06	75.90	4	3.53E-05	0.67
A2d	68.25	232.45	4.84E-08	3.81E-06	78.74	4	3.52E-05	0.73
A2d	69	233.2	5.14E-08	3.57E-06	69.37	4	3.39E-05	0.66
A2d	69.75	233.95	4.95E-08	3.58E-06	72.37	5	3.32E-05	0.67
A2d	70.5	234.7	5.03E-08	3.47E-06	69.02	4	3.25E-05	0.65
A2d	71.25	235.45	5.16E-08	3.30E-06	63.89	4	3.32E-05	0.64
A2d	72	236.2	4.91E-08	3.15E-06	64.18	4	3.26E-05	0.66
A2d	72.75	236.95	4.86E-08	3.13E-06	64.48	4	3.33E-05	0.69
A2d	73.5	237.7	4.60E-08	2.91E-06	63.29	4	3.07E-05	0.67
A2d	74.25	238.45	4.75E-08	2.98E-06	62.69	4	2.90E-05	0.61
A2d	75	239.2	4.75E-08	3.58E-06	75.42	4	3.15E-05	0.66
A2d	75.75	239.95	4.74E-08	3.29E-06	69.54	4	2.94E-05	0.62
A2d	76.5	240.7	4.60E-08	2.86E-06	62.11	4	2.73E-05	0.59
A2d	77.25	241.45	4.71E-08	2.82E-06	59.95	4	2.76E-05	0.59
A2d	78	242.2	4.88E-08	3.02E-06	61.90	4	3.14E-05	0.64
A2d	78.75	242.95	4.39E-08	2.85E-06	64.92	5	3.07E-05	0.70
A1a	30	243.4	4.85E-08	3.43E-06	70.76	4	3.40E-05	0.70

A1a	30.75	244.15	5.13E-08	3.36E-06	65.49	4	3.28E-05	0.64
A1a	31.5	244.9	4.69E-08	3.33E-06	71.06	4	3.47E-05	0.74
A1a	32.25	245.65	4.80E-08	3.85E-06	80.26	4	3.80E-05	0.79
A1a	33	246.4	4.98E-08	3.70E-06	74.32	4	3.78E-05	0.76
A1a	33.75	247.15	4.62E-08	3.80E-06	82.24	4	3.79E-05	0.82
A1a	34.5	247.9	4.79E-08	3.55E-06	73.95	5	3.80E-05	0.79
A1a	35.25	248.65	4.35E-08	3.97E-06	91.31	6	4.24E-05	0.97
A1a	36	249.4	4.18E-08	3.26E-06	78.01	6	3.44E-05	0.82
A1a	36.75	250.15	4.08E-08	3.19E-06	78.16	6	3.25E-05	0.80
A1a	37.5	250.9	4.00E-08	3.24E-06	80.91	5	3.15E-05	0.79
A1a	38.25	251.65	4.16E-08	3.40E-06	81.76	6	3.36E-05	0.81
A1a	39	252.4	4.49E-08	2.95E-06	65.70	6	2.88E-05	0.64
A1a	39.75	253.15	4.14E-08	3.42E-06	82.71	5	3.17E-05	0.76
A1a	40.5	253.9	4.11E-08	4.00E-06	97.36	5	3.50E-05	0.85
A1a	41.25	254.65	4.29E-08	3.80E-06	88.75	5	3.37E-05	0.79
A1a	42	255.4	4.36E-08	3.79E-06	87.07	6	3.32E-05	0.76
A1a	42.75	256.15	4.40E-08	3.61E-06	82.07	6	3.19E-05	0.73
A1a	43.5	256.9	4.94E-08	2.98E-06	60.24	6	2.70E-05	0.55
A1a	44.25	257.65	4.77E-08	2.96E-06	62.04	6	2.78E-05	0.58
A1a	45	258.4	4.80E-08	3.28E-06	68.26	6	2.91E-05	0.61
A1a	45.75	259.15	4.43E-08	3.35E-06	75.77	6	2.95E-05	0.67
A1b	45	259.9	4.59E-08	3.35E-06	72.96	6	3.03E-05	0.66
A1b	45.75	260.65	4.09E-08	3.49E-06	85.48	6	3.08E-05	0.75
A1b	46.5	261.4	4.42E-08	3.30E-06	74.53	5	2.92E-05	0.66
A1b	47.25	262.15	4.13E-08	3.51E-06	84.96	4	3.10E-05	0.75
A1b	48	262.9	4.97E-08	2.66E-06	53.49	4	2.42E-05	0.49
A1b	48.75	263.65	4.68E-08	2.94E-06	62.95	4	2.71E-05	0.58

A1b	49.5	264.4	5.34E-08	3.05E-06	57.22	5	2.89E-05	0.54
A1b	50.25	265.15	5.24E-08	3.37E-06	64.34	4	3.23E-05	0.62
A1b	51	265.9	4.80E-08	3.28E-06	68.35	4	3.21E-05	0.67
A1b	51.75	266.65	5.10E-08	3.10E-06	60.82	4	3.01E-05	0.59
A1b	52.5	267.4	4.94E-08	3.36E-06	67.90	5	3.58E-05	0.72
A1b	53.25	268.15	4.53E-08	2.69E-06	59.34	6	2.46E-05	0.54
A1b	54	268.9	4.34E-08	3.64E-06	83.78	6	3.28E-05	0.76
A1b	54.75	269.65	4.24E-08	3.33E-06	78.53	6	3.01E-05	0.71
A1b	55.5	270.4	4.35E-08	3.09E-06	71.16	4	2.79E-05	0.64
A1b	56.25	271.15	4.56E-08	2.97E-06	65.05	4	2.79E-05	0.61
A1b	57	271.9	4.68E-08	2.81E-06	59.98	4	3.09E-05	0.66
A1b	57.75	272.65	4.59E-08	2.68E-06	58.43	4	2.69E-05	0.59
A1b	58.5	273.4	4.43E-08	3.12E-06	70.54	4	3.51E-05	0.79
A1b	59.25	274.15	4.73E-08	3.00E-06	63.28	4	2.67E-05	0.56
A1b	60	274.9	4.29E-08	3.68E-06	85.59	6	3.15E-05	0.73
A1b	60.75	275.65	4.11E-08	3.42E-06	83.11	6	2.99E-05	0.73
A1b	61.5	276.4	4.20E-08	3.70E-06	87.98	4	3.33E-05	0.79
A1b	62.25	277.15	4.17E-08	4.41E-06	105.69	4	3.73E-05	0.90
A1b	63	277.9	4.11E-08	3.93E-06	95.83	4	3.35E-05	0.82
A1b	63.75	278.65	3.96E-08	3.10E-06	78.36	4	2.81E-05	0.71
A1b	64.5	279.4	4.38E-08	2.92E-06	66.63	4	2.66E-05	0.61
A1b	65.25	280.15	3.57E-08	3.15E-06	88.25	4	2.79E-05	0.78
A1b	66	280.9	4.14E-08	3.46E-06	83.58	5	3.18E-05	0.77
A1b	66.75	281.65	3.68E-08	3.58E-06	97.43	6	3.34E-05	0.91
A1b	67.5	282.4	3.42E-08	3.09E-06	90.44	6	2.78E-05	0.81
A1b	68.25	283.15	3.77E-08	3.24E-06	85.80	5	2.86E-05	0.76
A1b	69	283.9	3.94E-08	3.38E-06	85.67	5	3.07E-05	0.78

A1b	69.75	284.65	3.95E-08	2.85E-06	72.06	6	2.73E-05	0.69
A1b	70.5	285.4	3.88E-08	2.91E-06	75.01	4	2.78E-05	0.72
A1b	71.25	286.15	4.19E-08	3.20E-06	76.50	4	3.18E-05	0.76
A1b	72	286.9	4.40E-08	3.01E-06	68.40	4	2.83E-05	0.64
A1b	72.75	287.65	4.42E-08	3.40E-06	76.99	5	3.34E-05	0.76
A1b	73.5	288.4	4.15E-08	3.19E-06	76.81	4	3.04E-05	0.73
A1b	74.25	289.15	4.65E-08	2.72E-06	58.36	5	2.65E-05	0.57
A1b	75	289.9	4.68E-08	2.77E-06	59.15	4	2.72E-05	0.58
A1b	75.75	290.65	5.45E-08	3.02E-06	55.32	4	4.04E-05	0.74
A1b	76.5	291.4	5.41E-08	3.36E-06	62.21	4	4.84E-05	0.90
A1b	77.25	292.15	4.43E-08	3.78E-06	85.38	5	3.76E-05	0.85
A1b	78	292.9	4.55E-08	3.52E-06	77.45	5	3.60E-05	0.79
A1b	78.75	293.65	4.38E-08	3.71E-06	84.79	4	4.63E-05	1.06
A1b	79.5	294.4	4.74E-08	3.23E-06	68.07	4	3.15E-05	0.66
A1b	80.25	295.15	4.63E-08	3.69E-06	79.59	4	3.72E-05	0.80
A1b	81	295.9	5.02E-08	3.69E-06	73.54	4	5.84E-05	1.16
A1b	81.75	296.65	5.57E-08	3.39E-06	60.83	4	3.32E-05	0.60
A1b	82.5	297.4	5.72E-08	3.49E-06	60.96	4	3.55E-05	0.62
A1b	83.25	298.15	5.50E-08	3.72E-06	67.65	5	3.85E-05	0.70
A1b	84	298.9	4.42E-08	4.05E-06	91.54	5	4.02E-05	0.91
A1b	84.75	299.65	5.08E-08	3.84E-06	75.71	5	3.82E-05	0.75
A1b	85.5	300.4	5.00E-08	3.86E-06	77.14	5	4.01E-05	0.80
A1b	86.25	301.15	4.96E-08	3.83E-06	77.22	5	3.91E-05	0.79
A1b	87	301.9	4.66E-08	4.26E-06	91.39	4	4.50E-05	0.97
A1b	87.75	302.65	4.93E-08	4.09E-06	82.98	4	4.33E-05	0.88
A1b	88.5	303.4	5.09E-08	3.98E-06	78.31	4	4.18E-05	0.82
A1b	89.25	304.15	5.87E-08	3.87E-06	65.81	4	3.97E-05	0.68

A1b	90	304.9	5.53E-08	4.00E-06	72.28	4	4.13E-05	0.75
A1b	90.75	305.65	5.58E-08	4.34E-06	77.82	4	4.51E-05	0.81
A1b	91.5	306.4	5.70E-08	4.05E-06	71.03	6	4.34E-05	0.76
A1b	92.25	307.15	5.32E-08	4.43E-06	83.32	6	4.77E-05	0.90
A1b	93	307.9	4.93E-08	4.57E-06	92.67	4	4.93E-05	1.00
A1b	93.75	308.65	4.58E-08	4.72E-06	103.11	4	5.06E-05	1.11
A1b	94.5	309.4	5.58E-08	3.65E-06	65.45	5	3.77E-05	0.68
A1b	95.25	310.15	5.27E-08	4.06E-06	77.14	4	4.24E-05	0.80
A1b	96	310.9	5.03E-08	4.18E-06	83.05	4	4.39E-05	0.87
A1b	96.75	311.65	4.97E-08	4.00E-06	80.61	4	4.24E-05	0.85
A1b	97.5	312.4	4.77E-08	3.98E-06	83.44	4	4.24E-05	0.89
A1b	98.25	313.15	4.78E-08	4.12E-06	86.34	5	4.52E-05	0.95
A1b	99	313.9	4.24E-08	4.35E-06	102.73	6	4.74E-05	1.12
A1b	99.75	314.65	5.30E-08	4.19E-06	79.05	4	3.98E-05	0.75
A1b	100.5	315.4	5.29E-08	4.05E-06	76.59	4	4.04E-05	0.76
A1b	101.25	316.15	4.62E-08	4.46E-06	96.39	5	4.60E-05	0.99
A1b	102	316.9	4.65E-08	3.74E-06	80.41	4	3.58E-05	0.77
A1b	102.75	317.65	5.10E-08	3.58E-06	70.21	4	3.52E-05	0.69
A1b	103.5	318.4	5.00E-08	3.88E-06	77.56	4	3.92E-05	0.78
A1b	104.25	319.15	5.07E-08	3.81E-06	75.13	6	3.88E-05	0.76
A1b	105	319.9	4.78E-08	3.82E-06	79.87	6	3.99E-05	0.83
A1b	105.75	320.65	4.57E-08	3.93E-06	86.08	5	4.03E-05	0.88
A1b	106.5	321.4	4.66E-08	3.91E-06	84.02	5	4.14E-05	0.89
A1b	107.25	322.15	4.69E-08	3.80E-06	81.14	5	3.98E-05	0.85
A1b	108	322.9	4.97E-08	3.80E-06	76.53	4	3.97E-05	0.80
A1b	108.75	323.65	5.15E-08	3.65E-06	70.91	4	3.72E-05	0.72
A1b	109.5	324.4	5.11E-08	3.82E-06	74.65	4	4.05E-05	0.79

A1b	110.25	325.15	5.04E-08	3.53E-06	70.07	5	3.97E-05	0.79
A1b	111	325.9	4.58E-08	3.99E-06	87.01	6	4.29E-05	0.94
A1b	111.75	326.65	4.80E-08	3.97E-06	82.70	6	4.06E-05	0.85
A1b	112.5	327.4	5.75E-08	4.56E-06	79.22	6	4.52E-05	0.79
A1b	113.25	328.15	5.12E-08	4.01E-06	78.41	6	4.02E-05	0.79
A1b	114	328.9	5.16E-08	3.50E-06	67.77	5	3.51E-05	0.68
A1b	114.75	329.65	5.17E-08	3.88E-06	75.18	5	3.99E-05	0.77
A1b	115.5	330.4	4.64E-08	4.30E-06	92.64	6	4.68E-05	1.01
A1b	116.25	331.15	4.94E-08	4.09E-06	82.93	4	4.08E-05	0.83
A1b	117	331.9	4.98E-08	4.11E-06	82.53	4	4.02E-05	0.81
A1b	117.75	332.65	5.11E-08	3.84E-06	75.17	4	3.78E-05	0.74
A1b	118.5	333.4	5.08E-08	3.64E-06	71.56	4	3.82E-05	0.75
A1b	119.25	334.15	4.94E-08	3.85E-06	78.05	4	4.08E-05	0.83
A1b	120	334.9	4.49E-08	3.52E-06	78.34	4	4.64E-05	1.03
A1b	120.75	335.65	5.01E-08	3.45E-06	68.91	4	5.35E-05	1.07
A1b	121.5	336.4	4.86E-08	3.43E-06	70.62	4	5.04E-05	1.04
A1b	122.25	337.15	4.89E-08	3.94E-06	80.50	4	4.23E-05	0.86
A1b	123	337.9	4.80E-08	3.86E-06	80.44	4	4.19E-05	0.87
A1b	123.75	338.65	5.10E-08	4.01E-06	78.64	5	4.36E-05	0.85
A1b	124.5	339.4	5.19E-08	3.85E-06	74.23	5	3.78E-05	0.73
A1b	125.25	340.15	5.25E-08	4.09E-06	77.96	5	4.14E-05	0.79
A1b	126	340.9	4.79E-08	3.91E-06	81.55	6	4.03E-05	0.84
A1b	126.75	341.65	4.52E-08	4.01E-06	88.84	5	4.16E-05	0.92
A1b	127.5	342.4	4.37E-08	4.10E-06	93.85	5	4.21E-05	0.96
A1b	128.25	343.15	4.64E-08	3.90E-06	84.01	4	4.17E-05	0.90
A1b	129	343.9	4.50E-08	3.77E-06	83.61	4	4.25E-05	0.94
A1b	129.75	344.65	4.71E-08	3.15E-06	66.81	5	3.47E-05	0.74

A1b	130.5	345.4	4.78E-08	4.00E-06	83.71	5	3.99E-05	0.83
A1b	131.25	346.15	4.59E-08	4.96E-06	107.98	4	4.79E-05	1.04
A1b	132	346.9	5.02E-08	4.00E-06	79.76	4	4.14E-05	0.82
A1b	132.75	347.65	5.00E-08	4.09E-06	81.84	5	4.27E-05	0.85
A1b	133.5	348.4	5.02E-08	3.66E-06	72.86	4	3.78E-05	0.75
A1b	134.25	349.15	4.67E-08	3.75E-06	80.24	5	4.10E-05	0.88
A1b	139.5	354.4	4.70E-08	4.09E-06	86.88	5		
A1b	140.25	355.15	4.90E-08	4.03E-06	82.37	6		
A1b	141	355.9	5.79E-08	4.07E-06	70.27	5		
A1b	141.75	356.65	5.18E-08	3.70E-06	71.48	5		
A1b	142.5	357.4	5.08E-08	4.74E-06	93.28	6		
A1b	143.25	358.15	5.31E-08	4.43E-06	83.53	5		
A1b	144	358.9	5.21E-08	4.42E-06	84.71	5		
A1b	144.75	359.65	4.90E-08	5.32E-06	108.56	6		
A1b	145.5	360.4	4.96E-08	4.67E-06	94.25	6		
A1b	146.25	361.15	4.75E-08	4.90E-06	103.17	6		
A1b	147	361.9	4.71E-08	4.36E-06	92.58	6		
A1b	147.75	362.65	4.77E-08	4.60E-06	96.33	6		
A1b	148.5	363.4	5.22E-08	4.32E-06	82.71	6		
A1b	149.25	364.15	5.19E-08	4.24E-06	81.70	7		
A1b	150	364.9	4.84E-08	4.82E-06	99.53	7		
A1b	150.75	365.65	4.84E-08	4.78E-06	98.72	7		
A1b	151.5	366.4	4.48E-08	4.74E-06	105.91	5		
A1b	152.25	367.15	4.90E-08	4.24E-06	86.62	7		
A1b	153	367.9	4.98E-08	4.06E-06	81.40	7		
A1b	153.75	368.65	4.89E-08	3.85E-06	78.71	5		
A1b	154.5	369.4	4.89E-08	4.14E-06	84.66	6		

Alb	155.25	370.15	4.43E-08	4.10E-06	92.67	6
Alb	156	370.9	4.93E-08	4.28E-06	86.80	7
Alb	156.75	371.65	4.53E-08	4.04E-06	89.20	7
Alb	157.5	372.4	4.90E-08	4.16E-06	84.82	7
Alb	158.25	373.15	4.82E-08	4.12E-06	85.46	6
Alb	159	373.9	4.45E-08	4.47E-06	100.45	7
Alb	159.75	374.65	4.74E-08	4.19E-06	88.41	7
Alb	160.5	375.4	4.31E-08	4.82E-06	111.90	7
Alb	161.25	376.15	4.57E-08	4.24E-06	92.80	6
Alb	162	376.9	4.71E-08	4.57E-06	97.05	7
Alb	162.75	377.65	4.68E-08	5.06E-06	108.08	7
Alb	163.5	378.4	4.46E-08	4.94E-06	110.90	7
Alb	164.25	379.15	4.45E-08	4.94E-06	110.95	7
Alb	165	379.9	4.55E-08	4.57E-06	100.40	7
Alb	165.75	380.65	4.62E-08	4.92E-06	106.42	7
Alb	166.5	381.4	4.46E-08	4.84E-06	108.57	6
Alb	167.25	382.15	4.62E-08	4.87E-06	105.37	7
Alb	168	382.9	4.15E-08	4.94E-06	118.96	7
Alb	168.75	383.65	4.55E-08	4.71E-06	103.55	6
Alb	169.5	384.4	4.89E-08	4.06E-06	83.06	6
Alb	170.25	385.15	4.99E-08	4.52E-06	90.68	6
Alb	171	385.9	4.69E-08	4.56E-06	97.19	7
Alb	171.75	386.65	4.41E-08	4.77E-06	108.17	7
Alb	172.5	387.4	4.77E-08	4.33E-06	90.70	6
Alb	173.25	388.15	5.44E-08	4.03E-06	74.22	6
Alb	174	388.9	5.15E-08	4.22E-06	81.94	7
Alb	174.75	389.65	4.46E-08	4.51E-06	100.99	7

A1b	175.5	390.4	4.34E-08	4.83E-06	111.46	7
A1b	176.25	391.15	5.69E-08	4.47E-06	78.47	6
A1b	177	391.9	5.69E-08	3.59E-06	63.13	6
A1b	177.75	392.65	5.84E-08	3.82E-06	65.50	6
A1b	178.5	393.4	5.69E-08	3.55E-06	62.39	6
A1b	179.25	394.15	5.59E-08	3.79E-06	67.75	7
A1b	180	394.9	5.07E-08	4.18E-06	82.39	7
A1b	180.75	395.65	5.25E-08	4.11E-06	78.22	6
A1b	181.5	396.4	5.01E-08	3.87E-06	77.23	7
A1b	182.25	397.15	4.56E-08	4.14E-06	90.88	7
A1b	183	397.9	4.44E-08	4.12E-06	92.80	7
A1b	183.75	398.65	4.98E-08	4.10E-06	82.33	7
A1b	184.5	399.4	4.44E-08	4.51E-06	101.63	7
A1b	185.25	400.15	4.50E-08	4.22E-06	93.82	7
A1b	186	400.9	4.79E-08	4.26E-06	89.03	7
A1b	186.75	401.65	4.42E-08	4.34E-06	98.06	6
A1b	187.5	402.4	4.45E-08	4.79E-06	107.53	6
A1b	188.25	403.15	4.69E-08	4.62E-06	98.40	6
A1b	189	403.9	5.40E-08	4.68E-06	86.53	6
A1b	189.75	404.65	4.89E-08	4.30E-06	87.94	7
A1b	190.5	405.4	4.59E-08	4.55E-06	99.15	7
A1b	191.25	406.15	4.66E-08	4.33E-06	92.86	6
A1b	192	406.9	4.69E-08	4.00E-06	85.18	6
A1b	192.75	407.65	4.56E-08	4.11E-06	90.05	7
A1b	193.5	408.4	4.90E-08	3.69E-06	75.19	7
A1b	194.25	409.15	4.72E-08	4.16E-06	88.11	7
A1b	195	409.9	5.04E-08	4.15E-06	82.51	7

A1b	195.75	410.65	4.87E-08	3.99E-06	81.91	7
A1b	196.5	411.4	4.77E-08	4.02E-06	84.38	7
A1b	197.25	412.15	5.01E-08	4.28E-06	85.36	6
A1b	198	412.9	4.92E-08	4.19E-06	85.27	7
A1b	198.75	413.65	5.04E-08	4.10E-06	81.25	7
A1b	199.5	414.4	5.06E-08	4.16E-06	82.20	6
A1b	200.25	415.15	5.16E-08	3.88E-06	75.24	7
A1b	201	415.9	5.03E-08	4.21E-06	83.64	7
A1b	201.75	416.65	5.69E-08	3.83E-06	67.30	7
A1b	202.5	417.4	5.58E-08	3.77E-06	67.57	7
A1b	203.25	418.15	5.65E-08	4.21E-06	74.63	7
A1b	204	418.9	5.34E-08	4.40E-06	82.38	7
A1b	204.75	419.65	5.29E-08	4.56E-06	86.30	7
A1b	205.5	420.4	5.09E-08	4.55E-06	89.33	7
A1b	206.25	421.15	5.23E-08	4.51E-06	86.28	7
A1b	207	421.9	4.88E-08	4.53E-06	92.79	7
A1b	207.75	422.65	5.18E-08	4.22E-06	81.51	7
A1b	208.5	423.4	4.38E-08	4.64E-06	105.82	7
A1b	209.25	424.15	5.00E-08	4.48E-06	89.63	7
A1b	210	424.9	4.99E-08	4.40E-06	88.17	7
A1b	210.75	425.65	4.65E-08	4.38E-06	94.15	7
A1b	211.5	426.4	4.81E-08	4.39E-06	91.31	7
A1b	212.25	427.15	5.09E-08	4.07E-06	79.88	6
A1b	213	427.9	5.08E-08	3.95E-06	77.80	6
A1b	213.75	428.65	4.32E-08	4.33E-06	100.38	7
A1b	214.5	429.4	4.86E-08	4.03E-06	82.88	6
A1b	215.25	430.15	4.49E-08	4.09E-06	90.97	6

A1b	216	430.9	4.58E-08	4.29E-06	93.77	7
A1b	216.75	431.65	4.65E-08	4.29E-06	92.14	6
A1b	217.5	432.4	4.29E-08	3.98E-06	92.64	7
A1b	218.25	433.15	5.11E-08	4.07E-06	79.63	6
A1b	219	433.9	4.97E-08	4.11E-06	82.56	7
A1b	219.75	434.65	4.94E-08	4.12E-06	83.36	6
A1b	220.5	435.4	4.76E-08	4.08E-06	85.71	6
A1b	221.25	436.15	4.85E-08	3.94E-06	81.16	6
A1b	222	436.9	4.87E-08	3.83E-06	78.66	6
A1b	222.75	437.65	4.57E-08	4.06E-06	88.82	6
A1b	223.5	438.4	5.64E-08	4.01E-06	71.08	6
A1b	224.25	439.15	5.15E-08	4.08E-06	79.20	6
A1b	225	439.9	5.02E-08	3.97E-06	79.07	7
A1b	225.75	440.65	5.07E-08	3.91E-06	77.07	7
A1b	226.5	441.4	4.86E-08	3.98E-06	81.89	7
A1b	227.25	442.15	5.24E-08	3.73E-06	71.24	6
A1b	228	442.9	5.26E-08	3.38E-06	64.35	6
A1b	228.75	443.65	5.01E-08	3.49E-06	69.71	6
A1b	229.5	444.4	5.47E-08	3.88E-06	70.97	6
A1b	230.25	445.15	5.14E-08	4.09E-06	79.67	6
A1b	231	445.9	5.03E-08	3.75E-06	74.62	7
A1b	231.75	446.65	4.86E-08	3.83E-06	78.87	7
A1b	232.5	447.4	5.01E-08	3.87E-06	77.35	6
A1b	233.25	448.15	5.32E-08	4.08E-06	76.63	6
A1b	234	448.9	5.23E-08	4.19E-06	80.06	6
A1b	234.75	449.65	5.08E-08	4.21E-06	82.96	6
A1b	235.5	450.4	5.32E-08	4.30E-06	80.73	6

A1b	236.25	451.15	4.83E-08	4.44E-06	91.90	7
A1b	237	451.9	4.20E-08	4.94E-06	117.55	7
A1b	237.75	452.65	5.10E-08	4.45E-06	87.27	7
A1c	240	453.4	4.87E-08	4.23E-06	86.77	7
A1c	240.75	454.15	4.97E-08	3.87E-06	77.91	7
A1c	241.5	454.9	4.65E-08	4.16E-06	89.53	7
A1c	242.25	455.65	4.53E-08	4.07E-06	89.77	7
A1c	243	456.4	4.51E-08	4.43E-06	98.15	8
A1c	243.75	457.15	4.39E-08	4.41E-06	100.44	8
A1c	244.5	457.9	5.08E-08	4.22E-06	83.15	5
A1c	245.25	458.65	5.00E-08	4.12E-06	82.35	5
A1c	246	459.4	5.11E-08	4.08E-06	79.99	5
A1c	246.75	460.15	4.87E-08	4.26E-06	87.42	5
A1c	247.5	460.9	5.57E-08	4.16E-06	74.61	5
A1c	248.25	461.65	5.48E-08	4.29E-06	78.26	6
A1c	249	462.4	4.88E-08	4.25E-06	87.06	5
A1c	249.75	463.15	6.03E-08	4.21E-06	69.83	5
A1c	250.5	463.9	5.89E-08	3.98E-06	67.46	5
A1c	251.25	464.65	5.57E-08	4.42E-06	79.37	5
A1c	252	465.4	5.05E-08	4.55E-06	90.08	6
A1c	252.75	466.15	4.79E-08	4.76E-06	99.43	7
A1c	253.5	466.9	4.97E-08	4.24E-06	85.18	6
A1c	254.25	467.65	5.71E-08	3.90E-06	68.36	6
A1c	255	468.4	7.30E-08	4.12E-06	56.47	6
A1c	255.75	469.15	5.43E-08	5.16E-06	94.95	7
A1c	256.5	469.9	4.87E-08	3.99E-06	81.91	6
A1c	257.25	470.65	5.89E-08	4.32E-06	73.34	6

A1c	258	471.4	5.61E-08	4.57E-06	81.46	7
A1c	258.75	472.15	5.50E-08	4.41E-06	80.13	6
A1c	259.5	472.9	4.65E-08	4.48E-06	96.40	7
A1c	260.25	473.65	4.75E-08	4.68E-06	98.65	7
A1c	261	474.4	5.13E-08	3.68E-06	71.78	6
A1c	261.75	475.15	4.94E-08	4.16E-06	84.17	7
A1c	262.5	475.9	4.45E-08	4.38E-06	98.34	7
A1c	263.25	476.65	4.79E-08	3.68E-06	76.82	6
A1c	264	477.4	5.13E-08	4.57E-06	88.99	7
A1c	264.75	478.15	5.69E-08	4.75E-06	83.46	6
A1c	265.5	478.9	5.08E-08	4.48E-06	88.29	6
A1c	266.25	479.65	5.36E-08	3.94E-06	73.53	6
A1c	267	480.4	4.44E-08	3.67E-06	82.64	7
A1c	267.75	481.15	5.05E-08	4.12E-06	81.70	6
A1c	268.5	481.9	4.65E-08	4.44E-06	95.47	6
A1c	269.25	482.65	4.59E-08	4.44E-06	96.74	6
A1c	270	483.4	5.25E-08	4.25E-06	80.99	6
A1c	270.75	484.15	4.65E-08	4.35E-06	93.42	6
A1c	271.5	484.9	4.29E-08	5.49E-06	127.97	6
A1c	272.25	485.65	5.43E-08	4.40E-06	81.06	6
A1c	273	486.4	4.72E-08	4.56E-06	96.63	7
A1c	273.75	487.15	4.77E-08	4.17E-06	87.47	7
A1c	274.5	487.9	4.86E-08	4.32E-06	88.76	7
A1c	275.25	488.65	4.81E-08	4.28E-06	88.87	7
A1c	276	489.4	5.11E-08	4.40E-06	86.11	6
A1c	276.75	490.15	5.43E-08	4.20E-06	77.41	6
A1c	277.5	490.9	5.16E-08	4.37E-06	84.69	6

A1c	278.25	491.65	5.52E-08	4.40E-06	79.62	6
A1c	279	492.4	5.38E-08	4.35E-06	80.88	7
A1c	279.75	493.15	5.15E-08	4.53E-06	87.83	6
A1c	280.5	493.9	5.28E-08	4.49E-06	85.05	6
A1c	281.25	494.65	5.70E-08	4.64E-06	81.28	6
A1c	282	495.4	5.84E-08	4.52E-06	77.38	6
A1c	282.75	496.15	5.54E-08	4.32E-06	77.91	6
A1c	283.5	496.9	4.87E-08	4.29E-06	88.02	7
A1c	284.25	497.65	4.54E-08	3.94E-06	86.69	7
A1c	285	498.4	4.60E-08	4.12E-06	89.68	7
A1c	285.75	499.15	4.40E-08	4.41E-06	100.19	7
A1d	286.5	499.9	4.67E-08	4.32E-06	92.45	9
A1d	287.25	500.65	2.43E-08	2.27E-06	93.23	9
A1d	288	501.4	3.17E-08	3.73E-06	117.69	9
A1d	288.75	502.15	2.02E-08	1.66E-06	81.98	9
A1d	289.5	502.9	2.60E-08	2.59E-06	99.76	9
A1d	290.25	503.65	1.49E-08	1.12E-06	75.05	9
A1d	291	504.4	4.38E-08	3.62E-06	82.63	9
A1d	291.75	505.15	3.01E-08	4.58E-06	152.23	9
A1d	292.5	505.9	5.17E-08	4.11E-06	79.48	6
A1d	294	507.4	5.15E-08	4.07E-06	79.00	6
A1d	295.5	508.9	3.94E-08	3.83E-06	97.25	6
A1d	297	510.4	4.99E-08	3.85E-06	77.11	6
A1d	298.5	511.9	5.32E-08	3.83E-06	71.88	5
A1d	300	513.4	5.74E-08	3.85E-06	67.08	5
A1d	301.5	514.9	5.78E-08	4.22E-06	73.12	5
A1d	303	516.4	6.27E-08	3.97E-06	63.37	5

Ald	304.5	517.9	6.27E-08	4.30E-06	68.68	5
Ald	306	519.4	5.77E-08	4.44E-06	76.90	5
Ald	307.5	520.9	5.14E-08	4.33E-06	84.31	5
Ald	309	522.4	5.45E-08	4.16E-06	76.34	6
Ald	310.5	523.9	5.52E-08	4.22E-06	76.32	5
Ald	312	525.4	5.41E-08	4.13E-06	76.38	6
Ald	313.5	526.9	5.43E-08	4.38E-06	80.62	5
Ald	315	528.4	5.75E-08	4.63E-06	80.43	6
Ald	316.5	529.9	5.20E-08	4.48E-06	86.26	6
Ald	318	531.4	5.33E-08	4.65E-06	87.19	5
Ald	319.5	532.9	5.80E-08	4.52E-06	77.94	5
Ald	321	534.4	5.27E-08	4.49E-06	85.25	5
Ald	322.5	535.9	5.34E-08	6.08E-06	113.85	6
Ald	324	537.4	5.02E-08	6.56E-06	130.57	6
Ald	325.5	538.9	4.44E-08	3.70E-06	83.17	5
Ald	327	540.4	4.71E-08	5.40E-06	114.49	6
Ald	328.5	541.9	5.13E-08	4.54E-06	88.48	5
Ald	330	543.4	4.68E-08	4.03E-06	86.20	7
Ald	331.5	544.9	4.97E-08	4.01E-06	80.74	7
Ald	333	546.4	4.66E-08	3.86E-06	82.68	7
Ald	334.5	547.9	4.64E-08	4.16E-06	89.60	7
Ald	336	549.4	4.59E-08	4.21E-06	91.62	7
Ald	337.5	550.9	4.67E-08	4.29E-06	91.90	7
Ald	339	552.4	4.79E-08	4.27E-06	89.11	7
Ald	340.5	553.9	4.92E-08	3.94E-06	80.07	7
Ald	342	555.4	4.79E-08	4.63E-06	96.60	7
Ald	343.5	556.9	4.63E-08	4.02E-06	86.73	7

Ald	345	558.4	4.45E-08	4.10E-06	92.18	7
Ald	346.5	559.9	4.70E-08	3.94E-06	83.77	7
Ald	348	561.4	5.03E-08	4.58E-06	91.06	7
Ald	349.5	562.9	4.81E-08	3.94E-06	81.81	7
Ald	351	564.4	4.67E-08	3.85E-06	82.34	7
Ald	352.5	565.9	4.94E-08	4.89E-06	98.97	7
Ald	354	567.4	5.14E-08	3.61E-06	70.29	7
Ald	355.5	568.9	5.21E-08	3.35E-06	64.38	7
Ald	357	570.4	4.57E-08	3.66E-06	80.04	7
Ald	358.5	571.9	4.78E-08	3.33E-06	69.65	6
Ald	360	573.4	4.85E-08	3.18E-06	65.47	5
Ald	361.5	574.9	5.21E-08	4.06E-06	77.81	5
Ald	363	576.4	5.99E-08	4.03E-06	67.32	5
Ald	364.5	577.9	5.47E-08	5.36E-06	97.91	5
Ald	366	579.4	5.28E-08	5.81E-06	110.12	5
Ald	367.5	580.9	4.18E-08	4.36E-06	104.41	5
Ald	369	582.4	5.81E-08	3.90E-06	67.11	5
Ald	370.5	583.9	5.52E-08	4.16E-06	75.29	5
Ald	372	585.4	4.99E-08	4.58E-06	91.66	6
Ald	373.5	586.9	4.29E-08	4.65E-06	108.28	6
Ald	375	588.4	4.27E-08	4.78E-06	112.18	6
Ald	376.5	589.9	4.31E-08	4.72E-06	109.53	7
Ald	378	591.4	3.88E-08	4.02E-06	103.49	8
Ald	379.5	592.9	4.25E-08	4.44E-06	104.34	7
Ald	381.1	594.5	4.37E-08	4.25E-06	97.24	7
Ald	382.5	595.9	4.18E-08	4.17E-06	99.68	7
Ald	384	597.4	4.18E-08	3.79E-06	90.53	7

A1d	385.5	598.9	4.06E-08	4.10E-06	101.14	7
A1d	387	600.4	3.96E-08	3.86E-06	97.46	7
A1d	388.9	602.3	4.16E-08	4.30E-06	103.41	8
A1d	390	603.4	3.81E-08	5.17E-06	135.80	8
A1d	391.5	604.9	4.48E-08	3.74E-06	83.62	7
A1d	393	606.4	4.07E-08	3.87E-06	95.11	7
A1d	400.50	613.9	5.28E-08	5.93E-06	112.24	6
A1d	402.00	615.4	4.03E-08	5.29E-06	131.04	6
A1d	403.50	616.9	4.11E-08	3.90E-06	94.97	6
A1d	405.00	618.4	3.83E-08	3.55E-06	92.71	6
A1d	408.00	621.4	4.89E-08	5.99E-06	122.36	7
A1d	408.40	621.8	5.28E-08	5.14E-06	97.37	7
A1d	418.30	631.7	5.20E-08	4.35E-06	83.80	6
A1d	418.50	631.9	5.02E-08	4.40E-06	87.50	6
A1d	420.00	633.4	4.68E-08	4.34E-06	92.62	9
A1d	421.50	634.9	5.04E-08	3.79E-06	75.12	7
A1d	423.00	636.4	4.58E-08	4.05E-06	88.56	7
A1d	424.50	637.9	4.79E-08	4.03E-06	84.05	7
A1d	426.00	639.4	4.42E-08	4.21E-06	95.27	6
A1d	427.50	640.9	4.38E-08	4.23E-06	96.52	6
A1d	429.00	642.4	4.68E-08	4.38E-06	93.50	6
A1d	430.50	643.9	5.10E-08	4.12E-06	80.84	6
A1d	432.00	645.4	5.26E-08	3.93E-06	74.68	6
A1d	433.50	646.9	4.43E-08	3.81E-06	86.04	7
A1d	435.00	648.4	5.30E-08	4.11E-06	77.47	6
A1e	436.50	649.9	4.69E-08	3.93E-06	83.85	7
A1e	438.00	651.4	4.92E-08	3.87E-06	78.65	7

Ale	439.50	652.9	4.32E-08	3.95E-06	91.44	6
Ale	441.00	654.4	3.99E-08	3.86E-06	96.58	6
Ale	442.50	655.9	5.52E-08	3.78E-06	68.35	6
Ale	444.00	657.4	5.31E-08	3.66E-06	68.93	7
Ale	445.50	658.9	5.50E-08	3.82E-06	69.34	7
Ale	447.00	660.4	5.15E-08	3.85E-06	74.71	7
Ale	448.50	661.9	6.00E-08	3.74E-06	62.44	7
Ale	450.00	663.4	5.84E-08	3.64E-06	62.28	6
Ale	451.50	664.9	4.94E-08	4.06E-06	82.13	7
Ale	453.00	666.4	4.51E-08	4.31E-06	95.59	8
Ale	454.50	667.9	4.99E-08	4.22E-06	84.62	7
Ale	456.00	669.4	4.35E-08	4.40E-06	101.17	8
Ale	457.50	670.9	4.74E-08	4.38E-06	92.36	7
Ale	459.00	672.4	4.98E-08	5.86E-06	117.62	8
Ale	460.50	673.9	7.03E-08	6.51E-06	92.49	7
Ale	462.00	675.4	4.97E-08	4.39E-06	88.42	8
Ale	463.50	676.9	4.49E-08	4.99E-06	111.22	7
Ale	465.00	678.4	5.28E-08	6.95E-06	131.43	9
Ale	466.50	679.9	4.83E-08	3.78E-06	78.22	6
Ale	468.00	681.4	5.31E-08	4.31E-06	81.23	7
Ale	469.50	682.9	5.19E-08	4.37E-06	84.23	7
Ale	471.00	684.4	4.81E-08	4.32E-06	89.72	7
Ale	472.50	685.9	5.07E-08	3.92E-06	77.31	6
Ale	474.00	687.4	5.54E-08	3.46E-06	62.38	4
Ale	475.50	688.9	5.77E-08	3.79E-06	65.74	4
Ale	477.00	690.4	7.81E-08	3.68E-06	47.12	4
Ale	478.50	691.9	7.80E-08	3.81E-06	48.85	5

Ale	480.00	693.4	6.33E-08	3.75E-06	59.27	5
Ale	481.50	694.9	6.39E-08	3.44E-06	53.82	6
Ale	483.00	696.4	6.69E-08	3.45E-06	51.62	5
Ale	484.50	697.9	6.13E-08	3.94E-06	64.28	5
Ale	486.00	699.4	5.90E-08	3.83E-06	65.00	5
Ale	487.50	700.9	5.59E-08	3.86E-06	69.11	6
Ale	489.00	702.4	5.74E-08	4.03E-06	70.11	5
Ale	490.50	703.9	5.54E-08	4.12E-06	74.38	5
Ale	492.00	705.4	5.43E-08	4.01E-06	73.96	5
Ale	493.50	706.9	5.35E-08	3.93E-06	73.47	5
Ale	495.00	708.4	5.53E-08	4.11E-06	74.28	6
Ale	496.50	709.9	5.65E-08	3.63E-06	64.31	6
Ale	498.00	711.4	6.04E-08	3.10E-06	51.33	5
Ale	499.50	712.9	5.39E-08	4.08E-06	75.79	6
Ale	501.00	714.4	5.41E-08	4.23E-06	78.17	6
Ale	502.50	715.9	5.47E-08	4.20E-06	76.87	6
Ale	504.00	717.4	5.39E-08	4.18E-06	77.47	6
Ale	505.50	718.9	5.32E-08	4.33E-06	81.43	6
Ale	507.00	720.4	5.64E-08	4.87E-06	86.41	5
Ale	508.50	721.9	5.16E-08	4.85E-06	93.99	6
Ale	510.00	723.4	5.33E-08	4.59E-06	86.07	5
Ale	511.50	724.9	5.45E-08	4.29E-06	78.82	5
Ale	513.00	726.4	5.48E-08	4.40E-06	80.39	5
Ale	514.50	727.9	5.71E-08	4.12E-06	72.12	5
Ale	516.00	729.4	5.51E-08	4.16E-06	75.59	5
Ale	517.50	730.9	5.42E-08	4.09E-06	75.47	5
Ale	519.00	732.4	5.16E-08	4.33E-06	83.79	5

Ale	520.50	733.9	5.66E-08	3.91E-06	69.07	5
Ale	522.00	735.4	5.46E-08	3.55E-06	65.02	6
Ale	523.50	736.9	5.81E-08	4.06E-06	69.89	5
Ale	525.00	738.4	5.81E-08	4.26E-06	73.24	5
Ale	526.50	739.9	5.87E-08	4.24E-06	72.37	6
Ale	528.00	741.4	5.98E-08	4.46E-06	74.55	6
Ale	529.50	742.9	5.63E-08	4.23E-06	75.03	6
Ale	531.00	744.4	5.81E-08	4.60E-06	79.09	6
Ale	532.50	745.9	5.97E-08	4.46E-06	74.75	5
Ale	534.00	747.4	5.81E-08	4.53E-06	77.93	6
Ale	535.50	748.9	5.75E-08	3.77E-06	65.64	6
Ale	537.00	750.4	5.54E-08	4.83E-06	87.16	6
Ale	538.50	751.9	5.54E-08	4.14E-06	74.69	6
Ale	540.00	753.4	5.66E-08	4.04E-06	71.35	6
Ale	541.50	754.9	6.22E-08	4.03E-06	64.79	5
Ale	543.00	756.4	6.38E-08	4.29E-06	67.18	6
Ale	544.50	757.9	5.94E-08	4.13E-06	69.54	5
Ale	546.00	759.4	5.71E-08	3.95E-06	69.24	6
Ale	547.50	760.9	5.50E-08	3.69E-06	67.12	5
Ale	549.00	762.4	5.55E-08	3.47E-06	62.51	5
Ale	550.50	763.9	5.21E-08	3.81E-06	73.21	6
Ale	552.00	765.4	5.07E-08	3.90E-06	76.81	6
Ale	553.50	766.9	4.91E-08	3.88E-06	79.01	5
Ale	555.00	768.4	5.06E-08	4.08E-06	80.61	5
Ale	556.50	769.9	4.39E-08	4.87E-06	110.91	6
Ale	558.00	771.4	6.24E-08	5.16E-06	82.58	7
Ale	559.50	772.9	4.96E-08	6.16E-06	124.08	6

Ale	561.00	774.4	4.78E-08	6.48E-06	135.51	5
Ale	562.50	775.9	4.76E-08	6.85E-06	143.70	6
Ale	564.00	777.4	4.74E-08	6.04E-06	127.26	6
Ale	565.50	778.9	4.64E-08	4.93E-06	106.32	5
Ale	567.00	780.4	4.46E-08	4.57E-06	102.38	6
Ale	568.50	781.9	4.25E-08	4.48E-06	105.57	6
Ale	570.00	783.4	4.24E-08	4.52E-06	106.70	5
Ale	571.50	784.9	3.58E-08	3.85E-06	107.56	5
Ale	573.00	786.4	4.38E-08	4.08E-06	93.07	6
Ale	574.50	787.9	4.32E-08	3.96E-06	91.49	5
Ale	576.00	789.4	4.32E-08	3.56E-06	82.40	6
Ale	577.50	790.9	4.29E-08	3.61E-06	84.07	5
Ale	579.00	792.4	4.00E-08	3.20E-06	80.02	5
Ale	580.50	793.9	4.35E-08	3.39E-06	78.01	5
Ale	582.00	795.4	3.58E-08	2.89E-06	80.87	8

Vita

Michael L Newton

School: 526 Montclair Avenue, Bethlehem, PA 18015 610/758-5856 mln3@lehigh.edu
Home: 65 Clinton Road, Bedford Hills, NY 10507 914/234-6420
Birth: January 12, 1982; Mt. Kisco, NY
Parents: Simon and Julia Newton

Education

- M.S., Lehigh University, Earth and Environmental Sciences; anticipated completion May 2006
- B.A., Lehigh University, Economics; May 2005
- B.S., Lehigh University, Geological Sciences; May 2004

Related Experience

- *High Resolution Deformation Rates, southern Pyrenees, Spain* 5/05
  3 weeks measuring section, paleomagnetic drilling, collecting hand samples, and precision surveying for a rock magnetic study. Masters thesis.
- *Monument Hill 7.5' Quadrangle, Montana* 6/04
  4 weeks field mapping. Published an open file report with the Montana Bureau of Mines and Geology.
- *Paleomagnetic research on the Maringouin Formation, Canada* 8/03
  2 weeks field assistant collecting paleomagnetic samples. Honors B.S. thesis.
- *Digital mapping and strain analysis of deformed veins and intrusions* 6/03
  (University of Southern Maine) 6 weeks digital mapping.
- *Big Sheep Creek Basin, Montana* 7/02
  2 weeks mapping field assistant. Undergraduate thesis.
- *Field Camp* 6/02
  (Lehigh University) 6 weeks advanced training in mapping techniques

Skills

Computing: Microsoft Excel, Microsoft Word, Kaleidagraph, Analyseries, Adobe Illustrator, Adobe Photoshop.

Field Technology: GPS (precision surveying, Trimble 5700, handheld, total station), field mapping, air photo analysis.

Geotechnical: GIS (ArcMap, ArcInfo, Trimble Office), paleomagnetic sampling and analysis, well slug testing, water quality analysis.

Awards and Honors

- Donnel Foster Hewitt Award 2004

Awarded to the senior in the Earth and Environmental Sciences Department with the greatest promise for professional achievement

- David Hellekjaer Memorial Award 2004

Awarded to the senior best exemplifying rigorous participation in sports, dedicated commitment to the study of science, and loyalty and contribution to a fraternity or sorority

Scholarships and Grants

- Presidents Scholarship at Lehigh University 2004
  One year free tuition for students sustaining a GPA above 3.5 through 90 credits
- EDMAP grant number 04HQAG0099 2004
  From the National Cooperative Geologic Mapping Program of the U.S.G.S
- Morgan Miller Scholarship 2003
  Financial Aid scholarship
- J.D. Ryan Memorial Endowment Fund 2002
  Earth and Environmental Sciences Departmental summer field work support

Leadership

- President of Beta Sigma chapter of Theta Chi fraternity 8/03-8/04
- Interfraternity Council member 8/03-8/04

Professional Memberships

- Geological Society of America 2000-present
- Phi Eta Sigma honor fraternity 2001-present
- National Society of Collegiate Scholars 2001-present
- American Geophysical Union 2004-present
- US Ski and Snowboard Association 2002-2004
- American Association of Petroleum Geologists 2006-present

Publications

Anastasio, D.J., Hinnov, L.A., Newton, M.L., Kodama, K.P. (2005), Milankovitch Modulated Eocene Growth Strata From the Jaca Piggyback Basin, Spanish Pyrenees, Eos Trans. AGU, 86(52), Fall Meet. Suppl., Abstract PP51C-0618.

Regalla, C.A., Anastasio, D.J., Newton, M.L., Pazzaglia, F.J.,2005, The Monument Hill Fault Zone as a natural laboratory for studying the boundary of basin and range extension north of the Snake River Plain, Red Rock Valley, southwestern Montana, Geological Society of America *Abstracts with Programs*, Vol. 37, No. 7, p. 204.

Newton, M.L., Regalla, C.A., Anastasio, D. J., Pazzaglia, F.J., 2005, Bedrock and surficial geologic map of the Monument Hill 7.5' quadrangle, western Montana, Montana Bureau of Mines and Geology Open File Report 517, 15 page(s), scale 1:24,000.

Newton, M.L., Kodama, K.P (2004), A Paleomagnetic and Magnetic Anisotropy Study of the Carboniferous Maringouin Formation, New Brunswick, Canada: Possible

Evidence for Inclination Shallowing in Continental Red Beds, *Eos Trans. AGU, 85*(17), Jt. Assem. Suppl., Abstract GP31A-13.

Doyle, J., Kiser, B., Newton, M., Swanson, M.T., Bampton, M., 2004, Syntectonic granites and transpressional deformation at Pemaquid Point, mid-coast Maine, Geological Society of America *Abstracts with Programs*, Vol. 36, No. 2, p. 101.

Harkins, N.W. Newton, M., Anastasio, D.J., Pazzaglia, F.J. , 2004, Bedrock and surficial geologic map of the Caboose Canyon 7.5' quadrangle, southwest Montana, Montana Bureau of Mines and Geology Open File Report 494, 13 page(s), scale 1:24,000.

Harkins, N.W., Pazzaglia, F.J., Anastasio, D.J., Newton, M.L., 2003, Tectonic and rock-type influences on terraces and channel morphology; Big Sheep Creek, Beaverhead and Tendoy Mountains, southwest Montana, Geological Society of America *Abstracts with Programs,* Vol. 35, No.. 6, p. 72.

FOLDOUT
TOO LARGE
TO BE FILMED
AS A WHOLE
FILMED IN
SECTIONS
ONLY

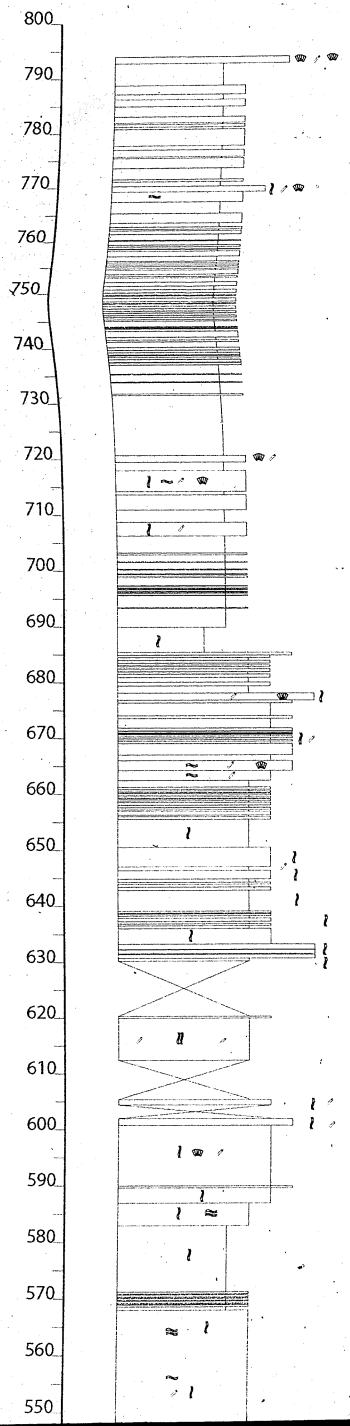

Legend

- Bryozoa
- Nummilites
- Equinoids
- Shell frags
- Vertical Bioturbation
- Horizontal Bioturbation
- Glauconite G.

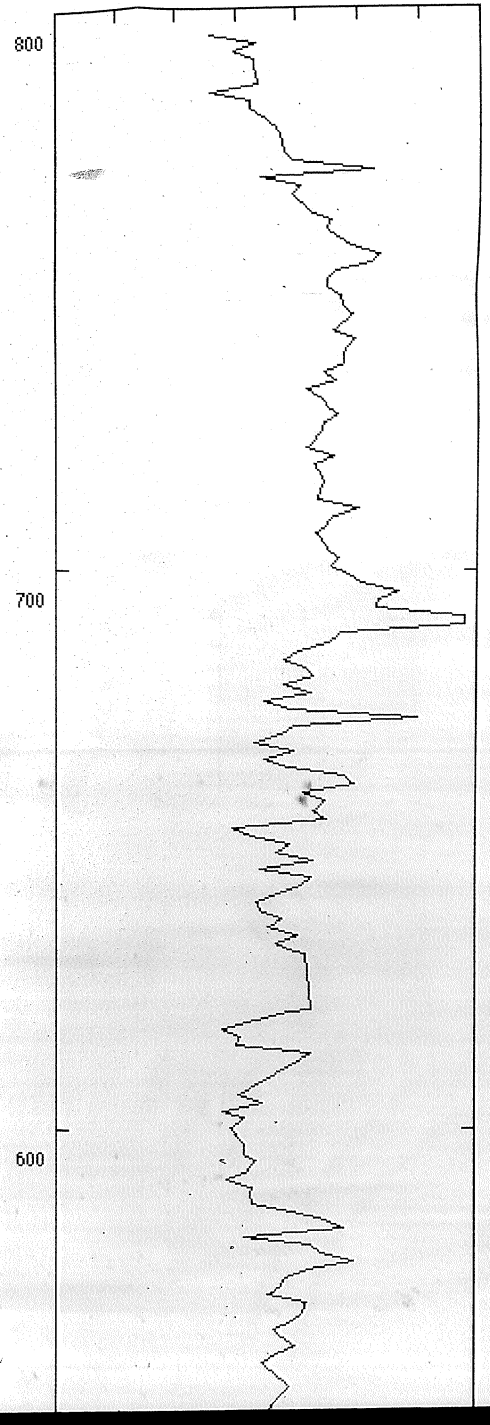

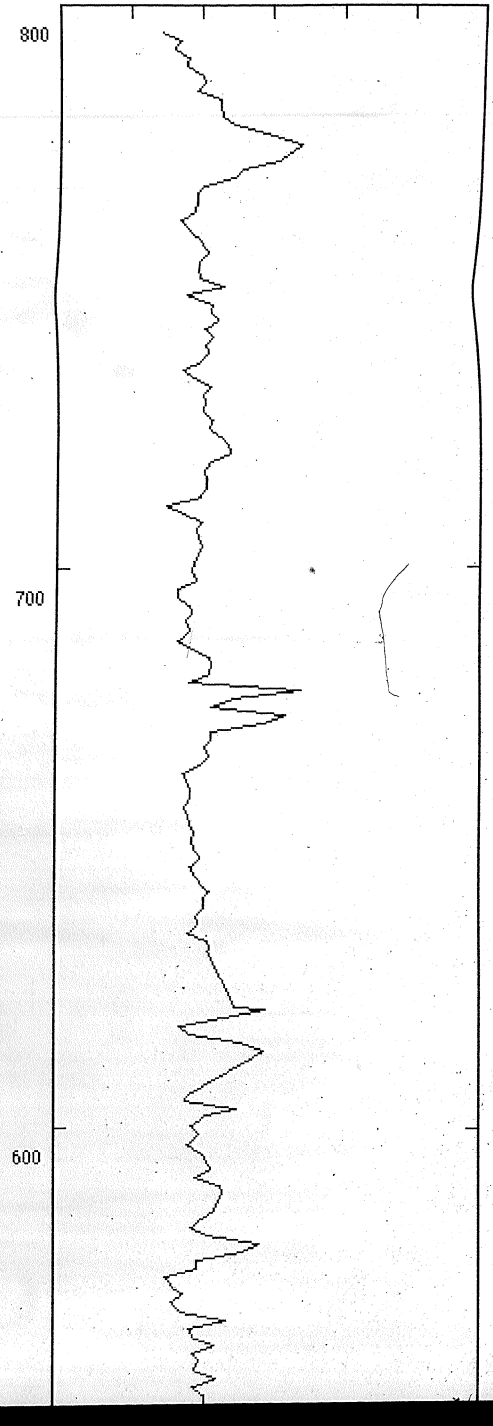

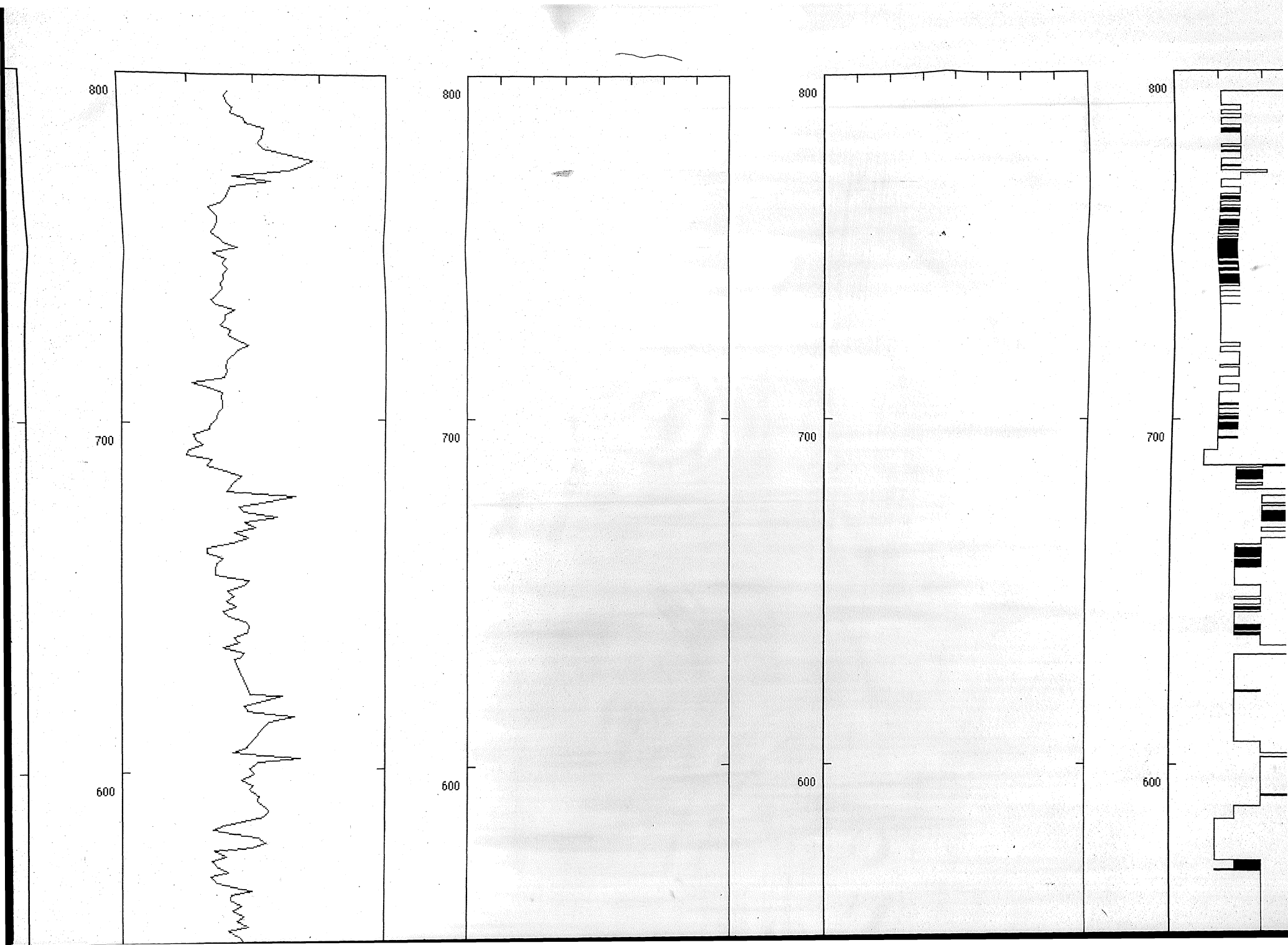
800
700
600
800
700
600
800
700
600
800
700
600

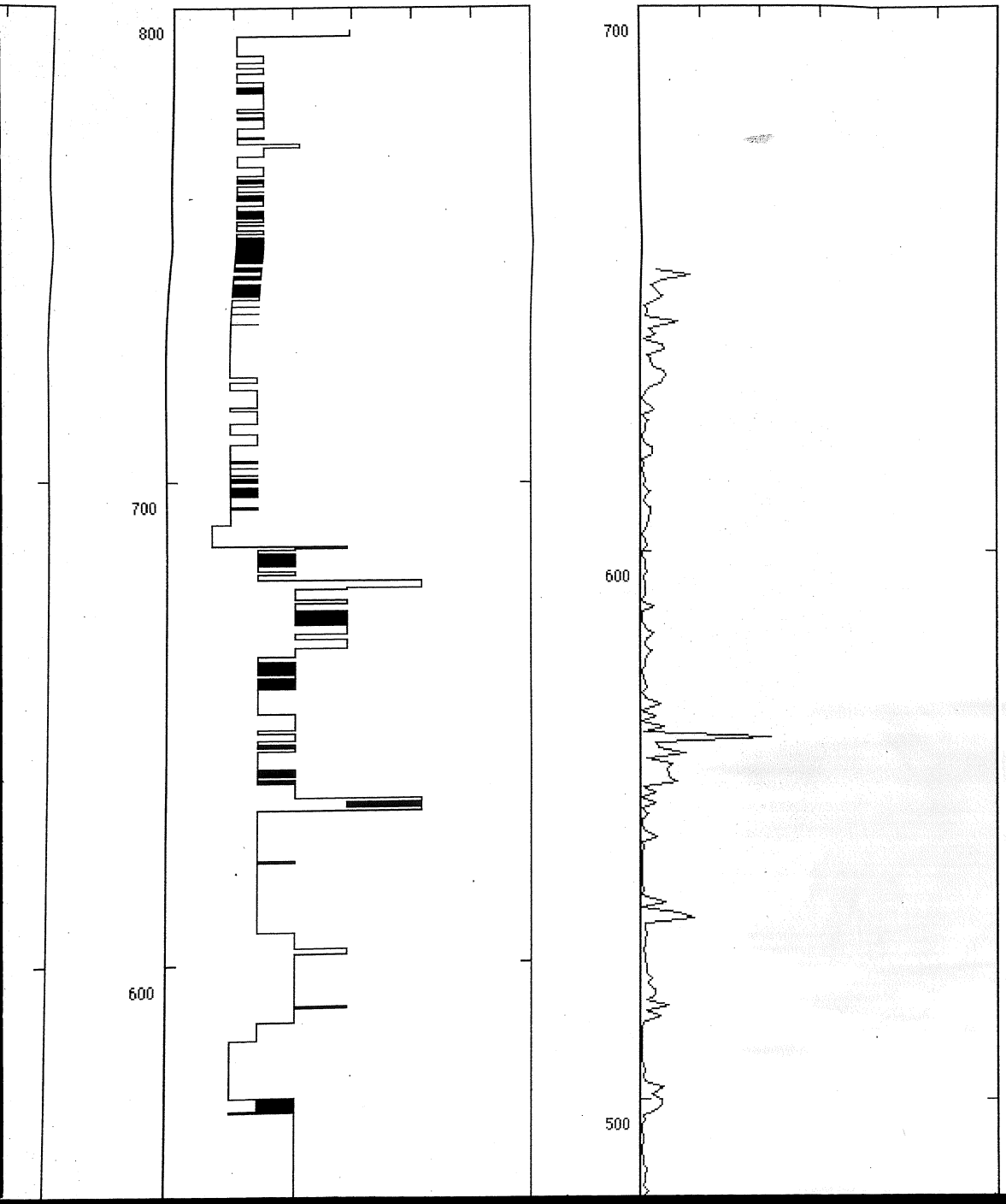
800
700
600
700
600
500

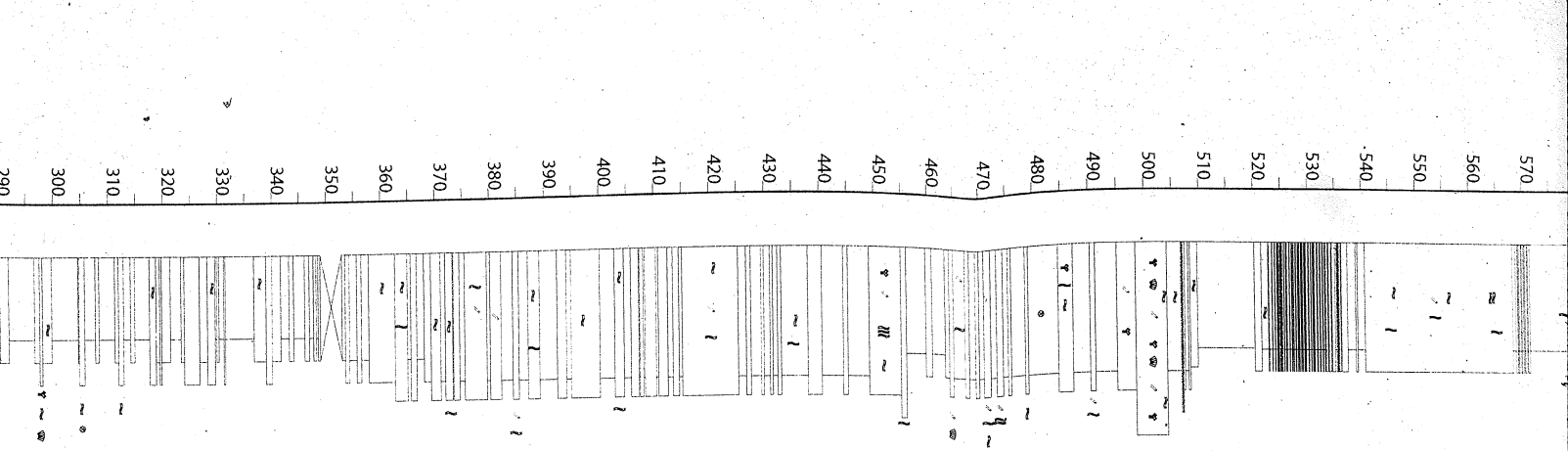
290
300
310
320
330
340
350
360
370
380
390
400
410
420
430
440
450
460
470
480
490
500
510
520
530
540
550
560
570

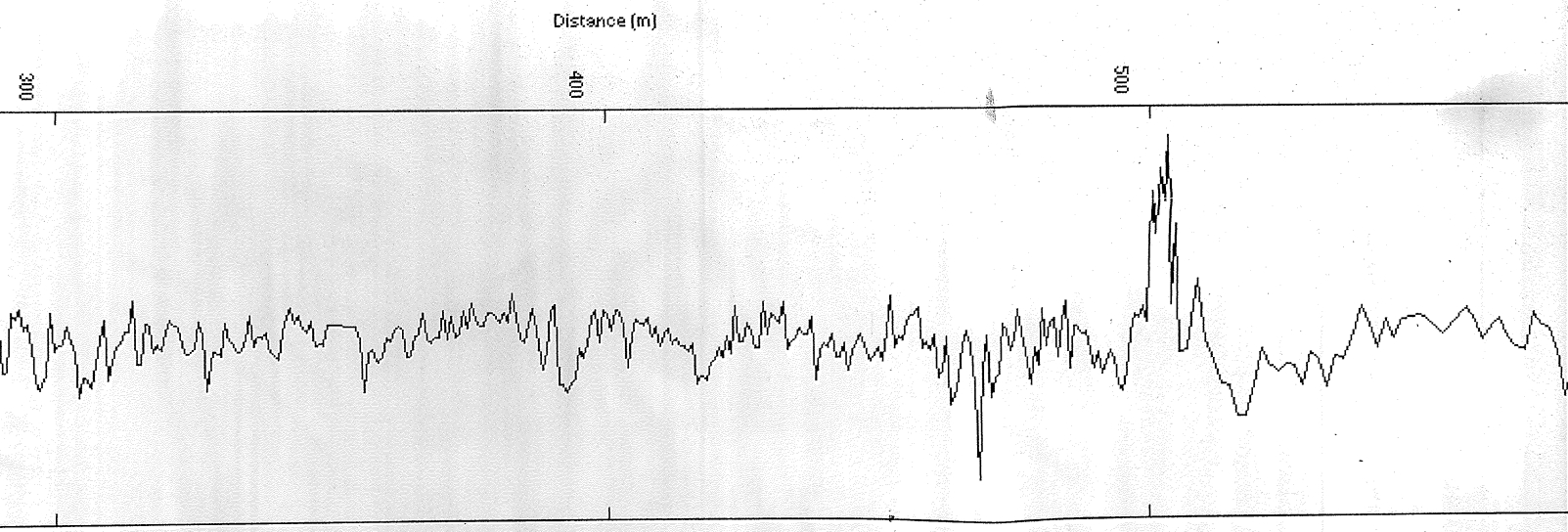
Distance (m)
300
400
500

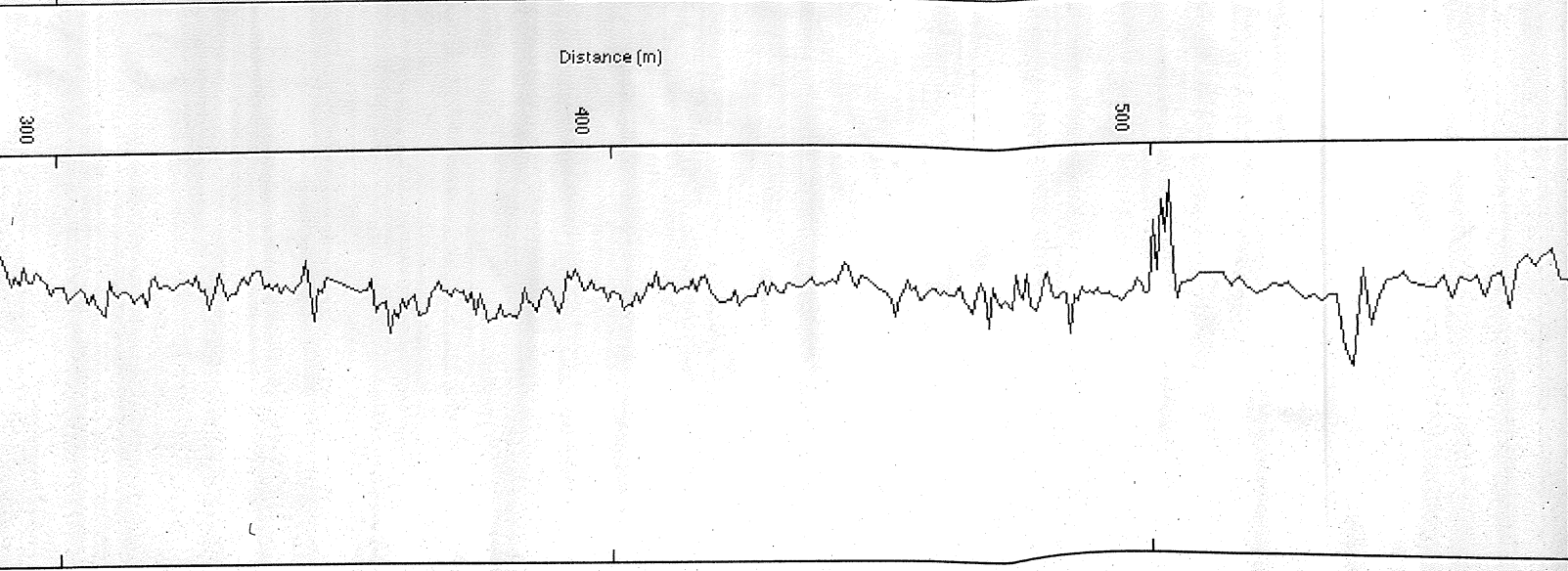
Distance (m)
300
400
500


Distance (m)
500

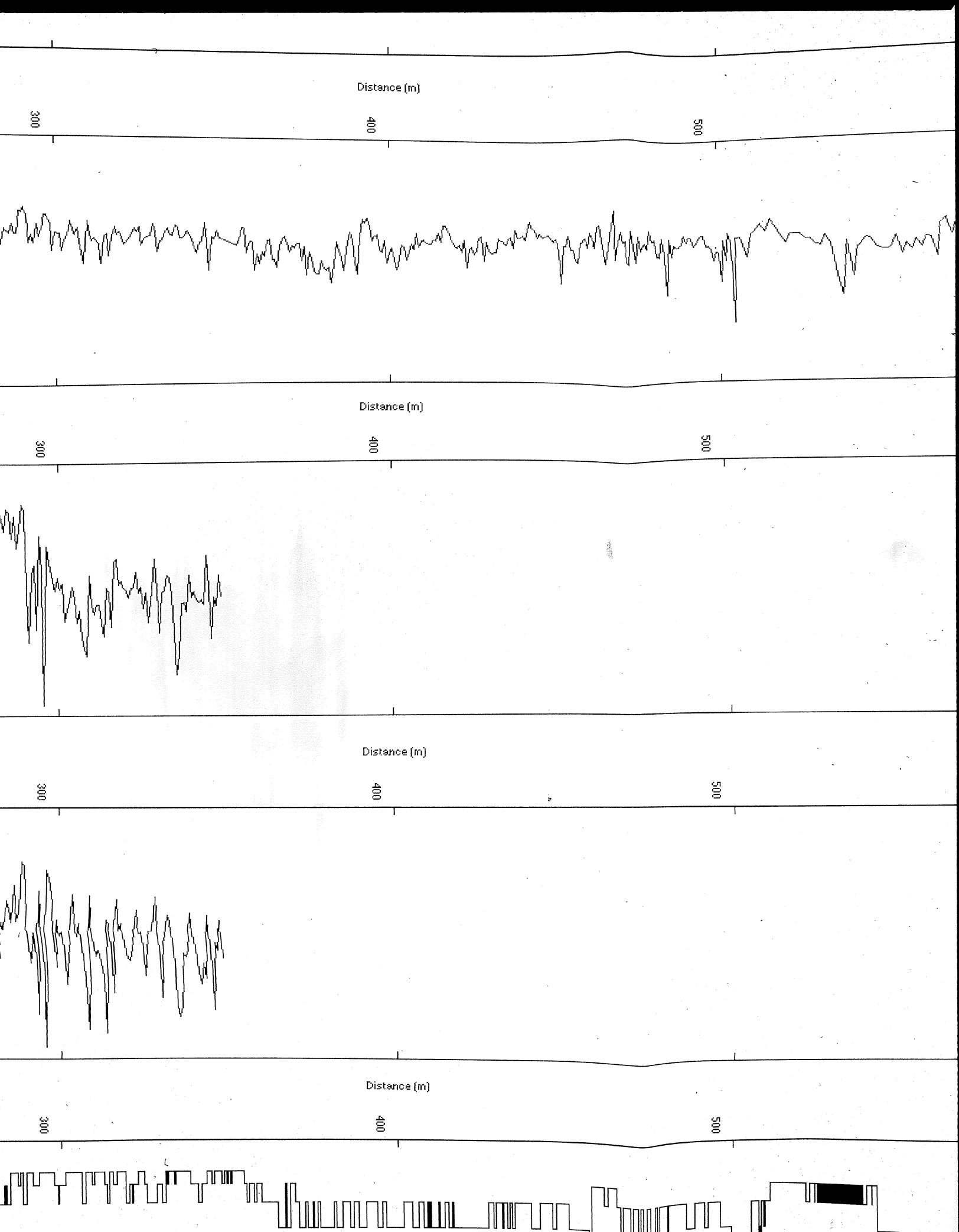
Distance (m)
300
400
500
Distance (m)
300
400
500
Distance (m)
300
400
500
Distance (m)
300
400
500

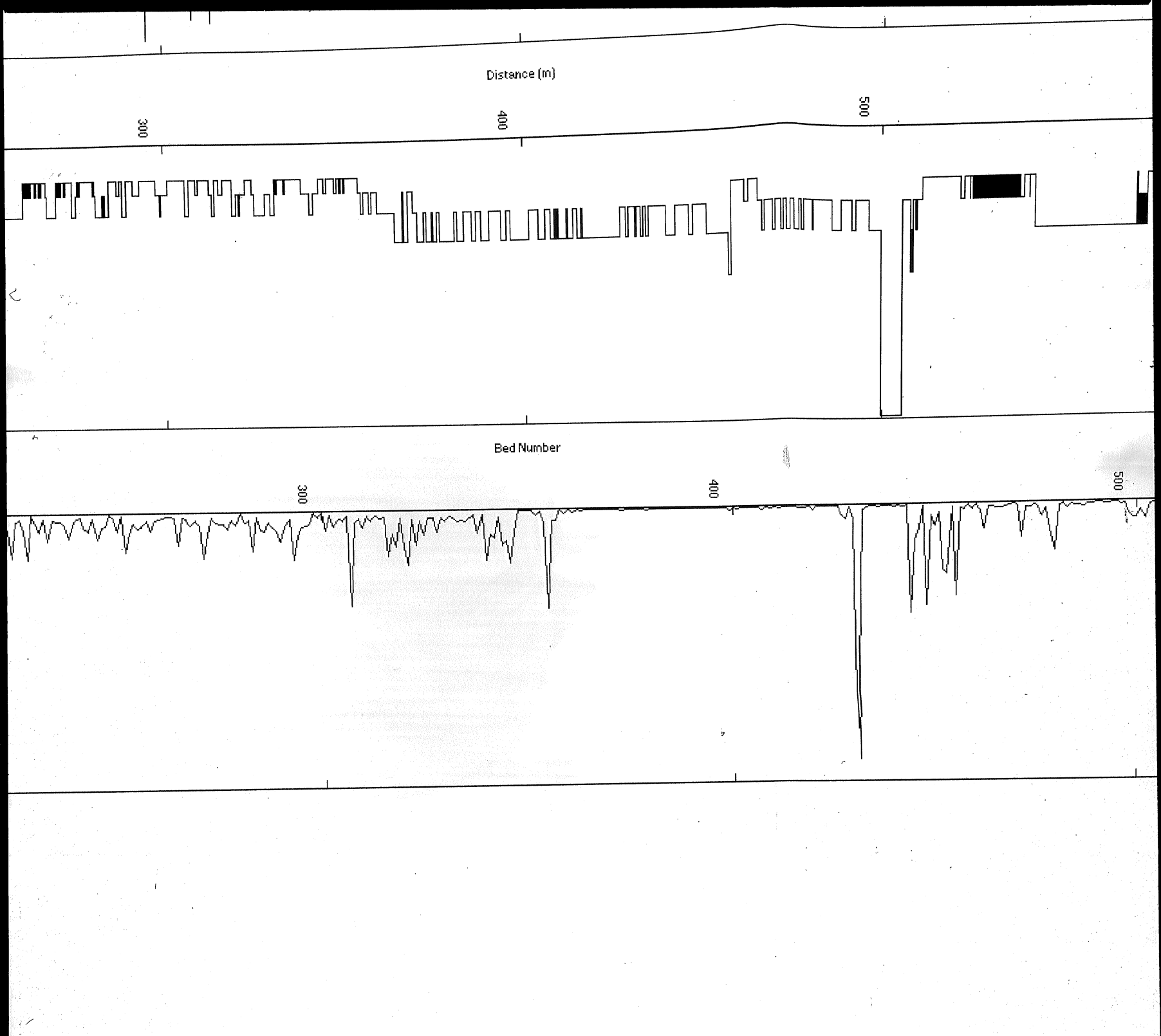
Distance (m)
300
400
500
Bed Number
300
400
500

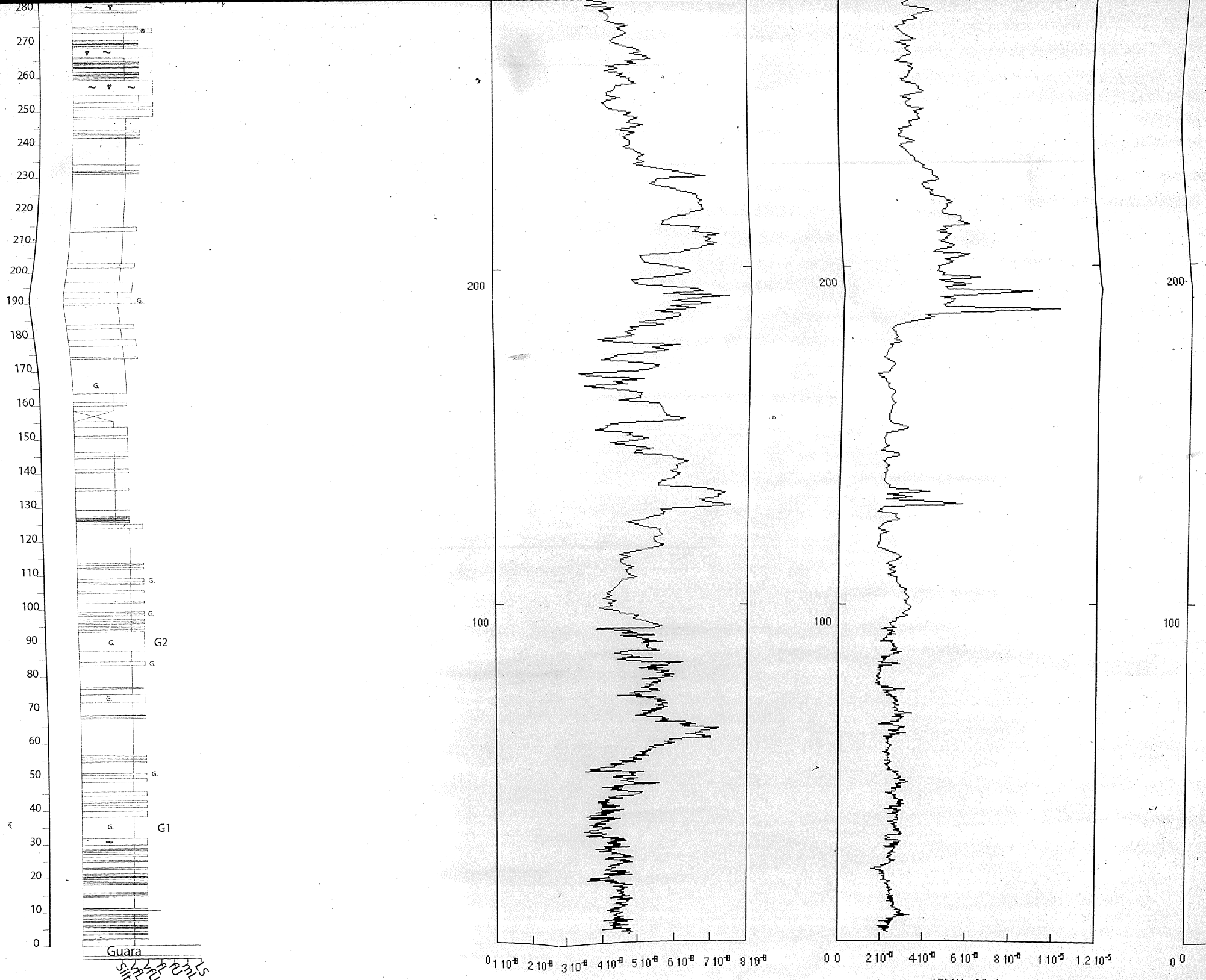
280
270
260
250
240
230
220
210
200
190
180
170
160
150
140
130
120
110
100
90
80
70
60
50
40
30
20
10
0
G.
G2
G1
Guara
200
100
0
1 10⁻⁸ 2 10⁻⁸ 3 10⁻⁸ 4 10⁻⁸ 5 10⁻⁸ 6 10⁻⁸ 7 10⁻⁸ 8 10⁻⁸
0 0
2 10⁻⁶ 4 10⁻⁶ 6 10⁻⁶ 8 10⁻⁶ 1 10⁻⁵ 1.2 10⁻⁵

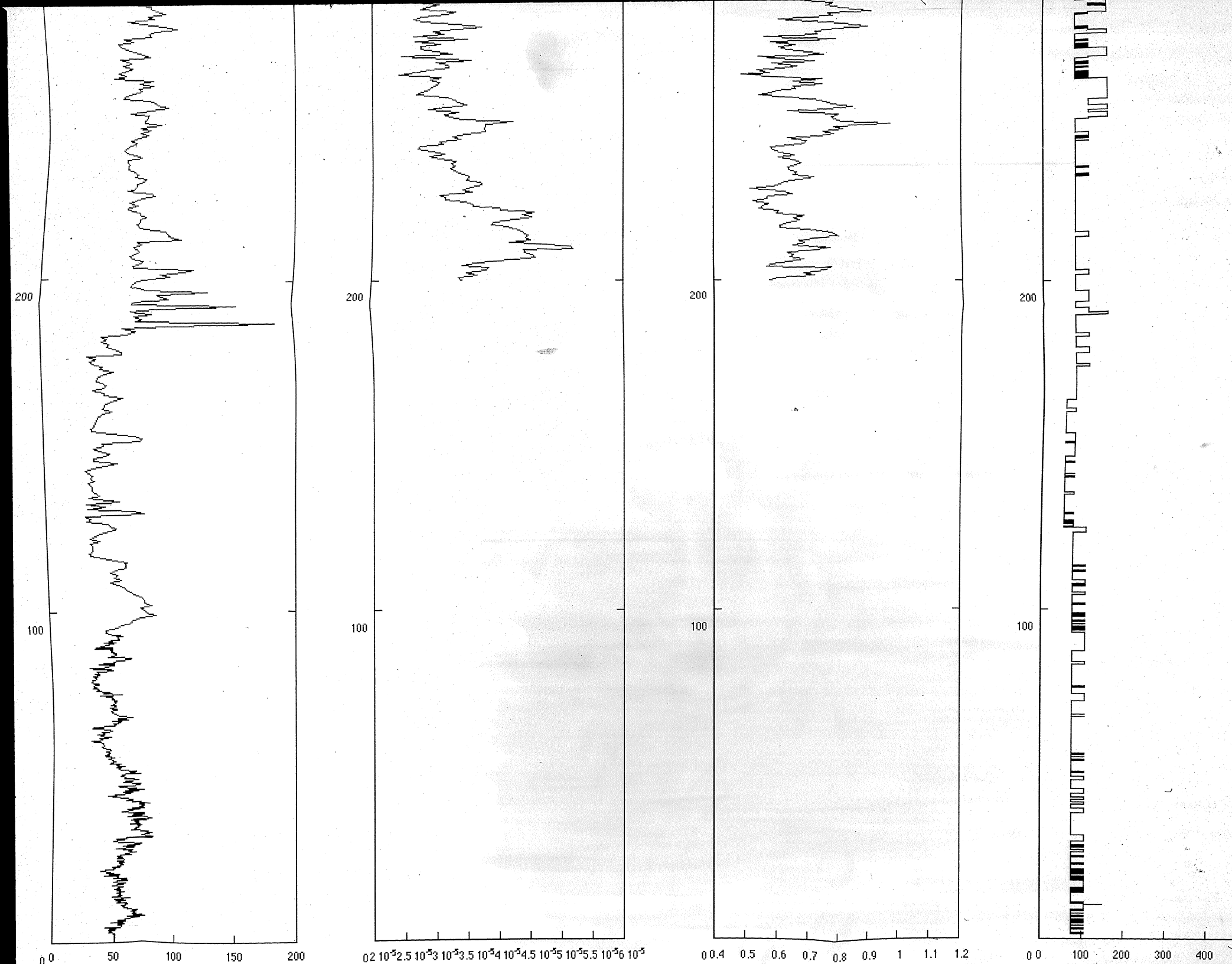
200
100
0 0
50
100
150
200
200
100
0 2 10^-5 2.5 10^-5 3 10^-5 3.5 10^-5 4 10^-5 4.5 10^-5 5 10^-5 5.5 10^-5 6 10^-5
200
100
0 0.4 0.5 0.6 0.7 0.8 0.9 1 1.1 1.2
200
100
0 0
100
200
300
400

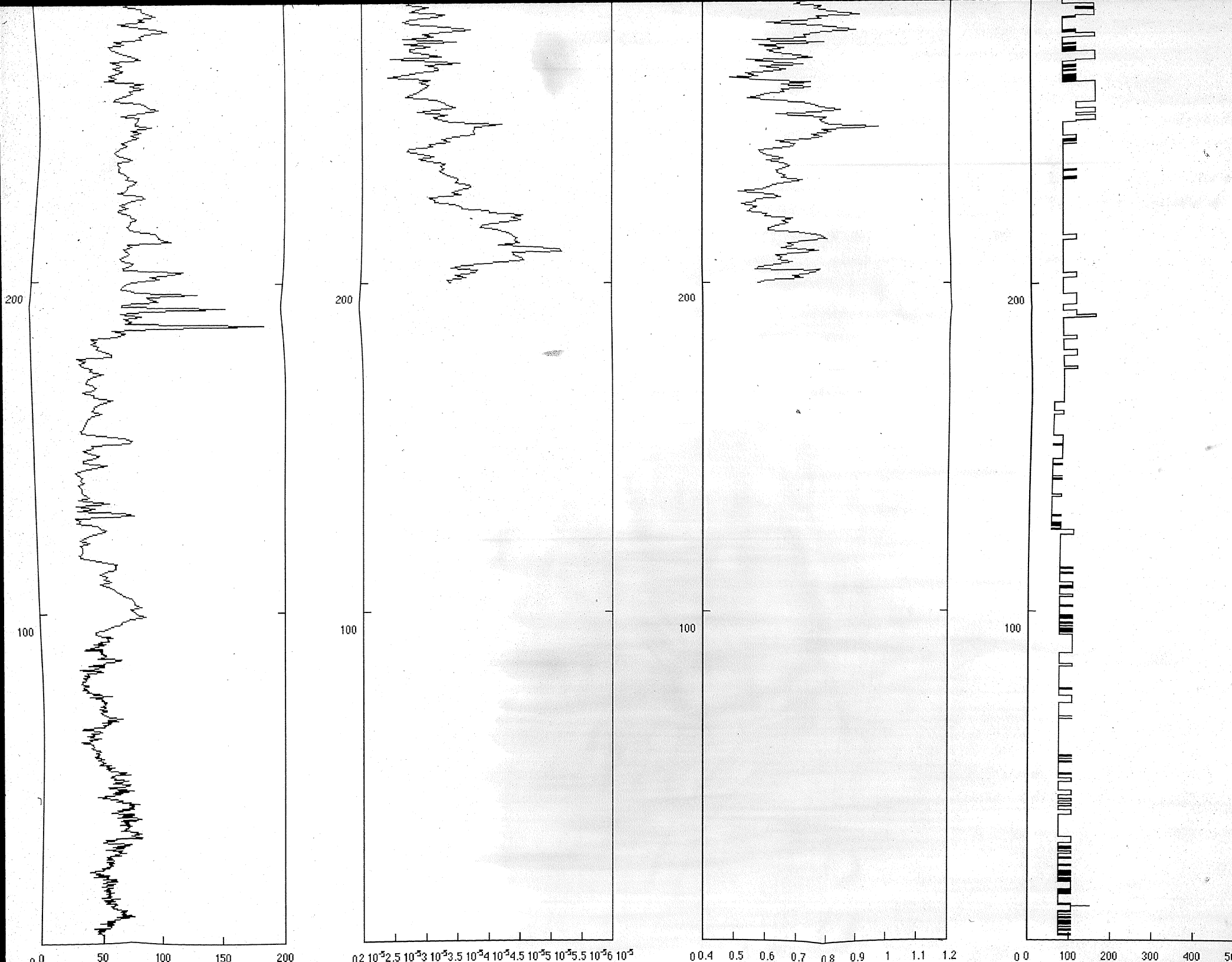
200
100
0 0
50
100
150
200
200
100
0.2 10^-5 2.5 10^-5 3 10^-5 3.5 10^-5 4 10^-5 4.5 10^-5 5 10^-5 5.5 10^-5 6 10^-5
200
100
0 0.4 0.5 0.6 0.7 0.8 0.9 1 1.1 1.2
200
100
0 0
100
200
300
400

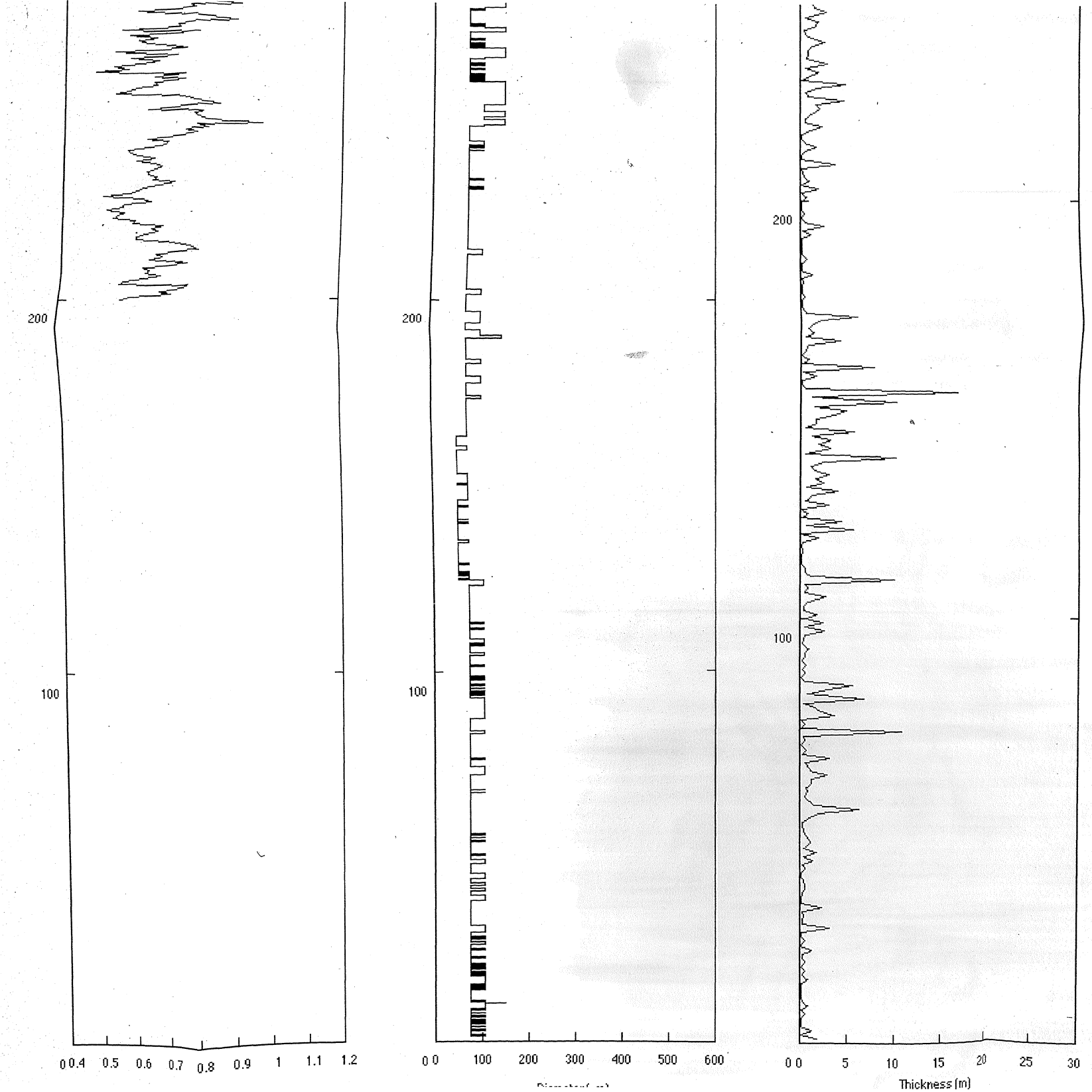
200
100
0 0.4 0.5 0.6 0.7 0.8 0.9 1 1.1 1.2
200
100
0 0 100 200 300 400 500 600
200
100
0 0 5 10 15 20 25 30
Thickness (m)

END OF TITLE